PB 2009 William Barclay Parsons Fellowship
Monograph 25

An Innovative Method For Assessing Tunnelling-Induced Risks To Adjacent Structures

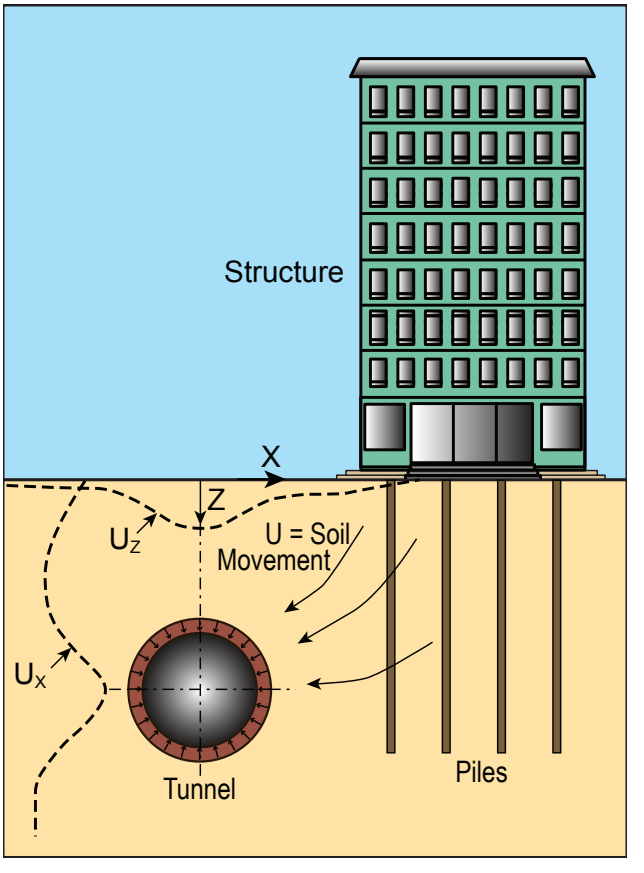

***Nagen Loganathan**, PhD*
Principal Professional Associate
January 2011

PB 2009 William Barclay Parsons Fellowship
Monograph 25

An Innovative Method For Assessing Tunnelling-Induced Risks To Adjacent Structures

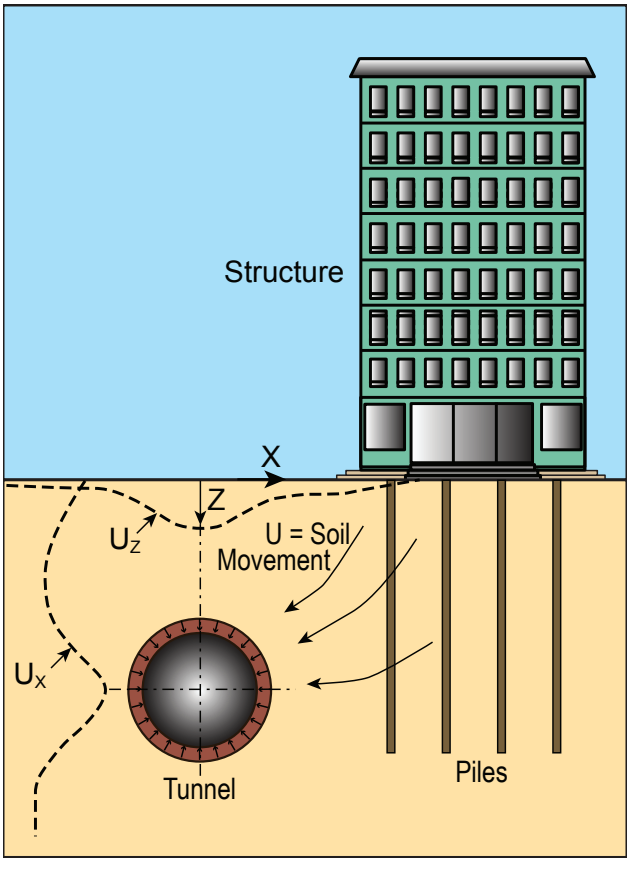

***Nagen Loganathan**, PhD*
Principal Professional Associate
January 2011

First Printing 2011
Copyright © 2011, Parsons Brinckerhoff Inc.

All rights reserved. No part of this work may be reproduced or used in any form or by an means—graphic, electronic, mechanical (including photocopying), recording, taping, or information or retrieval systems—without permission of the publisher.

Published by:
Parsons Brinckerhoff Inc.
One Penn Plaza
New York, New York 10119

Graphics Database: U609

CONTENTS

FOREWORD vii

ACKNOWLEDGEMENTS viii

1.0 INTRODUCTION 1

1.1 Purpose and Need 3

1.2 Research Outline 4

1.2.1 Prediction of Ground Loss 5

1.2.2 Closed-Form Solutions to Predict Ground Movement 5

1.2.3 Assessing Tunnelling-Induced Effects on Adjacent Structures 6

1.2.4 Building Risk Assessment Tool 6

2.0 LITERATURE REVIEW 7

2.1 Introduction 9

2.1.1 Ground Loss Components and Mechanisms 9

2.1.2 Ground Loss and Type of TBM 9

2.2 Earlier Research on Ground Loss 10

2.3 Earlier Research on the Available Methods for Predicting Tunnelling-Induced Ground Movements 14

2.3.1 Empirical Methods 14

2.3.2 Analytical Methods 17

2.3.3 Numerical Methods 18

2.4 Available Building Risk Assessment Methodologies 19

3.0 ESTIMATION OF TUNNELLING-INDUCED GROUND LOSS 25

3.1 Introduction 27

3.2 Definition of Ground Loss 27

3.3 Theoretical Background of Gap Parameters 28

3.3.1 Face Loss V_f 28

3.3.2 Shield Loss V_S 30

3.3.3 Tail Loss V_t 33

4.0 GROUND MOVEMENTS 35
4.1 Introduction 37
4.2 Closed-Form Solutions for Ground Movements 38
4.3 Summary - Green Field Ground Movements 43

5.0 TUNNELLING-INDUCED EFFECTS ON ADJACENT PILES 45
5.1 Introduction 47
5.2 Methodology 47
5.3 Parametric Study 49
5.4 Design Chart Concept 49
5.5 Design Charts for Short Piles 51
5.6 Design Charts for Long Piles 56
5.7 Summary 61

6.0 RISK ASSESSMENT METHODOLOGY FOR PILES . 63
6.1 Introduction 65
6.2 Ground and Pile Movement Path 65
6.3 Pile Location Specific Induced Effects 68
6.4 Summary 69

7.0 BUILDING RISK ASSESSMENT TOOL 71
7.1 Introduction 73
7.2 Risk Assessment Flow Chart 73
7.3 Tunnelling-Induced Building Risk Assessment for Shallow Foundations 75
7.4 Tunnelling-Induced Building Risk Assessment for Pile Foundations 80
7.5 Summary 82

8.0 CONCLUSIONS 83

9.0 REFERENCES 87

APPENDICES 93
Appendix A: Design Worksheets 95
A.1 Ground Loss Estimation 97
A.2 Ground Movement Predictions 99

Appendix B: General Pile Analysis (GEPAN) Computer Program 103

Appendix C: Typical Worksheets for Performing Building Damage Assessments 109

C.1 Typical Stage 2 Assessment Worksheet 111

C.2 Typical Stage 3 Assessment Worksheet 115

LIST OF FIGURES

Chapter 1

1.1 Examples of Tunnelling-Induced Building Failures 4

Chapter 2

2.1 Various Ground Loss Components 9
2.2 Grout and Bentonite Flow Mechanisms around an SPB TBM 11
2.3 (a) Typical EPB TBM Face Extrusion Pattern 12
2.3 (b) Typical Face Pressure Variation with Ground Loss. 12
2.4 Definition of Gap around Tunnel 13
2.5 Comparison of Various Surface Settlement Troughs. 16
2.6 Relationship of Damage to Angular Distortion and Horizontal Strain 20

Chapter 3

3.1 Circular and Oval Ground Deformation Patterns Around a Tunnel 27
3.2 Schematic of TBM Configuration with Cutter Bead and Tapered Shield 31
3.3 TBM Face Pressure Acting on the Shield Gap for EPB TBM 32
3.4 Ground Movement and Shield Gap Filling Mechanism for EPB TBM 33

Chapter 4

4.1 Tunnelling-Induced Ground Movements - Green Field. 37
4.2 Ground Deformation Patterns and Ground Loss Boundary Conditions 38
4.3(a) Subsurface Settlement 41
4.3(b) Lateral Deformation. 41
4.4 Comparison of Centrifuge Test Results 42
4.5 Key Diagram - Tunnel Dimensions 43

Chapter 5

5.1 Single Pile Adjacent to Tunnelling - The Basic Problem Analysed 48
5.2 Design Charts: Tunnelling-Induced Effects for Short Pile Base Case 52
5.3 Design Charts: Correction Factors for Strength - Short Pile. 53
5.4 Design Charts: Correction Factors for Pile Diameter - Short Pile. 54
5.5 Design Charts: Correction Factors for Pile Length/Tunnel Depth Ratio - Short Pile. 55
5.6 Design Charts: Tunnelling-Induced Effects for Long Pile Base Case 57
5.7 Design Charts: Correction Factors for Strength - Long Pile. 58
5.8 Design Chart- Correction Factors for Pile Diameter - Long Pile 59
5.9 Design Chart- Correction Factors for Pile Length/Tunnel Depth Ratio - Long Pile . 60

Chapter 6

6.1 Section and Plan View Showing Settlement Influence Zones and Pile Movements for Negative Face Loss 66
6.2 Section and Plan View Showing Settlement Influence Zones and Pile Movements for Positive Face Loss 67
6.3 Extent of Various Displacement Zones 68

Chapter 7

7.1 Risk Assessment Tool: Flow Chart for Assessing Potential Damage to Existing Buildings 74
7.2 Typical Settlement Contour Map with Building Footprints 76
7.3 Typical Worksheet for Stage 1 Risk Assessment 77
7.4 Definition of “Hogging” and “Sagging” 78
7.5 Building Risk Designation Plot 79
7.6 Pile Head Settlement Profile 81

LIST OF TABLES

Chapter 2

2.1 Recommended *i* Values by Various Researchers 15
2.2 Damage Assessment Criteria for Stage 1 and Stage 2 22

Chapter 4

4.1 Comparison of Estimated and Observed Surface Settlement Trough Parameters . 40

Chapter 6

6.1 Critical Tunnelling-Induced Values on Piles 69

Chapter 7

7.1 Damage Classifications - Typical Values for Maximum Building Slope and Settlement for Damage Risk Assessment (CIRIA PR30, 1996) 77

FOREWORD

Tunnelling-induced damage to adjacent structures and utilities is generally highly publicised by the media and has had negative consequences for the engineering industry as a whole. Owners, lending institutions, insurers, contractors, and many national and international tunnelling associations share a common goal: reduce the cost and risk associated with tunnelling and improve public perception of the tunnelling industry.

Urban tunnels are often excavated adjacent to high-rise buildings, beneath highways and bridge structures, and over or under other tunnels serving transportation or private and public utilities. The increasing need for urban tunnelling in such densely developed underground areas and the associated risks are leading clients to seek consultants equipped with innovative yet proven methods for assessing these risks and for mitigating them through design before construction begins. Key to developing such designs is an understanding of tunnelling-induced ground loss mechanisms and the associated displacements, and the risks they pose to adjacent buildings, structures and utilities.

This monograph presents an innovative method for assessing the tunnelling-induced risks to adjacent structures, especially at the early stages of project development, such as route selection and concept design. It is based on relatively complicated soft-ground tunnelling in an urban environment. This new risk assessment tool comprises:

- A new method for assessing the various components of the ground loss associated with tunnel boring machine (TBM) excavation in soft ground
- New closed-form solutions for predicting tunnelling-induced settlements
- Design charts for predicting tunnelling-induced effects on adjacent pile foundations
- A new risk assessment flow chart that includes shallow and pile foundations.

For the completeness of this subject (tunnelling-induced risk to adjacent structures) this monograph covers risk associated with buildings founded on pile foundations (findings of this research) and on shallow foundations (well established methods from literature).

This monograph is intended to be used as a “PB Guideline” for assessing tunnelling-induced risks to adjacent structures in urban environments. It is expected that it will also promote awareness of such risks among PB engineers who are involved in proposals, concept studies and detailed designs of tunnel projects. When we, in turn, make tunnel owners and builders aware of such risks at the early stages of the project, we help them to avoid financial risk to the project. In addition, our having more accurate information about tunnelling-induced risks in the early stages of project development will open avenues for working with major banks and insurance companies covering tunnelling projects in urban areas.

ACKNOWLEDGEMENTS

I wish to express my gratitude and appreciation to the Board of Directors of Parsons Brinckerhoff for establishing and supporting the William Barclay Parsons (WBP) Fellowship. This program was designed to introduce engineering innovations and best practices that advance the state-of-the-art, benefit our clients and enhance PB's leadership role in the industry. I am grateful also to the PB Career Development Committee for identifying the potential of my research proposal and supporting my work and completion of this monograph.

I am particularly indebted to Richard Flanagan, Principal Professional Associate of PB, for his direction, encouragement, constructive comments and support throughout this research. I also thank Doug Maconochie and Jim Rozek for their support as fellowship sponsors and reviews of this monograph.

I also thank my PB colleagues, Joe O'Carroll and Kenneth Xu, for their support and help, and PB Australia management for its support during my research. I sincerely thank Pedro Pablo Silva for his professional graphics works and type settings, and Lorraine Anderson for her professional editing of this monograph.

I thank Professor Harry Poulos, Senior Principal from Coffey Geosciences, for his support and advice on my previous research and my most recent work presented herein.

Finally, I thank my wife, Dilanthy, and our children, Ajaey and Dhaarani, for their love and support.

Nagen Loganathan, PhD
Principal Professional Associate
Parsons Brinckerhoff
Level 27, Ernst & Young Centre
680 George Street
Sydney NSW2001
Australia

1.0 INTRODUCTION

1.0 INTRODUCTION

1.1 PURPOSE AND NEED

Tunnelling is truly an international market and core business for PB. With the increase in urban tunnelling and associated risks, particularly those due to ground movements, clients continually seek consultants equipped with innovative yet proven methods to assess and mitigate these risks through design before going into construction.

Assessing tunnelling-induced ground loss is a major issue when predicting ground movements and their effects on adjacent structures. Presently, there are no methods available to tunnel designers for estimating the ground loss values for proposed tunnels based on tunnel configuration, construction method and ground conditions. Designers rely instead upon empirical assumptions made from similar projects. The problem in doing so is that no two tunnelling projects are the same, and the complexity, risk and consequence of failure seem to increase with every new project undertaken.

In urban environments, many high-rise buildings are supported by deep foundations that, if adjacent to a new tunnel excavation, are subject to axial and lateral forces caused by tunnelling-induced ground movements. These movements may jeopardize the integrity of the foundation elements themselves. Therefore, tunnelling-induced effects on adjacent structures should be assessed and added to the original design values of the adjacent structures to assess whether the total value exceeds the ultimate capacity of each foundation element.

Tunnelling-induced damage to adjacent structures and utilities is generally highly publicised by the media and has negative consequences for the industry as a whole. In recent years, insurers have had some significant financial losses and now insist on risk evaluation measures up front. Owners, lending institutions, insurers, contractors, and many national and international tunnelling associations share a common goal: reduce the cost and risk of tunnelling and improve public perception of the tunnelling industry.

The assessment of tunnelling-induced risks prior to construction is a challenge to designers, constructors and tunnel owners. Ground movements around tunnels are a critical factor in assessing tunnelling-induced risks; however, most existing methods for determining ground movements are inadequate, over-simplistic or overly complicated. The importance of accurately assessing ground loss and tunnelling-induced deformations has been emphasised in recent years due to an increase in the number of urban tunnelling projects. Further, the results of not doing so have been illustrated quite dramatically. For example, Figure 1.1 shows some of the major tunnelling-induced failures of recent times.

Figure 1.1 Examples of Tunnelling-Induced Building Failures

(a) Building on a Pile Foundation **(b) Building on a Shallow Foundation**

With property values as high as they are now in all major urban centres and the high risk of human loss or injury, it is critical that designers have a methodology that enables them to assess ground loss values accurately so they can minimise the risk of damage. Such a method must use geotechnical parameters and take into account the TBM configuration and TBM operational parameters. This methodology can then be used to determine the appropriate TBM configuration and operational parameters to minimise ground movements for any given project considering the risk profiles of buildings along the alignment.

1.2 RESEARCH OUTLINE

The research conducted under the PB 2009 William Barclay Parsons (WBP) Fellowship builds upon the author's previous research work and extensive experience in assessing tunnelling-induced effects on adjacent structures. His analytical solutions for tunnelling-induced ground movements for stiff ground (soil) conditions with lateral earth pressure coefficient of one (k_0=1) have been published previously. This monograph essentially brings to culmination the previous research efforts and incorporates the outcomes of this current research, capturing the entire knowledge base in one unified model. It includes examples of the input parameters, development of design charts, output results, actual field data and comparisons to existing methods. The results presented herein can be used worldwide, and they provide PB with a step-up in the tunnelling industry.

The various technical aspects of the fellowship research are outlined below.

1.2.1 Prediction of Ground Loss

Tunnelling-induced ground movements during pressurised faced TBM tunnelling in soft ground occur in the radial and longitudinal directions with ground moving into the tunnel excavated face (both face and sides). The volume of soil that intrudes into the tunnel owing to the pressure release at the excavated face will be excavated eventually. The movement of soil into this opening can be related to the concept of "loss of ground," which is defined as the volume of material (through face or radial encroachment over and around or behind the TBM shield) that has been excavated in excess of the theoretical design volume of excavation. Ground loss for a TBM excavated tunnel occurs in three stages:

- Face loss (longitudinal ground movement into the tunnel face)
- Shield loss (radial ground movement into the gap created by TBM overcut)
- Tail loss (due to the gap closure at the tail).

In this study, the ground loss components at each stage of the tunnel excavation are estimated to understand the ground movement patterns and the induced effects on adjacent piles, these effects being:

- Settlement of pile head
- Maximum lateral movement of pile
- Down drag forces
- Bending moments.

It is demonstrated that these effects result in stressing and destressing on the adjacent foundation, and that these impacts on the foundation can be minimised by controlling the various ground loss components. TBM face pressures, TBM configuration (cutter bead thickness, shield taper, thickness of tail skin, clearances for segment erection, etc.) and grouting procedures are the major factors discussed.

A design worksheet developed for estimating various ground loss values is also presented. It will be a valuable guide for designers to follow when assessing one of the most crucial elements of risk when tunnelling adjacent to pile foundations.

1.2.2 Closed-Form Solutions to Predict Ground Movement

A ground movement prediction will be of practical use only if it takes into account the effects of a number of parameters, such as:

- Excavation and tunnel construction methods
- Tunnel depth and diameter
- Groundwater conditions
- Initial stress state
- Stress-strain-strength behaviour of the soil around tunnel.

Current “rules” for estimating ground settlement from tunnelling operations have been derived generally from empirical correlations between some of these parameters and observed

settlement data. Hence, they account for only a few of the significant factors, so extrapolation to other cases is questionable at best because generally similar conditions are not fulfilled.

In this monograph, closed-form solutions for predicting ground deformation are presented for various ground loss components and the ground movements experienced by adjacent pile foundations during TBM excavation.

1.2.3 Assessing Tunnelling-Induced Effects on Adjacent Structures

Design charts developed to assess the tunnelling-induced effects on adjacent deep-pile foundations are presented herein. These charts will help designers to estimate the tunnelling induced effects on an adjacent pile foundation at various stages of the excavation.

In addition, based on these charts, designers may assess TBM face pressures required to minimise ground movements and the associated impacts on nearby foundations.

1.2.4 Building Risk Assessment Tool

The risk assessment tool presented in this monograph is applicable to buildings founded on both shallow and pile foundations (including combined footings). The risk assessment procedure for shallow foundations is based on commonly adopted published information. Risk assessment for buildings on pile foundations is based on the findings of this research.

2.0 LITERATURE REVIEW

2.0 LITERATURE REVIEW

2.1 INTRODUCTION

This chapter presents a review of some of the considerable research performed by others in the fields of ground loss, ground movement and risk of tunnelling-induced damage to buildings. Before the review is a brief introduction to ground loss components and mechanisms, and to the ground loss mechanisms for the two types of TMBs used for soft-ground excavation.

2.1.1 Ground Loss Components and Mechanisms

Tunnel excavation is associated inevitably with ground loss, which, in turn, results in associated ground movement. It is important, therefore, to minimize ground loss when tunnelling through urban areas. To do so requires that designers understand the components and mechanisms associated with ground loss during TBM operations.

The various ground loss components that can occur during tunnel excavation are shown in Figure 2.1.

Figure 2.1 Various Ground Loss Components

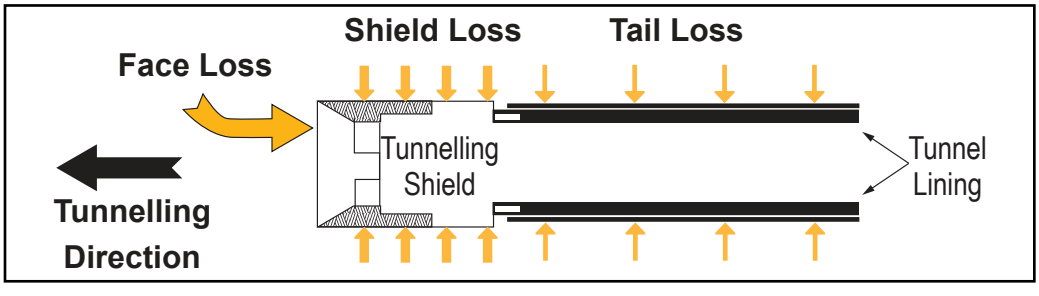

The mechanisms associated with the ground loss components are as follows:

- **Face loss** occurs when the change in ground stress at the TBM face causes longitudinal ground movement into the tunnel face.
- **Shield loss** occurs when the ground moves radially into the gap created around the tunnel shield by TBM overcut. This overcutting of the ground is done to minimise the friction between the ground and the TBM. Overcutting is also carried out at curves during tunnel excavation.
- **Tail loss** results from shrinkage and/or incomplete filling of the grout or pea gravel that is applied to the tail gap immediately after the segmental lining leaves the TBM shield.

2.1.2 Ground Loss and Type of TBM

The ground loss mechanisms for the two types of TBMs used most commonly for soft soil tunnelling—earth pressure balance (EPB) and slurry pressure balance (SPB)—are similar with

one exception. It is accepted that SPB TBMs control shield loss better than EPB TBMs by better stabilising the gap around the shield as the TBM advances.

A brief summary of the two types of TBMs is as follows:

- **Earth pressure balance** (EPB). EPB TBMs use the excavated soil to apply a support pressure to the tunnel face. Often various additives are injected into the soil as it is excavated to ensure appropriate muck properties to achieve the optimum TBM advance rate without causing excess ground loss.
- **Slurry pressure balance** (SPB). Slurry shields stabilize the tunnel face by applying a pressurised bentonite slurry that is mixed into the soil during TBM operations and then separated later, after the soil has been excavated, in a separation and recovery plant.

2.2 EARLIER RESEARCH ON GROUND LOSS

Many research works have been performed to understand the ground loss mechanisms. Bezuijen and Bakker (2007) carried out detailed numerical analyses and field monitoring to understand the gap grout flow and face slurry flow mechanism and, from this, to estimate the ground loss associated with the gap closure around the TBM shield.

Figure 2.2 shows three possible grout flow mechanisms around an SPB tunnel shield. These mechanisms depend on the magnitude of the slurry pressure and gap grout pressure. The three possible flow conditions illustrated occur as explained below:

1. **(Top):** Grout flows from the tail to the face and bentonite flows from the face to the tail. This condition occurs when shield loss occurs due to bleeding of the grout or penetration of the bentonite into the soil. For this condition, the lowest pressure will occur where the grout and bentonite meet.
2. **(Middle):** Bentonite flows back to the tail and pushes the grout out of the gap between the TBM and soil. The pressure will be highest at the tunnel face and will decrease when going towards the tail. This condition cannot be continuous but can occur temporarily.
3. **(Bottom):** Grout flows to the tunnel face and pushes the bentonite with it. The pressure is highest at the tail close to the grout injection points and decreases toward the face.

Figure 2.2 Grout and Bentonite Flow Mechanisms around an SPB TBM (Bezuijen & Bakker, 2007)

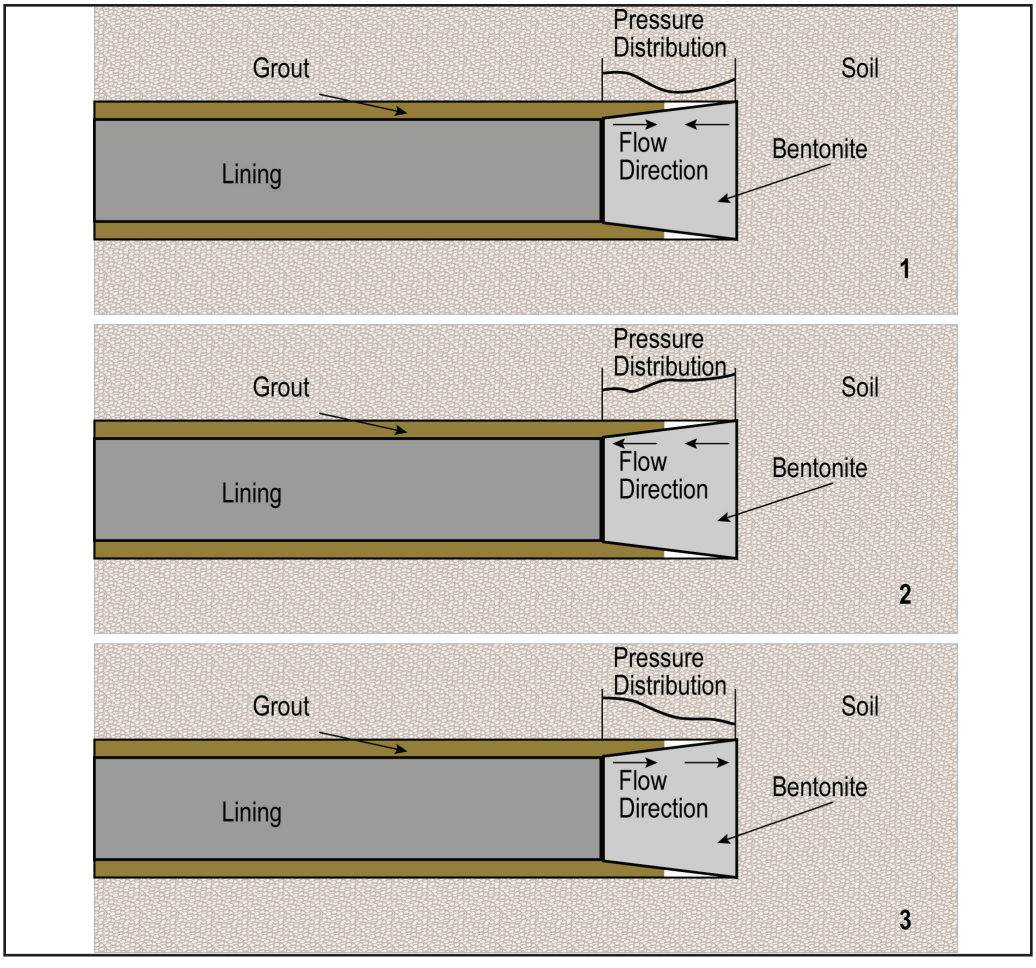

The realistic ground loss around the shield should include the ground displacement around the gap; however, the ground displacement equilibrium state should be assessed. These aspects were explored further as part of the WBP Fellowship research to establish ground loss mechanisms.

Gatti & Cassani (2007) reported various methods for estimating the ground loss for an EPB TBM. Figure 2.3 (a) shows typical face extrusion values. More ground is extruded at the centre of the TBM and less at the shield skin. This observation was attributed to the friction resistance between the soil and the shield skin at the face. This aspect was studied in detail as part of this WBP Fellowship research to assess the face loss component.

Figure 2.3 (b) shows a typical variation of face loss with the earth pressure at the TBM face. As indicated, the face loss decreased as the face pressure increased.

Figure 2.3 (a) Typical EPB TBM Face Extrusion Pattern

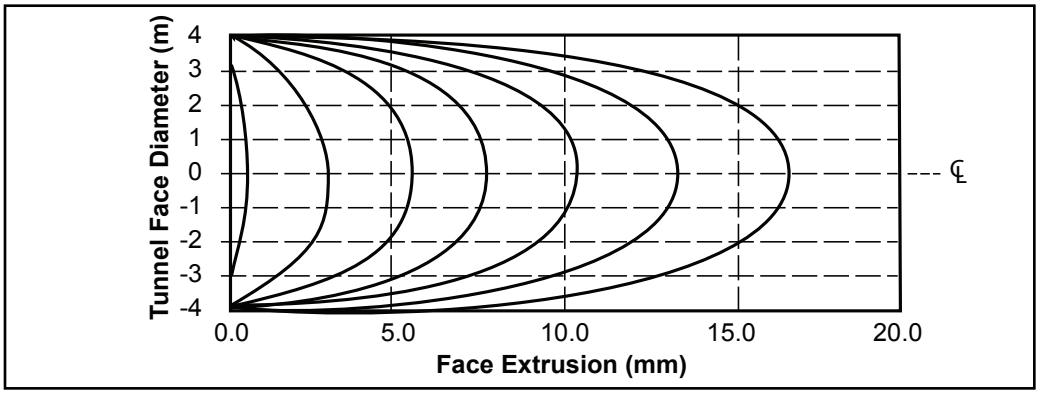

Figure 2.3 (b) Typical Face Pressure Variation with Gound Loss

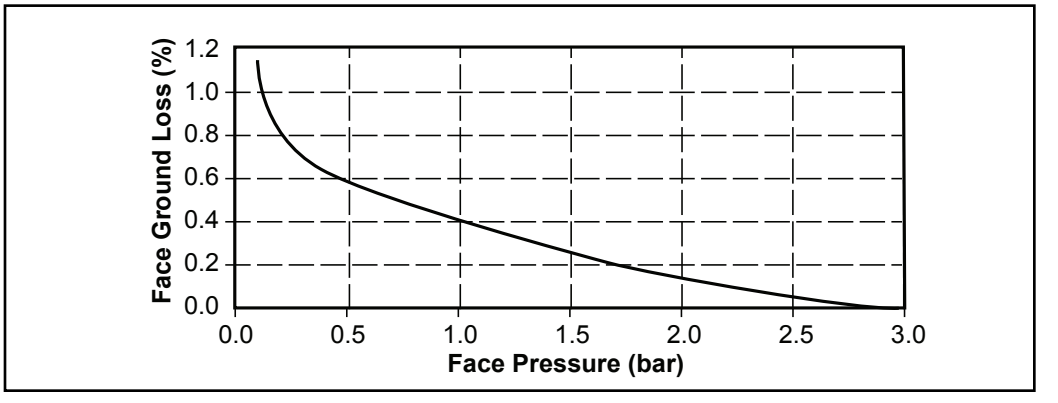

Rowe and Lee (1992) established a method to predict the equivalent two-dimensional "gap" at the tunnel crown considering ground movements in longitudinal and radial directions. They defined gap parameters as:

$$g = G_p + U^*_{3D} + \omega \qquad (2.1)$$

Where:

G_p = the physical gap (usually the difference between the theoretical maximum outside diameter of the tunnelling machine and the outside diameter of the lining for a circular tunnel)

U^*_{3D} = the three dimensional (3-D) elasto-plastic deformation into the tunnel face

ω = the gap due to the overcutting bead.

Figure 2.4 shows the tunnel head and the 2-D plane strain representation of the tunnel heading.

Figure 2.4 Definition of Gap around Tunnel

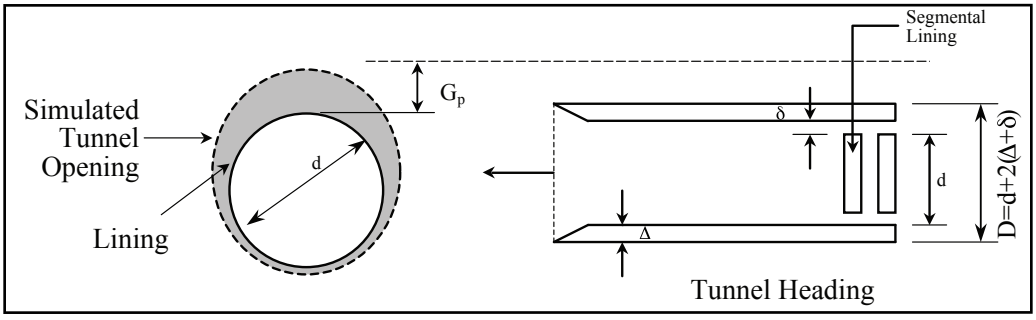

Rowe and Lee (1992) defined the physical gap as:

$$G_p = 2\Delta + \delta \tag{2.2}$$

Where:

Δ = the thickness of the tailpiece

δ = the clearance for erecting the lining.

The free-field stress state at a given section is modified as the excavation of the tunnel approaches it, as follows:

- If pressure on the tunnel face is lower than the free field stress, then the soil mass will move towards the tunnel face.
- If pressure on the tunnel face is larger than free field stress, then the earth will be pushed outside and result in negative face loss.

The volume of soil that intrudes into the tunnel face owing to pressure release at the face will be excavated eventually. The elasto-plastic deformation component, U^*_{3D} , is defined as:

$$U^*_{3D} = (k/2)\ \delta_x \tag{2.3}$$

Where:

k = soil-cutter resistance factor

δ_x = face intrusion.

Lo et al. (1984) derived an expression for the elasto-plastic plane strain displacement (U_i) for cohesive soils at the tunnel crown as:

$$\frac{U_i}{R} = 1 - \left(\frac{1}{1 + \frac{2(1+\nu_u)c_u}{E_u}\left[\exp\left(\frac{N-1}{2}\right)\right]^2} \right)^{1/2} \tag{2.4}$$

Where:

R = tunnel radius
E_u = undrained Young's Modulus
c_u = undrained strength of the soil
v_u = undrained Poisson's ratio
N = stability number.

The smallest of $0.6G_p$ and $(1/3)U_i$ is chosen and designated as ω^*, (the gap due to the overcutting bead). The value of ω includes the radial ground loss due to the overcutting beads and copy cutters, which provide additional gap to minimise the friction between the TBM and the ground. (Overcutting can also occur at tunnel curves.)

The concept of using gap parameters has been studied further to develop a method for assessing various ground loss components, as discussed in Chapter 3.

2.3 EARLIER RESEARCH ON THE AVAILABLE METHODS FOR PREDICTING TUNNELLING-INDUCED GROUND MOVEMENTS

Methods of estimating soil movement associated with tunnelling may be classified broadly into three categories; empirical, analytical and numerical. The usage and the limitations of each category are discussed below.

2.3.1 Empirical Methods

Surface Settlements. The well-established empirical methods available to date are used primarily to estimate surface settlements in soft ground. The one used most commonly was proposed by Peck (1969), who found that based on a number of field measurements, the surface settlement trough could be represented by a shape of a probability distribution curve, or error curve, as shown in Equation 2.5:

$$S = S_{\max} \cdot \exp\left(\frac{-x^2}{2i^2}\right) \tag{2.5}$$

Where:

S = surface settlement at a transverse distance x from the tunnel centre line
S_{max} = maximum settlement at x=0
i = location of maximum settlement gradient or point of inflexion.

A significant amount of research involving field observations and model tests has been devoted to the estimation of S_{max} and the i values for different ground conditions. The estimations of i values by various researchers are shown in Table 2.1.

Table 2.1 Recommended *i* Values by Various Researchers

Name	*i*- value	Remark
Peck (1969)	$\frac{i}{R} = \left(\frac{z_0}{2R}\right)^n$: n = 0.8 to 1.0	Based on field observations
Atkinson & Potts (1979)	$i = 0.25(z_0 + R)$: for loose sand, $i = 0.25(1.5z_0 + 0.5R)$: for dense sand and over consolidated clay	Based on field observations and model tests
O'Reilly & New (1982)	$i = 0.43z_0 + 1.1$: cohesive soil $i = 0.28z_0 - 0.1$: granular soil	Based on field observations of UK tunnels
Mair (1993)	$i = 0.5z_0$	Based on field observations worldwide and centrifuge test
Attewell (1977)	$\frac{i}{R} = \alpha.\left(\frac{z_0}{2R}\right)^n$:α = 1 and n = 1	Based on field observations of UK tunnels
Clough & Schmidt (1981)	$\frac{i}{R} = \alpha.\left(\frac{z_0}{2R}\right)^n$:α = 1 and n = 0.8	Based on field observations of US tunnels

Note: z_0 is the depth of tunnel below ground (at tunnel springline) and R is the tunnel radius.

The maximum settlement can be estimated using Equation 2.6 as proposed by Mair (1993):

$$S_{\max} = \frac{0.313V_L D^2}{i} \tag{2.6}$$

Where:

V_L = ground loss (ratio of ground loss volume/tunnel volume per meter length)
D = diameter of the tunnel.

Figure 2.5 shows a comparison of various predicted surface settlement troughs for a hypothetical 6-m (20-foot) diameter tunnel at a 30-m (98-foot) depth. The ground loss volume/tunnel volume ratio was assumed as 1 percent. As shown, the maximum surface settlements predicted by various methods are in the range of 7 mm to 10 mm (0.3 inch to 0.4 inch). The surface settlement trough width, i, varies from 8.3 m to 15 m (27.2 feet to 49.2 feet). These results show the variability of empirical predictions proposed by various researchers due to the variability in the databases they used for the derivation of i values.

Figure 2.5 Comparison of Various Surface Settlement Troughs

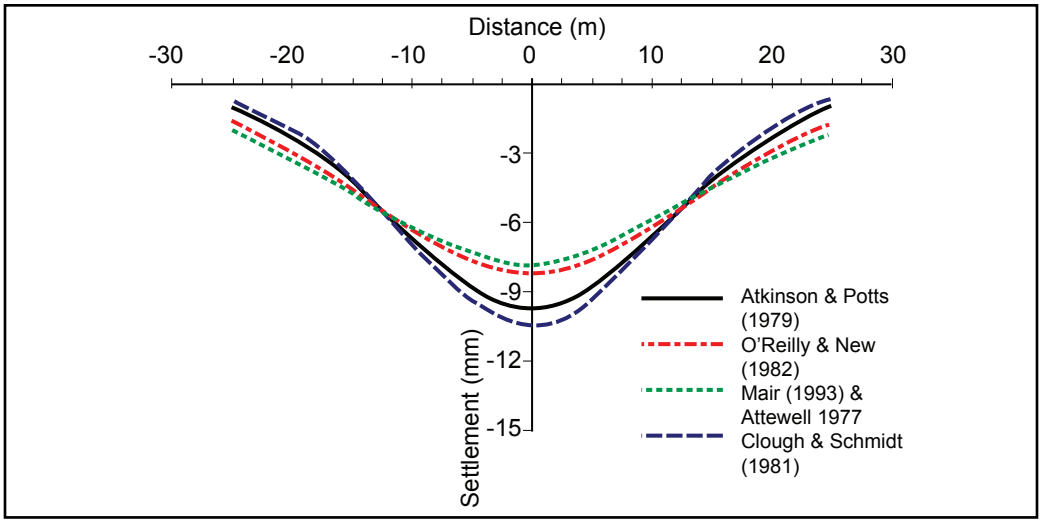

Subsurface Settlements. At present, few empirical methods are available to predict subsurface settlement profiles. The two used most widely are those proposed by Mair (1993) and Atkinson & Potts (1979).

Mair (1993) stated that it is often assumed that the shapes of subsurface settlement profiles developed during tunnel construction are characterised by a Gaussian distribution in the same manner as for surface settlement profiles. His empirical method proposed for estimating the subsurface settlements is as follows:

$$S_z = S_{z,\max} \exp\left(\frac{-x^2}{2i_z}\right) \tag{2.7}$$

Where:

$i_z = k(Z_o\text{-}Z)$

$$k = \frac{0.175 + 0.325\left(1 - \frac{Z}{Z_0}\right)}{1 - \frac{Z}{Z_0}}$$

Therefore,

$$\frac{S_{z,\max}}{R} = \frac{1.25V_L}{0.175 + 0.325\left(1 - \frac{Z}{Z_0}\right)} \cdot \frac{R}{Z_0}$$

Atkinson & Potts (1979) proposed the following method, which is based on model tests, to estimate subsurface settlements for shallow tunnels:

$$\frac{S_z}{S_{z,\max}} = 1.0 - \alpha\left(\frac{Z - R}{2R}\right) \tag{2.8}$$

Where:

α = 0.57 for dense sand
α = 0.40 for loose sand
α = 0.13 for over-consolidated clays
S_z = settlements at depth z
$S_{z,\max}$ = maximum settlement at depth z.

Vermeer and Bonnier (1991) proposed a similar empirical formula:

$$S_z = \left(\frac{z_0}{z_0 - z}\right)^{0.8} S_{z,\max} \exp\left(\frac{-x^2}{2i_z}\right) \tag{2.9}$$

Norgrove et al (1979) established an empirical relation as a ratio of the subsurface settlement:

$$S_x = \frac{x}{z_0} S_z \tag{2.10}$$

Where:

S_x = lateral deflection
S_z = settlement at depth z
x = lateral distance from the tunnel centreline
Z_0 = depth of the tunnel.

These empirical methods do not give highly accurate results, however, as they are subject primarily to two important limitations:

- Their applicability to different ground conditions and construction techniques
- The limited empirical relationships established to predict horizontal movements and subsurface settlements.

2.3.2 Analytical Methods

As mentioned, ground deformation prediction should account for the effects of a number of parameters if it is to be of use. These parameters include:

- The construction method and tunnel driving details
- Tunnel depth and diameter
- Ground water conditions
- The initial stress state
- The stress-strain-strength behaviour of the soil around the tunnel excavation.

Current "rules" for estimating ground settlement from tunnelling operations were derived generally from empirical correlations between some of those variables and the settlements observed in actual tunnels, as described in Section 2.3.1. Hence, they account for only a few of the significant factors, and extrapolation to other cases is questionable mainly because similar conditions are generally not fulfilled. Only a few attempts to develop analytical methods (closed-form solutions) that incorporate all factors contributing to ground deformations have appeared:

- Sagaseta (1987) presented closed-form solutions for obtaining the strain field in an initially isotropic and homogeneous incompressible soil due to near-surface ground loss from tunnelling.
- Verruijt and Booker (1996) presented an analytical solution for tunnels in homogeneous elastic half spaces using an approximate method suggested by Sagaseta (1987) for the case of ground loss.

The solution given by Verruijt and Booker is a generalisation of Sagaseta's solution in that it:

- Gives the solutions for the case of ground loss for the incompressible case and for arbitrary values of Poisson's ratio
- Includes the effect of ovalisation (tunnel lining deformation) in the long term.

Verruijt and Booker's closed-form solutions for the estimation of settlements and lateral deformations are as follows:

Estimation of settlements:

$$U_z = -\varepsilon R^2\left(\frac{z_1}{r_1^2}+\frac{z_2}{r_2^2}\right)+\delta R^2\left(\frac{z_1(kx^2-z_2^2)}{r_1^4}+\frac{z_2(kx^2-z_2^2)}{r_2^4}\right)$$
$$+\frac{2\varepsilon R^2}{m}\left(\frac{(m+1)z_2}{r_2^2}+\frac{mz(x^2-z_2^2)}{r_2^4}\right)-2\delta R^2 h\left(\frac{x^2-z_2^2}{r_2^4}+\frac{m}{m+1}\frac{2zz_2(3x^2-z_2^2)}{r_2^6}\right) \quad (2.11)$$

Estimation of lateral deformations:

$$U_x = -\varepsilon R^2\left(\frac{x}{r_1^2}+\frac{x}{r_2^2}\right)+\delta R^2\left(\frac{z_1(x^2-kz_1^2)}{r_1^4}+\frac{x(x^2-kz_2^2)}{r_2^4}\right)$$
$$-\frac{2\varepsilon R^2 x}{m}\left(\frac{1}{r_2^2}-\frac{2mzz_2}{r_2^4}\right)-\frac{4\delta R^2 xh}{m+1}\left(\frac{z_2}{r_2^4}+\frac{mz(x^2-3z_2^2)}{r_2^6}\right) \quad (2.12)$$

Where:

ε = uniform radial ground loss
δ = long term ground deformation due to the ovalization of the tunnel lining
$z_1 = z\text{-}H$
$z_2 = x+H$
$r_1^2 = x^2+z_1^2$
$r_2^2 = x^2+z_2^2$
R and h = tunnel radius and depth
$m = 1(1\text{-}2v)$
$k = v/(1\text{-}v)$
ν = Poisson's ratio of soil.

2.3.3 Numerical Methods

Some of the limitations in empirical methods (and, consequently, analytical methods) may be overcome by the finite element method, which indeed has been used widely for tunnelling analyses. For example, Rowe and Kack (1983) found in their analyses of some case

histories that their finite element technique generally gave good estimates of soil settlements as compared with those measured, although unfavourable comparisons were found in some cases. Successful predictions of lateral soil movements by the finite element method were also reported by Lee et al. (1992). Gunn (1993) reported that a finite element analysis gave poor predictions for surface settlements, however, even with a refined constitutive soil model. Gunn found that the surface settlement trough was too wide and shallow compared with those given by the empirical methods (error curve) and field measurements.

Simpson et al. (1996) concluded from their analyses of excavation in London Clay that the predicted surface settlement trough was substantially influenced by the anisotropic shear modulus, but that it was little influenced by non-linearity of ground stiffness. Addenbrooke (1997) reported that better predictions could be achieved by using sophisticated soil models that accounted for non-linear soil behaviour at small strain.

The findings of various researchers appear contradictory in terms of the selection of appropriate soil models for predicting tunnelling-induced ground deformations. Finite element predictions require considerable expertise, modelling and interpretation skill to obtain accurate results. Further, the following aspects need to be modelled accurately:

- The realistic stress path that soil (soil-structure interaction mechanism) experiences during the tunnel excavations for different tunnelling methods
- The three-dimensional effect of various ground loss components, typically face loss and the radial ground loss
- The stress-strain behaviour of the soil around the tunnel.

2.4 AVAILABLE BUILDING RISK ASSESSMENT METHODOLOGIES

In practice, building damage assessments are carried out in three stages to simplify the assessment procedure, as suggested by Mair (1996). As the first step, settlement contours are plotted along the project corridor and all existing building footprints plotted onto the settlement contour maps. Maximum settlement and angular distortions have been estimated for each structure.

To focus the assessment on the buildings most susceptible to damage, an initial assessment, Stage 1, is conducted to filter out those properties where the risk of damage was anticipated to be low (negligible or slight damage category on Table 2.2 at the end of this chapter). Stage 2 and Stage 3 evaluations are then carried out on buildings where a higher potential for damage (moderate and severe damage category) was predicted in the Stage 1 assessment.

Stage 1 - Preliminary Assessment

This assessment is based upon the estimation of ground settlement magnitude and slope under assumed “green field” conditions. Six risk categories ranging from 0 (negligible) to 5 (very severe) are used to define the possible degree of damage. Table 2.2 shows the criteria for the preliminary assessment.

Stage 2 - Second Stage Assessment

In this stage, the interaction between the ground and the building is considered and the

horizontal and shear strains induced on the building are estimated. A criterion based on critical strain developed at the building-ground interface and proposed by Burland (1997) and Boscardin & Cording (1989) is used (refer to Table 2.2).

The Stage 2 assessment is considered conservative because it assumes the building has no stiffness and deflects to conform to the green field settlement trough. In practice, however, the actual level of damage is likely to be less than the assessed category due to the contribution of the structural stiffness of the building.

Figure 2.6 shows an alternative method proposed by Boscardin & Cording (1989) based on angular distortion and horizontal strain. This method has been used at the early stages of studies for cut and cover tunnels. Both methods proposed by Boscardin & Cording (1989) and Burland (1997) provide consistent damage classification.

Figure 2.6 Relationship of Damage to Angular Distortion and Horizontal Strain (Boscardin & Cording, 1989)

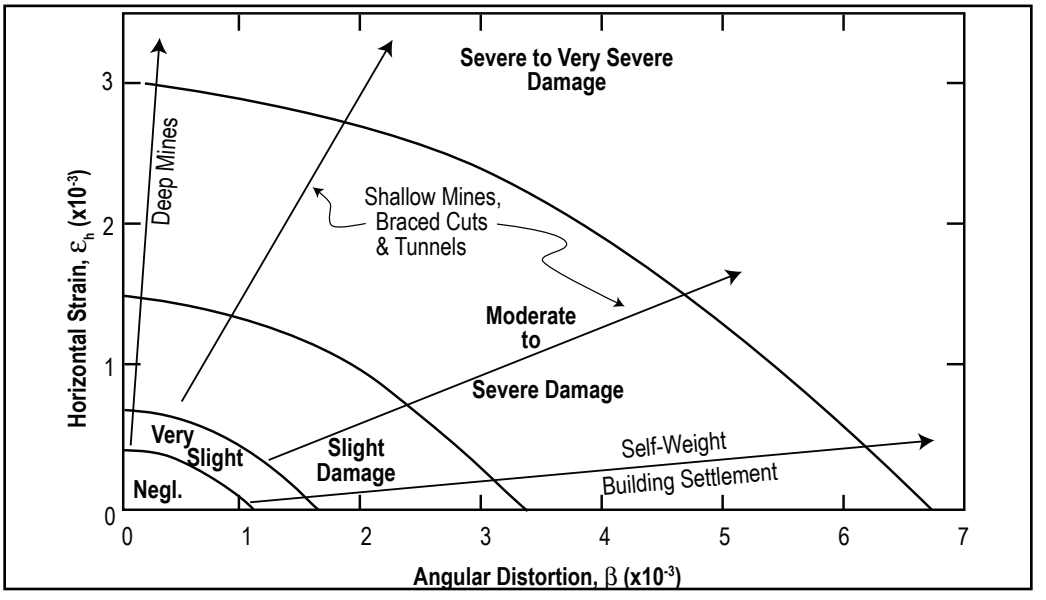

Stage 3 - Detailed Evaluation

Detailed evaluation is undertaken for buildings classified in Category 3 and above (moderate or worse) during the Stage 2 assessment. In Stage 3, the potential risk induced by tunnel excavation, the consequences of the risk, and the type of building with respect to implementing observational risk management plans are considered.

The Stage 3 evaluation starts with a site visit for visual inspection and assessment of the building stiffness, existing conditions and potential consequences of the damage. Based on site inspections and review of existing information, the risk designation of the building can be revised considering the following:

- Geotechnical conditions, sub-surface profile and groundwater conditions
- Stiffness of the building (timber, masonry or framed buildings)
- Foundation type
- Details of heritage listing of the building and the age of the building
- Sensitivity and usage of the building such as office, private home, public building, sports facility etc.

Any building that is designated as “moderate” risk or worse after the site inspection will be subjected to a detailed study considering the relative stiffness of the building and the ground based on the method proposed by Addenbrook et al. (1997) and to an intensive monitoring programme.

For buildings on pile foundations, only detailed evaluations (Stage 3) are performed using numerical methods. At present, various numerical approaches are used to estimate pile group responses due to combinations of external loadings. The computer programs available for such analysis vary in the type of approach used and in the sophistication of their treatment of different aspects of group behaviour. Among the most widely used general programs are PGROUP (Banerjee and Driscoll, 1976), DEFPIG (Poulos, 1979, 1990), and PIGLET (Randolph, 1980). These programs are based on elastic continuum analysis, although DEFPIG can also be extended into the non-linear range by specifying limiting values of skin friction and lateral pressure along the pile.

Table 2.2: Damage Assessment Criteria for Stage 1 and Stage 2

Building damage classification After Burland (1995), and Mair et al (1996)					Approximately equivalent ground settlement and slopes (after Rankin 1988)	
1	2	3	4	5	6	7
Risk Cat	**Description of degree of damage**	**Description of typical and likely forms of repair for typical masonry buildings**	**Approx. crack width (mm)[1]**	**Max. tensile strain %[2]**	**Max. slope of ground[3]**	**Max. settl. of building (mm)[3]**
0	Negligible	Hairline cracks.		Less than 0.05		
1	Very slight	Fine cracks easily treated during normal redecoration. Perhaps isolated slight fracture in building. Cracks in exterior visible upon close inspection.	0.1 to 1.0	0.05 to 0.075	Less than 1:500	Less than 10
2	Slight	Cracks easily filled. Redecoration probably required. Several slight fractures inside building. Exterior cracks visible; some repainting may be required for weather-tightness. Doors and windows may stick slightly.	1 to 5	0.075 to 0.15	1:500 to 1:200	10 to 50
3	Moderate	Cracks may require cutting out and patching. Recurrent cracks can be masked by suitable linings. Brick pointing and possible replacement of a small amount of exterior brickwork may be required. Doors and windows sticking. Utility services may be interrupted. Weather tightness often impaired.	5 to 15 or a number if cracks greater than 3	0.15 to 0.3	1:200 to 1:50	50 to 75
4	Severe	Extensive repair involving removal and replacement of walls especially over door and windows required. Window and door frames distorted. Floor slopes noticeably. Walls lean or bulge noticeably. Some loss of bearing in beams. Utility services disrupted.	15 to 25 but also depends on number of cracks	Greater than 0.3	1:200 to 1:50	Greater than 75
5	Very severe	Major repair required involving partial or complete reconstruction. Beams lose bearing, walls lean badly and required shoring. Windows broken by distortion. Danger of instability.	Usually greater than 25 but depends on number of cracks		Greater than 1:50	Greater than 75

Notes:

1) Crack width is only one factor of assessing the category of damage and should not be used on its own as a direct measurement of it.
2) Local deviation of slope from the horizontal or vertical of more than 1/100 will normally be clearly visible. Overall, deviations in excess of 1/150 are undesirable.
3) Columns 6 and 7 also indicate "green field" settlements and settlement trough slopes and are based on the methods of Rankin (1987). Category of damage using the Rankin method are approximately equivalent to those proposed by Burland, although in some cases there may be significant differences.

Considering the existing methods of building damage assessment for shallow foundations, a global procedure that includes both shallow and deep pile foundations is presented in this monograph (Chapter 7).

3.0 ESTIMATION OF TUNNELLING-INDUCED GROUND LOSS

3.0 ESTIMATION OF TUNNELLING-INDUCED GROUND LOSS

3.1 INTRODUCTION

The accurate assessment of tunnelling-induced effects on adjacent structures depends on the accuracy of the predicted tunnelling-induced ground loss values and ground deformation. At present, ground loss values are assumed, based on past experience and the outcomes of previous tunnelling projects under similar conditions. In reality, ground loss values are likely to vary depending on tunnelling methods, tunnel configuration, soil types and other factors. The fact that such variation in empirical observations exists suggests the need for a more logical approach to estimating ground loss due to tunnelling.

A new method for assessing the various ground loss components, such as face loss, shield void loss and tail void loss, was developed as part of this WBP fellowship research. This work took into consideration the various aspects of ground loss mechanisms covered in the published works by other researchers, as discussed in Chapter 2.

This new method can be used prior to construction to predict ground loss parameters based on known TBM geometry, geotechnical conditions and the tunnel configuration.[1] The total ground loss prediction has been verified for case histories (Loganathan et al, 2005; Loganathan et al, 2000 and Loganathan and Flanagan, 2001). Prediction of various components of ground loss presented in this monograph has not yet been verified; however, such verification is planned for the future. It will be based on either field measurements or/and three dimensional numerical modelling, and after it is completed, this monograph will be updated.

3.2 DEFINITION OF GROUND LOSS

Ground loss is defined as the volume of material (through face or radial encroachment over and around or behind the shield) that has been excavated in excess of the theoretical design volume of excavation. In this study, ground loss estimation assumes uniform radial ground movement (average ground loss) and is denoted as V_L (%). In practice, the soil movement around a tunnel is non-uniform due to the oval-shaped gap at the crown caused by the gravity effect. Figure 3.1 shows the uniform and "actual" shapes of the gap around the tunnel.

Figure 3.1 Circular and Oval Ground Deformation Patterns Around a Tunnel

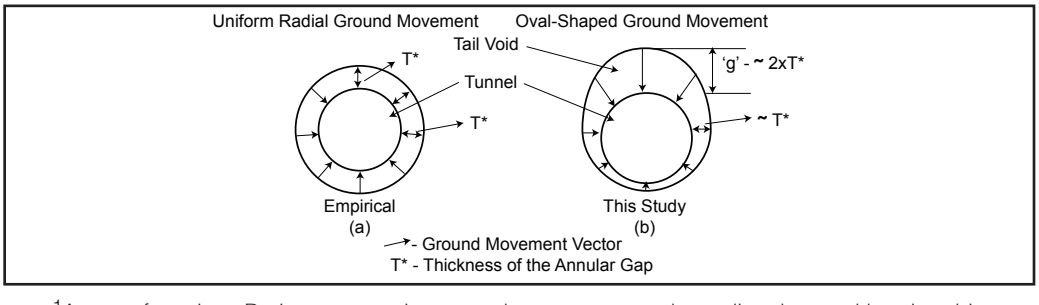

[1]A note of caution: During construction, even the most accurately predicted ground loss is subject to the human factor, the TBM operator.

The equivalent average undrained ground loss (V_L), which is also referred to as ε_o in this monograph, is defined with respect to the gap parameter as follows:

$$\varepsilon_o = V_L = \frac{\pi(R + \frac{g}{2})^2 - \pi R^2}{\pi R^2} \; x \; 100\% \; = \frac{g}{R} x 100\% \qquad (3.1)$$

Where:

R = radius of the tunnel

g = estimated gap at the crown.

The second order gap (g^2) has been neglected because it has only a negligible effect on the ground loss value; i.e., the second order ground loss component for 1 percent ground loss is about 0.01 percent (only 1 percent error in ground loss estimation).

The ground loss components at various stages of the tunnel excavation are estimated to help designers understand the ground movement patterns and the induced effects on adjacent structures. With this information, they will be better able to determine appropriate methods for controlling ground loss and to recommend the appropriate face pressure and TBM configuration for minimising the physical gap.

3.3 THEORETICAL BACKGROUND OF GAP PARAMETERS

The estimated ground loss deformation patterns are greatly influenced by the ground loss parameter. As discussed and illustrated in Section 2.1.1, the ground loss occurs in three stages, each represented by the following variables.

- Face Loss, V_f
- Shield Loss, V_s
- Tail Loss, V_t.

3.3.1 Face Loss V_f

The volume of soil that intrudes into the tunnel face owing to pressure release at the face will be excavated eventually. Thus, there is a volume of lost ground equal to the amount of over-excavated material at the face called the face loss. Lee et al. (1992) presented a method to estimate the radial equivalent gap parameter, g_f, (radial ground movement towards the lining) of the longitudinal ground movement towards the tunnel face.

Based on Equation 3.1, the face loss, V_f can be specified as:

$$V_f = \frac{g_f}{R} x 100\% \qquad (3.2)$$

Where:

g_f = equivalent gap at the crown of the face loss

R = tunnel radius.

Lee et al. (1992) established a method to determine the g_f value based on numerical modelling. The relationship they derived is:

$$g_f = \frac{k}{2} \frac{\Omega R P_0}{E} \qquad (3.3)$$

Where:

k = the coefficient representing the resistance between the intruding soil and the TBM chamber skin

Ω = dimensionless axial displacement ahead of the tunnel face

R = tunnel radius

P_0 = total stress removal at the tunnel face

E = elastic modulus at the tunnel spring line (typically the undrained Young's modulus in extension).

The k variable. Peck (1969) indicated that the frictional forces between the skin of the shield and the surrounding soil, which are caused by the shoving action of the shield, can develop longitudinal tensile stresses that tend to cause failure and plastic flow into the tunnel face and the annular void between the tail skin. Lee et al. (1992) performed a series of 3D elastoplastic finite element method (FEM) modelling to establish the friction factor "k." Their results are shown in Equation 3.3a.

$$k = \begin{cases} 0.7 & \text{stiff ground (qu >100 kPa or N>10)} \\ 0.9 & \text{soft ground (qu = 25 to 100 kPa or N = 3 to10)} \\ 1.0 & \text{very soft ground (qu <25 or N<3).} \end{cases} \quad (3.3a)$$

Where:

N = SPT blow count for 300mm penetration

qu = unconfined compression strength = 2 x C_u (undrained shear strength).

Most tunnelling works are carried out through stiff material with qu being greater than 100 kPa (undrained shear strength greater than 50 kPa). Therefore, k=0.7 is an appropriate factor to assume for the ground loss estimation, as shown in Equation 3.3a.

The Ω variable. Determination of the factor Ω is based on extensive numerical analysis performed by Lee et al. (1992) for various stability ratios, N_R, as shown in Eq. 3.3b.

$$\Omega = \begin{cases} 1.12 \text{ for } N_R<3 \\ 0.63N_R-0.77 \text{ for } 3<N_R<5 \\ 1.07N_R-2.55 \text{ for } N_R>5. \end{cases} \quad (3.3b)$$

Where:

$$N_R = \frac{\gamma H - P_i}{C_u}$$

P_i = TBM face pressure

H = tunnel depth to spring line

C_u = undrained shear strength at the spring line.

The P_0 variable. The total stress removal at the tunnel face due to the excavation can be estimated using Equation 3.3c.

$$P_0 = k_0 P_v + P_w - P_i \quad (3.3c)$$

Where:

k_0 = lateral earth pressure coefficient

P'_v = effective ground pressure at the spring line

P_w = water pressure
P_i = TBM face pressure.

In practice, few methods are available to estimate TBM face pressure. The two used commonly are:

- **Sliding model** (Sternath & Bauman, 1997)

  This method calculates the TBM face pressure by analysing a prismatic soil body acting above the crown of the tunnel face with an underlying wedge acting in front of the TBM cutterhead

- **Terzarghi's Silo Theory** (Terzarghi, 1959)

  This method estimates the effective soil column that imposes a load on the TBM as a result of soil arching effects.

In this study, Terzarghi's Silo Theory has been used to estimate TBM face pressure as shown in Appendix A1.

The actual mobilised TBM face pressure may be slightly different from theoretical predictions. The applied TBM face pressure at the site depends on two types of factors:

- **Static:** Soil type, soil stiffness/strength, tunnel configuration and groundwater table
- **Dynamic:** Tunnel advance rate, mode of tunnelling (undrained or drained), and the stand-up time of the soil.

In practice, only static factors are considered in theoretical earth pressure estimations (sliding model and Terzarghi's Silo Theory). Dynamic factors determine how much theoretical earth pressure is mobilised during tunnel excavation. Refer to Loganathan et al. (2005) for further information on dynamic factors.

3.3.2 Shield Loss V_s

The TBM shield consists of the cutter head and the shield, with cutter heads being designed slightly larger than the shield to minimise friction between the TBM and the surrounding ground. Beads are provided at the periphery of the cutter head for overcutting. In modern days, TBM shields are tapered, having a slightly smaller diameter at the tail, and some TBMs have both a cutter bead and tapered shield. In this study, the shield loss concept was derived for TBMs with both features, as illustrated in Figure 3.2 (not to scale).

Figure 3.2 Schematic of TBM Configuration with Cutter Bead and Tapered Shield

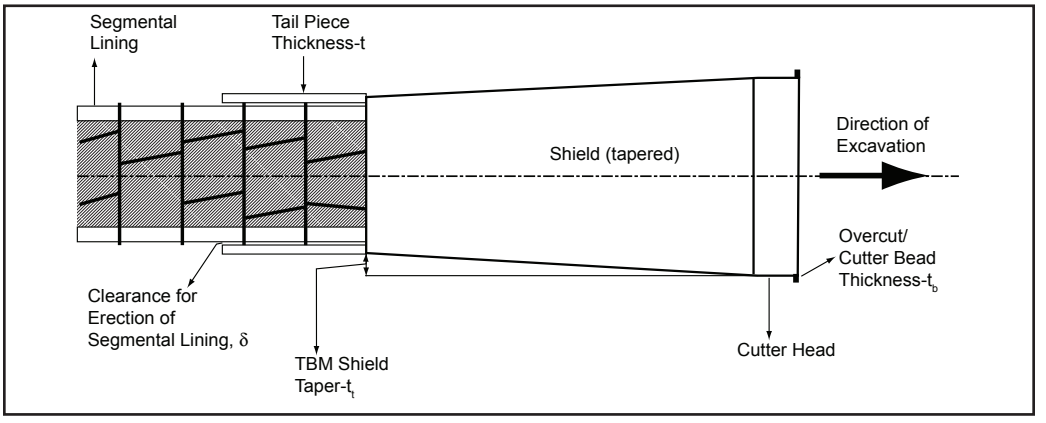

The thickness of the cutter bead is shown as t_b and the shield taper is shown as t_t. These values are typically in the range of 5 to 15 mm (0.2 to 0.6 inch) for t_b and 30 to 60 mm (1.2 to 2.4 inches) for t_t, although they can vary depending on project requirements.

Generally, the gap created by over-excavation due to the cutter bead and tapered shield is filled with slurry or groundwater when the TBM face is pressurised. In stable ground, the TBM is operated without face pressure. To assess the worst case condition, however, it was assumed that the shield gap is unsupported until the lining is assembled and the tail void grouting is done through the tail skin.

A detailed study carried out by Bezuijen and Bakker (2007) indicated that the stress around the tunnel shield changes depends on the radial movement of the soil into the gap, as shown in Equation 3.4.

$$\Delta_\sigma = 2 \frac{\Delta_r}{r} G \tag{3.4}$$

Where:

G = shear modulus of the ground = E/[2(1+ν)]

r = radius

Δr = radial movement.

The change in stress is expressed as:

$$\Delta\sigma = \gamma H + P_w - P_i$$

Where P_i will be the applied TBM face pressure.

It is assumed that a fluid pressure equivalent to P_i will act on the shield gap due to the pressure connectivity between the mixing chamber and the shield gap via the gap into the mixing chamber. An appropriate P_i value should be used for the SPB slurry shield, the combination mix shield machine (operates in either SPB or EPB mode) and the standard EPB machine.

Figure 3.3 shows how the TBM face pressure is transferred to the shield gap.

Figure 3.3 TBM Face Pressure Acting on the Shield Gap for EPB TBM

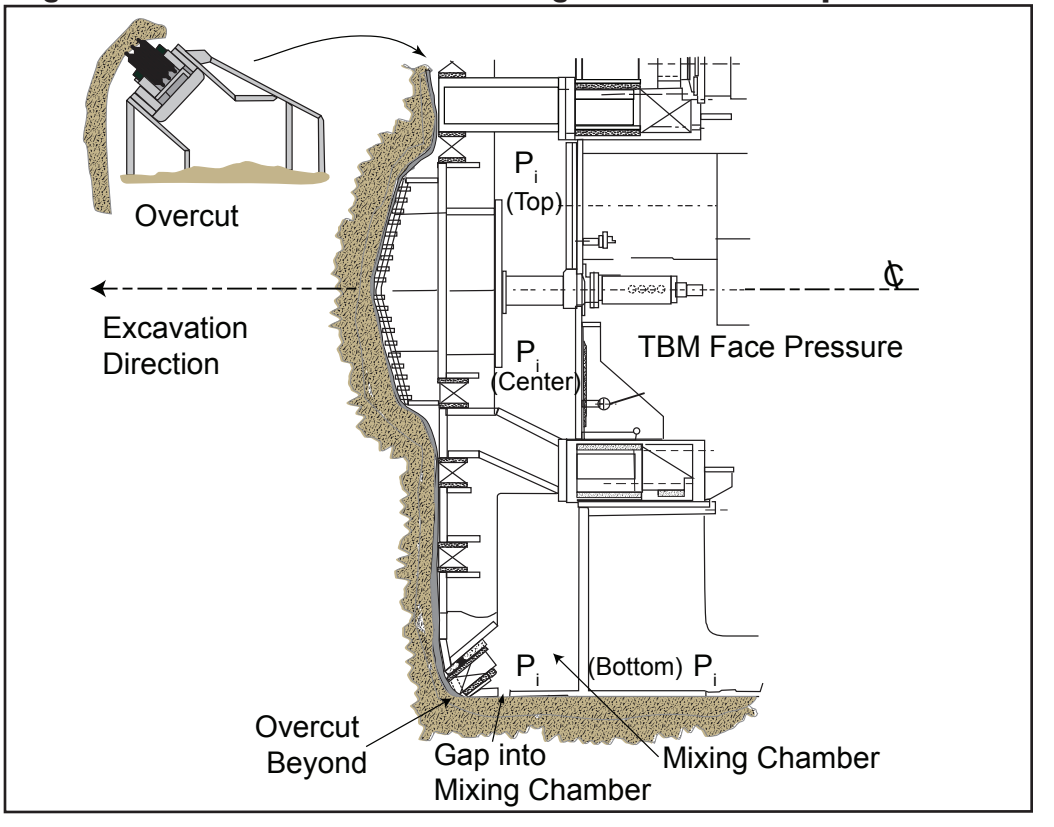

Based on Equation 3.4, the ground movement into the shield gap can be derived as follows:

$$U_i = R(1+\nu)\frac{(\gamma H + p_w - p_i)}{E} \tag{3.5}$$

Bezuijen and Bakker's (2007) detailed study also indicated that the tail void grout for slurry machines intrudes at least half way to the shield when the grout is pumped from the tail. It can be assumed, therefore, that shield loss will occur due to the radial ground movement to fill the gap created by the cutter bead and half of the shield taper.

Figure 3.4 shows the details of a typical EPB TBM that has a flap at the end of the tail shield to prevent grout flow forward along the shield gap. With EPB TBMs, the groundwater from the mixing chamber flows along the shield gap up to the end of the shield. To consider the worst case condition, however, it was assumed that the ground closure can happen for half the shield length, as for the slurry TBM.

The shield loss can be estimated using Equation 3.6.

$$V_s = \frac{g_s}{R} x\,100\% \tag{3.6}$$

If Ui > t_t+t_b, then $g_s = 0.5(t_t+t_b)$
If not, then $g_s = 0.5Ui$.

Figure 3.4 Ground Movement and Shield Gap Filling Mechanism for EPB TBM

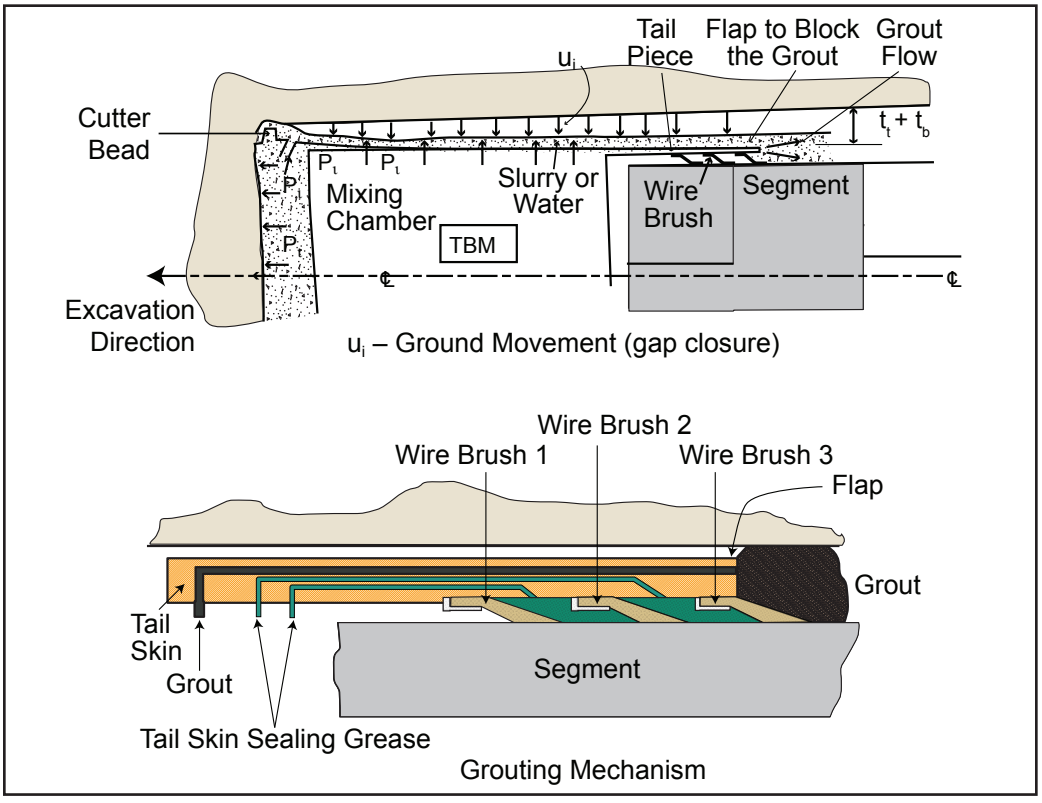

3.3.3 Tail Loss V_t

A physical gap is created in the tail due to the thickness of the tail skin, t, and the provision of clearance, δ, for the erection of the segmental lining. This gap will be grouted immediately after the erection of the lining to minimise the ground loss. In practice, however, there will be a time-dependent shrinkage in the grout-soil mix due to cement hydration. Lagerblad et al. (2010) reported that a volume change (shrinkage) of about 7 to 8 percent occurs for cement paste with a water/cement ratio of 0.4. Similarly, laboratory tests carried out on cement-soil mix by Ingles (1972) indicated about 7 to 10 percent reduction of thickness in the cement-soil mix samples. Therefore, if grouting is used to fill the physical gap, the value of the final tail loss gap is assumed to be about 7 to10 percent of the total tail gap. Considering the possible voids in the grout due to poor workmanship, it is assumed that about 10 percent shrinkage will occur in tunnelling practice.

The upper bound shrinkage percentage has been assumed to accommodate any possible volume reduction due to incomplete filling of the grout or pea gravel.

The equivalent gap formed due to the shrinkage of the grout is expressed as:

$$g_t = 0.1(t+\delta).$$

The ground loss component due to grout shrinkage at the tail can be estimated as:

$$V_s = \frac{g_s}{R} x\, 100\% \qquad (3.7)$$

The total ground loss during TBM excavation can be derived by adding face loss and the radial losses.

A worksheet developed to assess the ground loss values based on the methodology described in this chapter is provided in Appendix A1.

4.0 GROUND MOVEMENTS

4.0 GROUND MOVEMENTS

4.1 INTRODUCTION

Current “rules” to estimate ground settlement from tunnelling operations have been derived generally from empirical correlations between various parameters and the observed settlements in actual tunnels, as described previously (Sections 2.3.1 and 2.3.2). These rules account for only a few of the significant factors, and extrapolation to other cases is questionable. Hence, a method is needed to predict surface, subsurface and lateral ground movements so that designers can better assess the effects that tunnelling-induced ground movements will have on adjacent foundations and utilities.

A closed-form solution is presented in this chapter to predict these movements—surface, subsurface and lateral. This solution has been tested for its accuracy using case histories, centrifuge model test results, and FLAC3D numerical predictions. The formulas presented below are being used successfully by practicing engineers to predict tunnelling-induced ground movements.

Figure 4.1 shows the tunnelling-induced green field ground movements.

Figure 4.1 Tunnelling Induced Ground Movements - Green Field

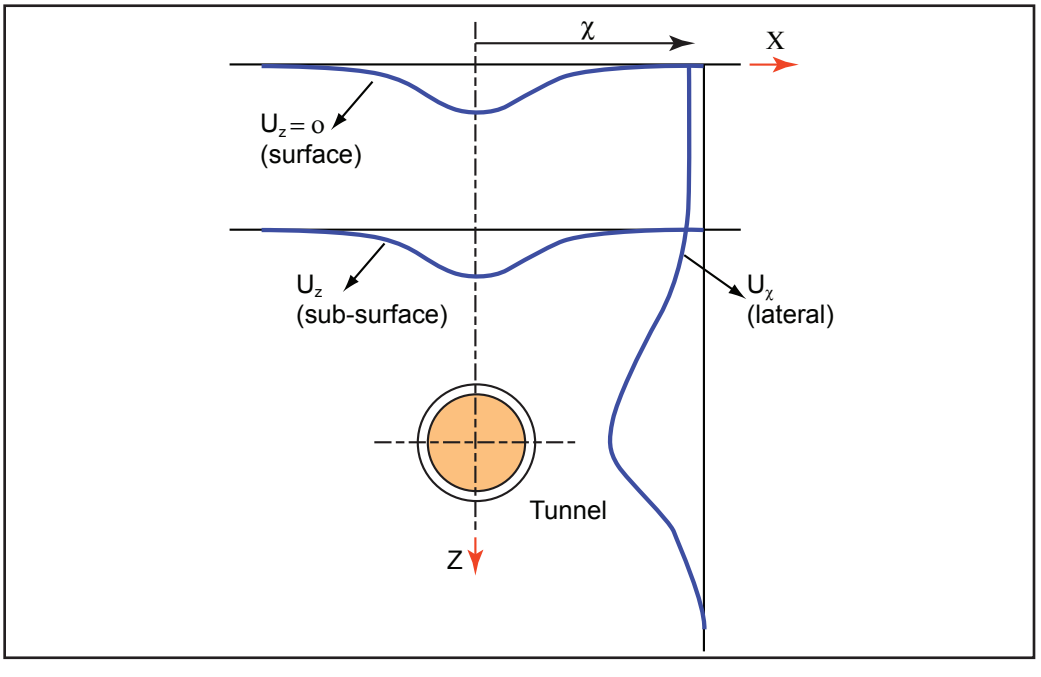

4.2 CLOSED-FORM SOLUTIONS FOR GROUND MOVEMENTS

Only a few attempts have been made to develop analytical methods (closed-form solutions) that incorporate all factors contributing to ground deformation:

- Sagaseta (1987) presented closed-form solutions for determining the strain field in initially isotropic and homogeneous incompressible ground due to near-surface ground loss caused by tunnel excavation.
- Verruijt and Booker (1996) presented an analytical solution for tunnels in a homogeneous elastic half space, using an approximate method suggested by Sagaseta (1987) for the case of ground loss.

Loganathan and Poulos (1998) modified the Veruijt and Booker solution by incorporating realistic ground loss boundary conditions that occur during tunnel excavation, as shown in Figure 4.2. An oval shaped gap was introduced at the tunnel crown because ground loss occurs at various stages of excavation (as discussed in Chapter 3).

Figure 4.2 Ground Deformation Patterns and Ground Loss Boundary Conditions

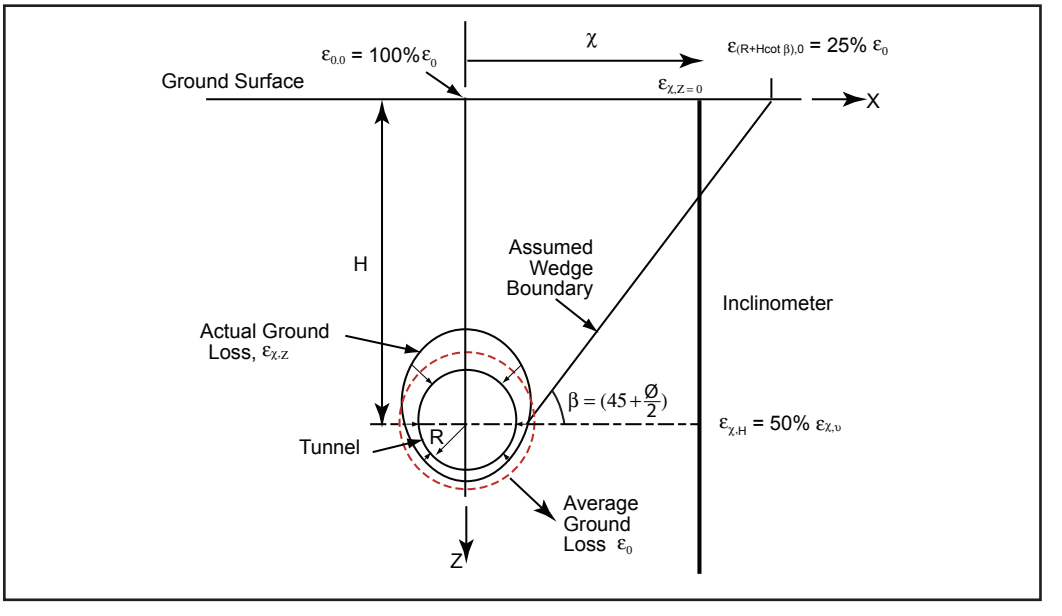

Based on the geometry of the oval-shaped gap formed around the tunnel, it is estimated that about 75 percent of vertical ground movement occurs within its upper annulus. Figure 4.2 shows the vertical ground movement influence zone where most of the soil displacement occurs. In sandy soil, the limit angle, β, is defined as (45° + ϕ/2), where ϕ= the angle of shearing resistance of the sand.

For soft to stiff clay, β may be assumed to be 45° based on the observations made by Cording and Hansmire (1975). That is, it is assumed that the ground movement occurs predomi-

nantly within the (45° + ϕ/2) wedge between the ground surface and the tunnel. It is estimated that the magnitude of horizontal movement at the tunnel spring line is approximately half of the vertical movement at the tunnel crown (which causes 75 percent of the ground movement into the upper annulus of the oval shaped gap around the tunnel).

The closed-form solutions presented by Loganathan and Poulos are shown in Equations 4.1, 4.2 and 4.3. These solutions predict the tunnelling-induced ground movements reasonably well, as will be demonstrated below.

Surface Settlement

$$U_{z=0} = \varepsilon_0 R^2 \cdot \frac{4H(1-\nu)}{H^2 + x^2} \cdot \exp\left\{-\frac{1.38x^2}{(H\cot\beta + R)^2}\right\} \tag{4.1}$$

Subsurface Settlement

$$U_z = \varepsilon_0 R^2 \left(-\frac{z-H}{x^2 + (z-H)^2} + (3-4\nu)\frac{z+H}{x^2 + (z+H)^2} - \frac{2z[x^2 - (z+H)^2]}{[x^2 + (z+H)^2]^2} \right) \cdot \exp\left\{-\left[\frac{1.38x^2}{(H\cot\beta + R)^2} + \frac{0.69z^2}{H^2}\right]\right\} \tag{4.2}$$

Lateral Deformation

$$U_x = -\varepsilon_0 R^2 x \left[\frac{1}{x^2 + (H-z)^2} + \frac{3-4\nu}{x^2 + (H+z)^2} - \frac{4z(z+H)}{(x^2 + (H+z)^2)^2} \right] \cdot \exp\left\{-\left[\frac{1.38x^2}{(H\cot\beta + R)^2} + \frac{0.69z^2}{H^2}\right]\right\} \tag{4.3}$$

Where:

$U_{z=0}$ = ground surface settlement
U_z = subsurface settlement
U_x= lateral soil movement
R = tunnel radius
z = depth below ground surface
H = depth of tunnel axis level
ν = Poisson's ratio of soil
ε_0 = average ground loss ratio (not a displacement)
x = lateral distance from tunnel centre line
β = Limit angle = 45 + ϕ/2.

These equations allow rapid estimation of ground deformation and require only an estimate of the Poisson's ratio (ν) of the soil. Poisson's ratio indirectly represents the characteristics of coefficient of lateral earth pressure (k_0) value of the ground. The k_0 values should be estimated from the relationship shown in Equation 4.4.

(Bowles, 1996) $$k_0 = \frac{\nu}{(1-\nu)} \tag{4.4}$$

Although Equations 4.1, 4.2 and 4.3 appear long, they are easy to work with using a simple worksheet (see Appendix A2). In addition, these closed-form solutions can be easily incorporated in numerical modelling programmes to impose ground movements external to the model soil-structure interaction problem to predict induced effects on adjacent piles.

The ground strength and stiffness and its elasto-plastic behaviour are considered in the estimation of the ground loss values. In most cases, tunnel excavation is carried out within the elastic strain range of the ground. The tunnelling-induced strain around the excavated face is controlled by applying the appropriate face pressure, installing the tunnel support system on time, or improving the ground around the tunnel.

The settlement trough width *i* is considered an important parameter for determining surface settlement using empirical methods. The relationship between the normalised parameters *i/R* and the *H/2R* parameters for the proposed analytical solution is shown in Equation 4.5:

$$\frac{i}{R} = \frac{1.15}{(\tan\beta)^{0.35}} \left(\frac{H}{2R}\right)^{\frac{0.9}{(\tan\beta)^{0.23}}} \quad (4.5)$$

A comparison of the maximum surface settlement and the surface settlement trough width *i* parameter derived by using various methods and observed values for reported case histories (Loganathan and Poulos, 1998) is shown in Table 4.1. The table shows that the predictions made using Equation 4.5 are in good agreement with empirical predictions and field observations. The case histories reported in Table 4.1 describe only the tunnels excavated through stiff to soft clayey soil.

Table 4.1 Comparison of Estimated and Observed Surface Settlement Trough Parameters

Case	Maximum surface settlement (mm)				Trough width, i (m)		
	Mair et al (1981)	Clough & Schmidt (1981)	Loganathan and Poulos (1998)	Observed	Mair et al (1981)	Clough& Schmidt (1981)	Loganathan and Poulos (1998)
Heathrow Express Trial Tunnel, UK	32.5	38.1	36.3	39	9.5	8.1	12.2
Thunder Bay Tunnel, Canada	49.0	65.6	40.0	50	5.35	4.0	6.4
Green Park Tunnel, UK	6.0	8.9	5.8	6	14.7	10.0	16.9
Barcelona Subway Network, Barcelona	29.0	30.3	23.2	24	5.0	4.8	6.8
Bangkok Sewer Tunnel, Thailand	14.8	21.8	11.8	12	9.2	6.3	10.6

The closed-form formulas (Equations 4.1, 4.2 and 4.3) have been tested and proven by various researchers and practicing engineers. For example, when Phienwej et al. (2007) used these equations to predict ground movements for the Bangkok Subway tunnel project, their results were very close to field measurements, as shown in Figure 4.3 (a) and (b).

Figure 4.3(a) Subsurface Settlement

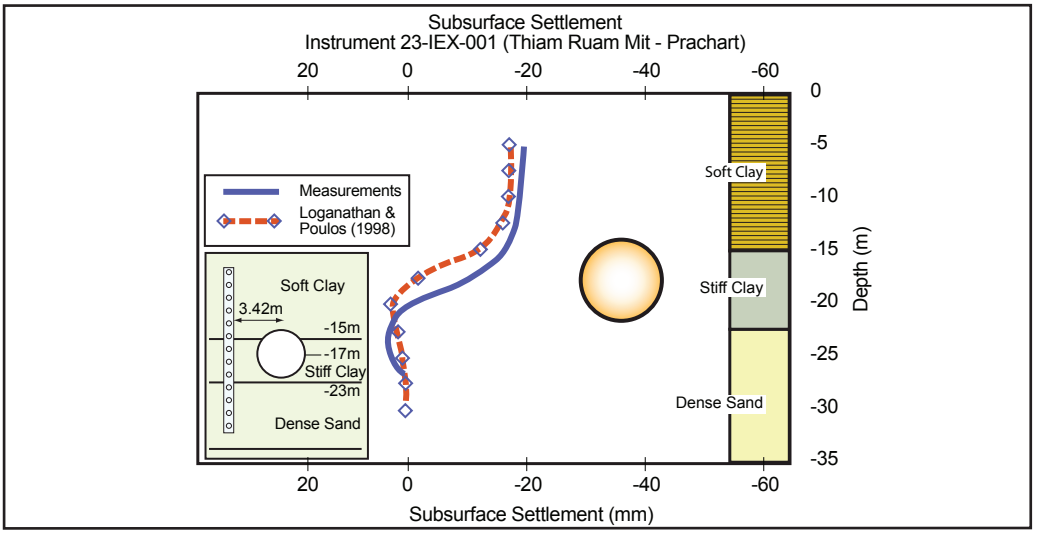

Figure 4.3(b) Lateral Deformation

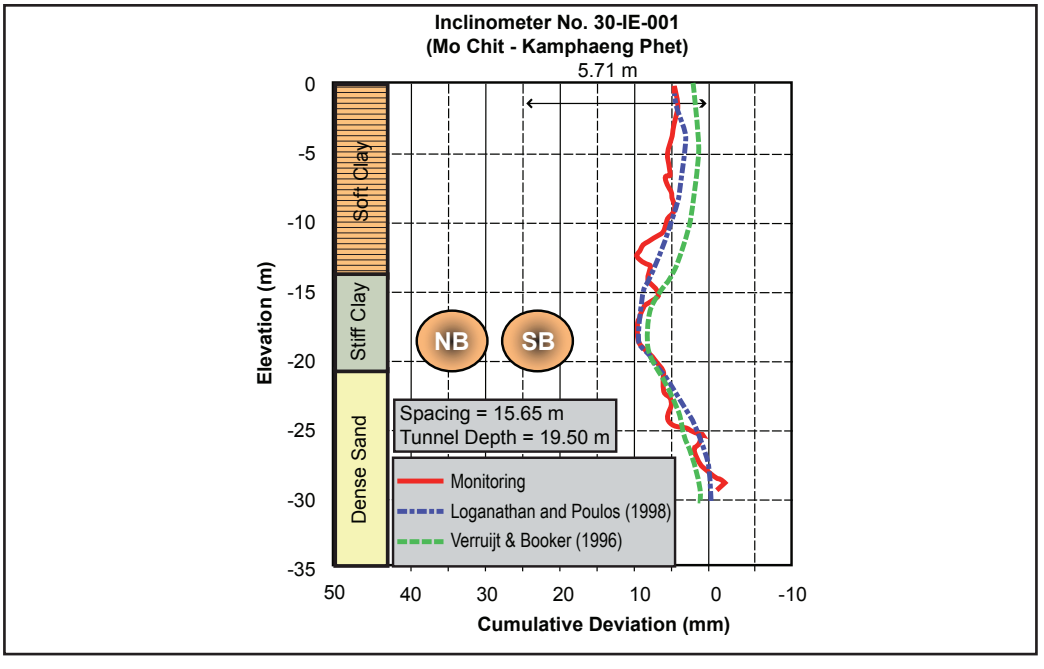

Figure 4.4 shows the comparison of the:

- Predictions made by using Loganathan and Poulos's method
- Measured values from centrifuge tests
- Predictions made by using other empirical methods for identical ground loss value.

Figure 4.4 Comparison of Centrifuge Test Results

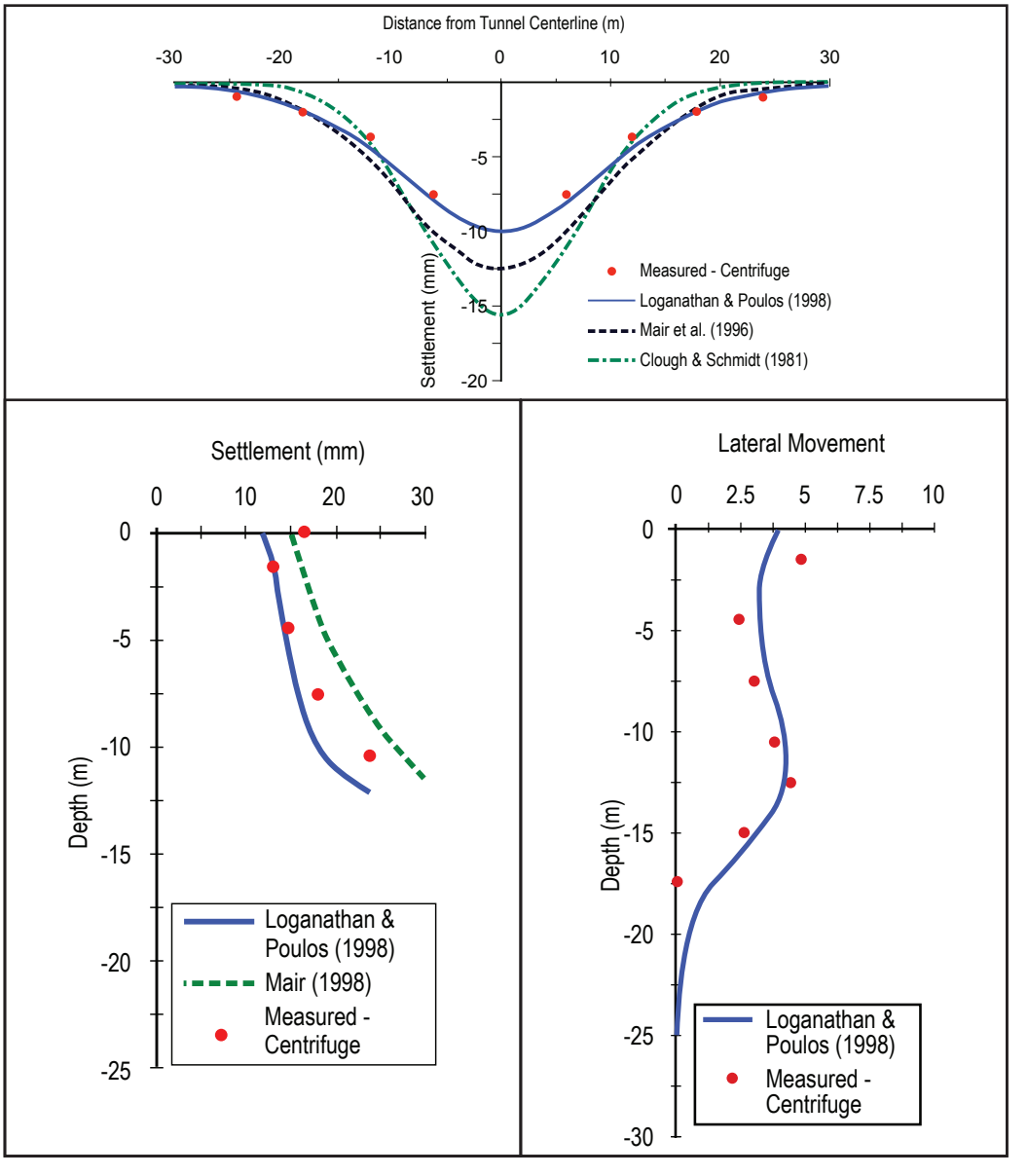

4.3 SUMMARY – GREEN FIELD GROUND MOVEMENTS

Closed-form solutions presented in this study predict the tunnel excavation induced ground movements reasonably well. Figure 4.5 shows a key diagram of tunnel dimensions.

Figure 4.5 Key Diagram - Tunnel Dimensions

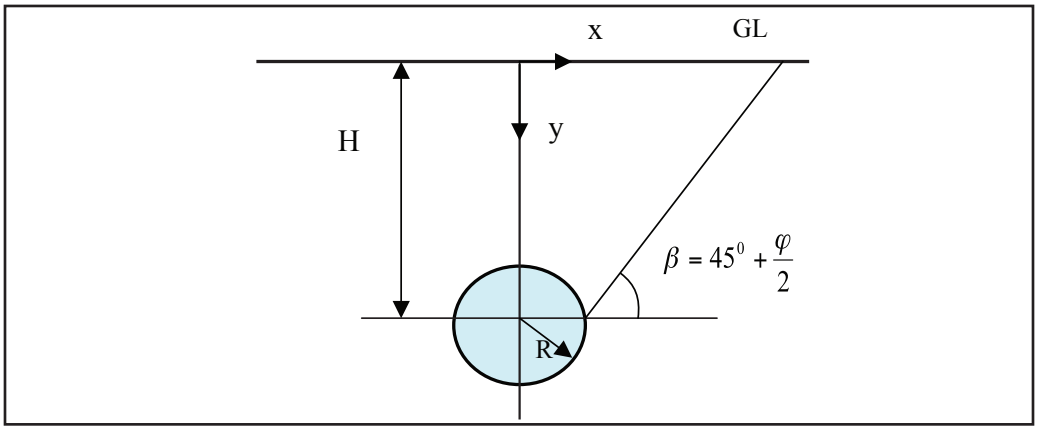

The summary of the closed-form solutions is as follows:

Surface Settlement

$$U_{z=0} = \varepsilon_0 R^2 . \frac{4H(1-\nu)}{H^2 + x^2} . \exp\left\{ - \frac{1.38x^2}{(H \cot\beta + R)^2} \right\}$$

Subsurface Settlement

$$U_z = \varepsilon_0 R^2 \left(- \frac{z-H}{x^2 + (z-H)^2} + (3-4\nu) \frac{z+H}{x^2 + (z+H)^2} - \frac{2z[x^2 - (z+H)^2]}{[x^2 + (z+H)^2]^2} \right)$$
$$\cdot \exp\left\{ - \left[\frac{1.38x^2}{(H \cot\beta + R)^2} + \frac{0.69z^2}{H^2} \right] \right\}$$

Lateral Deformation

$$U_x = -\varepsilon_0 R^2 x \left[\frac{1}{x^2 + (H-z)^2} + \frac{3-4\nu}{x^2 + (H+z)^2} - \frac{4z(z+H)}{(x^2 + (H+z)^2)^2} \right]$$
$$\cdot \exp\left\{ - \left[\frac{1.38x^2}{(H \cot\beta + R)^2} + \frac{0.69z^2}{H^2} \right] \right\}$$

Poisson's ratio values should be estimated lateral earth pressure coefficient (k_0) values using the following equation:

$$k_0 = \frac{\nu}{(1-\nu)}$$

5.0 TUNNELLING-INDUCED EFFECTS ON ADJACENT PILES

5.0 TUNNELLING-INDUCED EFFECTS ON ADJACENT PILES

5.1 INTRODUCTION

Relative movements of ground, as described in Chapter 4, induce bending moments and down-drag forces on piles. In current practice, the induced effects are estimated using numerical analysis tools, such as the finite element method, the finite difference method and the boundary element method These tools can provide a comprehensive picture of ground movements throughout the soil around the tunnel and the adjacent structures; however, they rely on appropriate ground models that include soil parameters. In addition, numerical modelling is time consuming and a high level of expertise is required to perform the analysis.

Such detail is rarely available at the early stages of the project, such as route selection and conceptual design. Yet, at these stages it has become equally important to be able to determine with reasonable accuracy what the tunnelling-induced effects on adjacent piles will be. The design charts presented in this chapter give us a tool to do just that. They are easy to use and provide reliable results.

These design charts have been validated using commercially available numerical modelling software and published centrifuge test model tests. It is recommended for detailed designs, however, that users perform project-specific validation with numerical modelling.

It should be noted that the design charts provided here may not predict the tunnelling-induced effects for extremely large ground loss values (typically greater than 2.5 percent) accurately because the ground-interaction mechanism changes under such conditions.

5.2 METHODOLOGY

Design charts presented in this monograph have been developed by performing series of numerical modellings.

To assess the tunnelling-induced ground movement interaction with the adjacent piles, it is important to have a numerical method to model the soil-structure interaction. After exploring many numerical methods to model soil-structure interaction, it was decided to use the boundary element programme, GEPAN (GEneral Pile ANalysis) developed by Xu and Poulos (1999) at the University of Sydney, Australia. GEPAN uses a three-dimensional boundary element method together with the virtual image technique for an elastic half-space to carry out analyses of multiple single piles and pile groups. It incorporates the effects of external soil movements due to tunnels, open cut excavations and embankment constructions. The closed-form solutions for predicting tunnelling-induced ground movements, as presented in Chapter 4, have been incorporated in the GEPAN program, which provides a complete ground movement analysis around the tunnel.

GEPAN considers non-linear behaviour of the soil-pile interaction by specifying limiting values of skin friction and lateral pressure along the pile. A typical pile-tunnel configuration used for the analysis is shown in Figure 5.1. The details of GEPAN are provided in Appendix B.

Figure 5.1 Single Pile Adjacent to Tunnelling - The Basic Problem Analysed

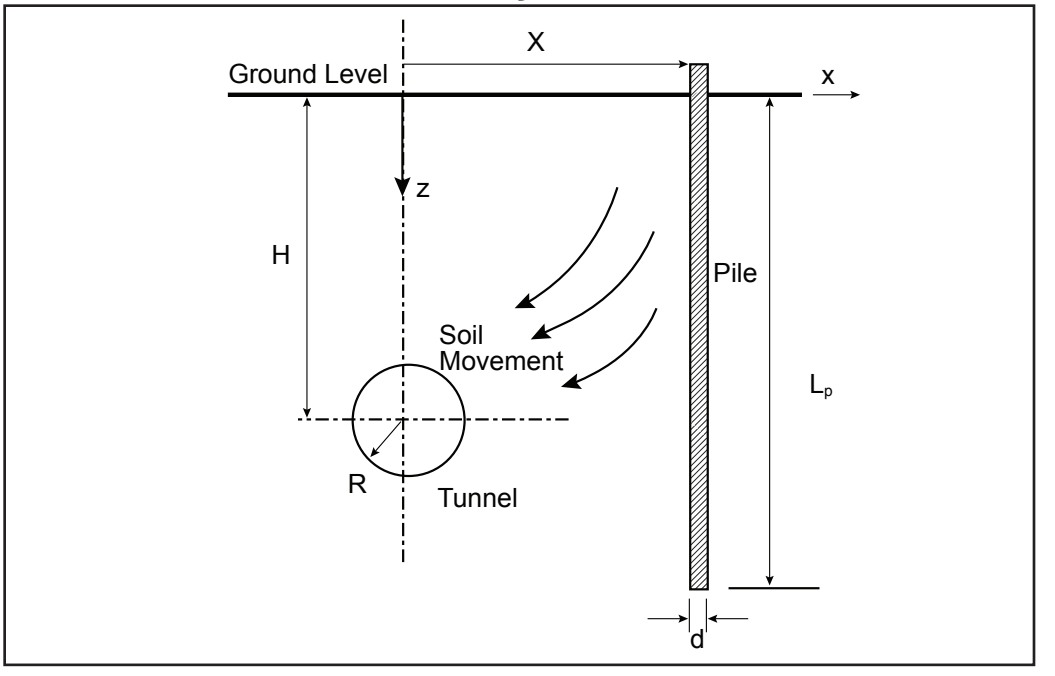

Short-pile and long-pile cases were analysed to assess the effect of pile length with respect to the tunnel depth. Each case indicates considerably different tunnelling-induced behaviour on the pile, as described below.

- **Short Pile.** The tunnel axis is located below the tip of the existing pile (Lp/H<1). Anlyses show significant pile settlement is induced, together with additional bending moments, lateral deformations and pile rotations. The pile head settlement exceeded the ground surface settlement for a pile located about half the tunnel depth away horizontally.
- **Long Pile.** The tunnel axis is located above the tip of the existing pile (Lp/H>1). Analyses show the induced bending moments are significant in this case. The pile head settlements are less than the ground settlement and, therefore, the pile head settlement trough may be considered in the assessment of potential building damage due to tunnelling-induced ground movements.

The difference between the short- and long-pile behaviours may be attributed to the pile fixity and the slenderness effects with respect to the non-uniform ground movements with the depth induced by the tunnel excavation. Short piles have a tendency to move with the soil movements, whereas long piles resist soil movement. Soil can fail around the long pile, however, due to the resistance; whereas generally, short piles will show elastic behaviour of the pile-soil interaction.

Based on the above observations, two sets of design charts were developed, one for long piles and one for short piles.

5.3 PARAMETRIC STUDY

Parametric studies were carried out to investigate the influences of various parameters on the pile responses. In these studies, the following parameters were varied:

- Tunnel radius, R
- Ground loss ratio, ε_F
- Undrained soil shear strength, c_u
- Depth of tunnel axis level, H
- Pile diameter, d
- Pile length, L_p.

The following observations were made:

1. **Increasing tunnel radius R and ground loss ratio, ε_F,** resulted in increases in the:
   - Maximum bending moment M_{max}
   - Lateral pile deflection ρ_{max}
   - Compressive axial force ($+P_{max}$)
   - Tensile axial force ($-P_{max}$)
   - Pile head settlement v_{max}.

   It is appropriate, therefore, to normalise the ground loss with the tunnel radius by introducing a factor "ground loss ratio, ε_F" where $\varepsilon_F = R^2\varepsilon_0$.
2. **Increasing the strength of the ground, c_u,** resulted in increases in:
   - M_{max}, ρ_{max}, $+P_{max}$, and $-P_{max}$ because of an increase of the lateral soil pressure and skin friction
   - Pile head settlement, v_{max}.
3. **Increasing the pile diameter,** d, tended to:
   - Increase induced bending moment on pile, M_{max}
   - Decrease lateral deflection of the pile, ρ_{max} (due to an increase of pile lateral rigidity)
   - Increase $+P_{max}$, and $-P_{max}$
   - Decrease v_{max}.
4. **The effects of the depth of tunnel axis level, H, and the pile length, L_p,** depend on the ratio L_p/H. The maximum pile responses could either increase or decrease with changing L_p/H depending on the other parameters.

5.4 DESIGN CHART CONCEPT

Based on the above parametric studies, it was found that within the range of parameters examined, the various maximum pile responses may be approximated as follows:

Lateral response:

$$M_{\max} = M_b \,.k_{cu}^{M} \;.k_d^{M} \,.k_{L_p/H}^{M} \tag{5.1}$$

$$\rho_{\max} = \rho_b \,.k_{cu}^{\rho} \;.k_d^{\rho} \,.k_{L_p/H}^{\rho} \tag{5.2}$$

Axial response:

$$+P_{\max} = +P_b \,.k_{cu}^{+P} \;.k_d^{+P} \,.k_{L_p/H}^{+P} \tag{5.3}$$

$$-P_{\max} = -P_b \,.k_{cu}^{-P} \;.k_d^{-P} \,.k_{L_p/H}^{-P} \tag{5.4}$$

$$v_{\max} = v_b \,.k_{cu}^{v} \;.k_d^{v} \,.k_{L_p/H}^{v} \tag{5.5}$$

Where:

M_{max} =	maximum induced bending moment
M_b =	maximum induced bending moment on the pile for base case
ρ_b =	maximum lateral deflection of the pile for base case
ρ_{max} =	maximum induced lateral deflection
$+P_{max}$ =	maximum induced compressive axial force
$+P_b$ =	maximum positive axial force induced on the pile for base case
$-P_b$ =	maximum negative axial force induced on the pile for base case
$-P_{max}$ =	maximum induced tensile axial force
v_{max} =	maximum induced pile head settlement
v_b =	pile head settlement derived for base case.

Based on the parametric study (by changing various factors), the following correction or influence factors were derived for the various parameters that affect the magnitude of the tunnelling-induced effects on piles:

- **Undrained shear strength.** Correction factors are k^{M}_{cu}, k^{ρ}_{cu}, k^{+P}_{cu}, k^{-P}_{cu}, and k^{v}_{cu}.
- **Pile diameter.** Correction factors are k^{M}_{d}, k^{ρ}_{d}, k^{+P}_{d}, k^{-P}_{d}, and k^{v}_{d}.
- **Ratio of pile length to tunnel axis level.** Correction factors are $k^{M}_{Lp/H}$, $k^{\rho}_{Lp/H}$, $k^{+p}{}_{Lp/H}$, $k^{-p}{}_{Lp/H}$, and $k^{v}_{Lp/H}$.

The base case, a single pile and a tunnel configuration as shown in Figure 5.1, was analysed to develop the design charts. Details of the base case are as follows:

- The tunnel is excavated through homogeneous clay with the undrained shear strength of 60 kPa.
- Tunnel outer diameter, OD, is 6 m (20 feet).
- Tunnel depth to centreline, H, is 20 m (66 feet).
- Pile diameter, d, is 0.5 m (1.6 feet)
- Pile length, L_p, is 15 m (50 feet) for the short pile case and L_p is 25 m (82 feet) for the long pile case.
- Young's modulus of the pile is 30 GPa.
- Ground loss is 1 percent.

5.5 DESIGN CHARTS FOR SHORT PILES

The maximum pile responses for the short-pile case were established for the base case. Based on the observations made from the parametric study, it was decided to adopt normalised ground loss factor $\varepsilon_F = R^2\varepsilon_0$ to produce the design charts for the base case. Correction factors will be assessed based on the differences between the parameters for a specific project and those for the base case.

- **Figure 5.2** shows the tunnelling-induced effects on short piles for the base case with the ground loss factor $\varepsilon_{FB} = R^2\varepsilon_0 = 3^2 \times 1\% = 0.09$.
- **Figure 5.3** shows the variation of correction factors for the undrained shear strength of the soil varying from 10 kPa to 300 kPa.
- **Figure 5.4** shows the variation of correction factors for the pile diameter varying from 0.25 m to 1.5 m (0.8 feet to 5 feet).
- **Figure 5.5** shows the variation of the correction factors for the pile length/tunnel depth ratio varying from 0.5 to 1.0. This ratio has the most influence on the response of the pile.

The steps involved in using the design charts are as follows:

STEP 1: Estimate the ground loss ratio, ε_F for a given problem using $\varepsilon_F = R^2\varepsilon_0$. Estimate the factor, $L_R = \varepsilon_{F/}\varepsilon_{FB}$, where $\varepsilon_{FB} = 0.09$.

STEP 2: Estimate the tunnelling-induced base behaviour from Figure 5.2 for the given horizontal distance, x, and multiply these values by the factor L_R.

STEP 3: Estimate undrained soil shear strength, pile diameter, and pile length/tunnel depth ratio correction factors from Figures 5.3, 5.4 and 5.5 and multiply the values estimated in Step 2 by these correction factors (via Equations 5.1 to 5.5).

Figure 5.2 Design Charts: Tunnelling-Induced Effects for Short Pile Base Case

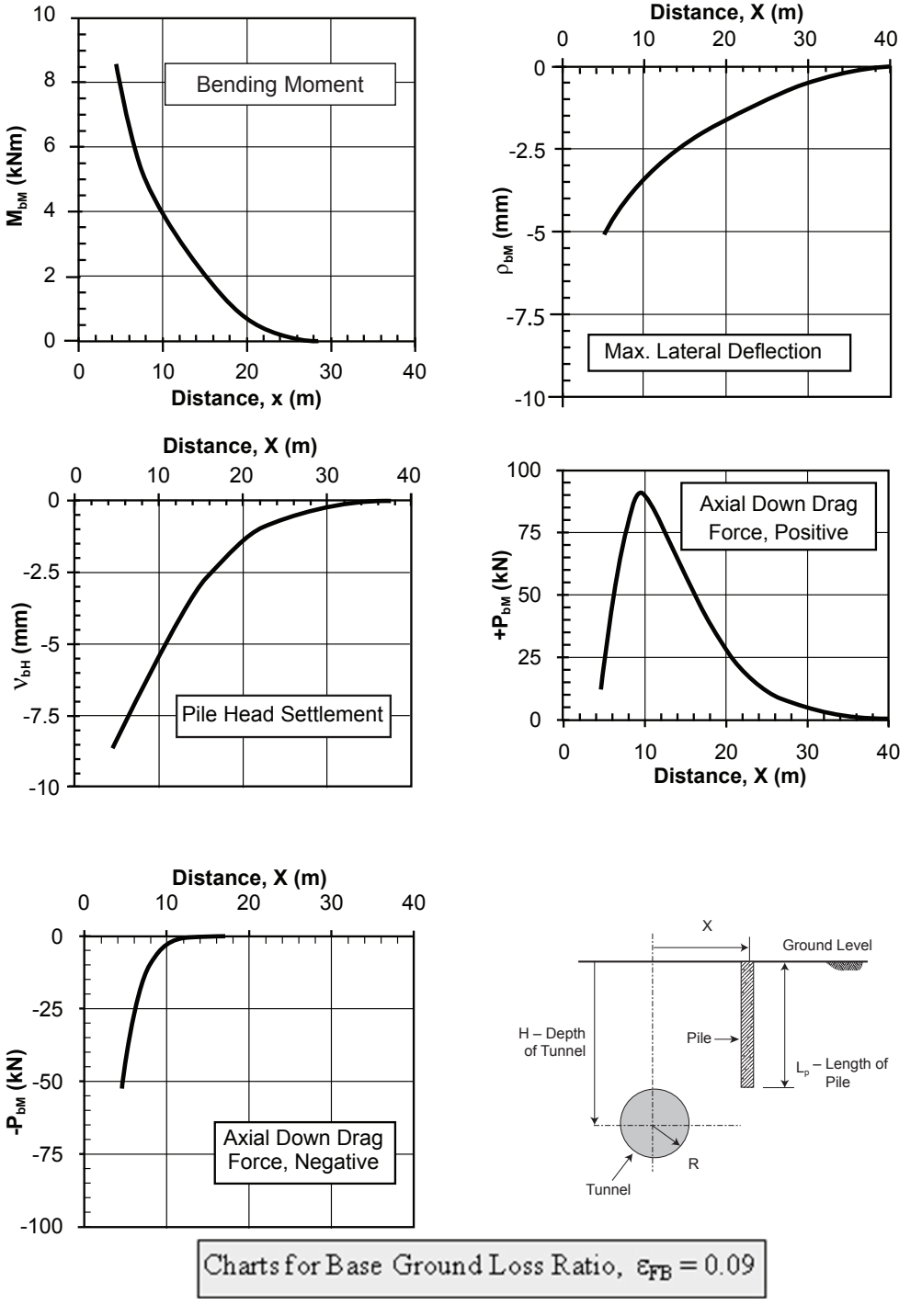

Charts for Base Ground Loss Ratio, $\varepsilon_{FB} = 0.09$

Figure 5.3 shows the correction factors for the undrained shear strength of the soil. It can be seen that all the tunnelling-induced behavior parameters are increasing with increasing soil strength except the pile settlement. Pile settlement reduces with increased soil strength. It is also noted that axial down drag force varies considerably with the undrained shear strength of the soil.

Figure 5.3 Design Charts: Correction Factors for Strength - Short Pile

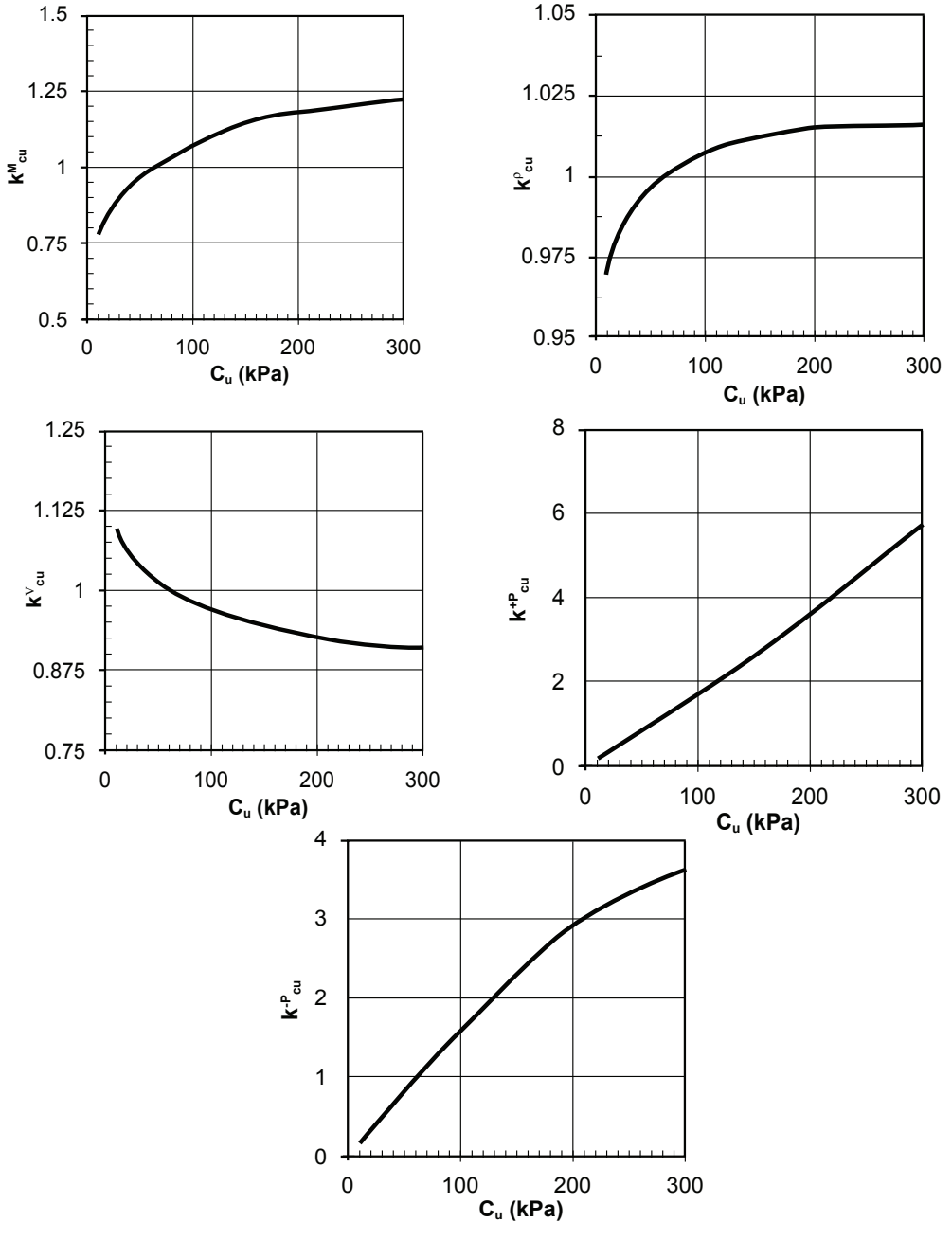

Figure 5.4 shows the correction factors for varying pile diameters. It can be seen that induced bending moments and axial down drag force are increasing with increasing pile diameter, but that the lateral deflection and settlement of the pile decrease with increasing pile diameter. Down drag forces also decrease as the distance from the tunnel increases.

Figure 5.4 Design Charts: Correction Factors for Pile Diameter - Short Pile

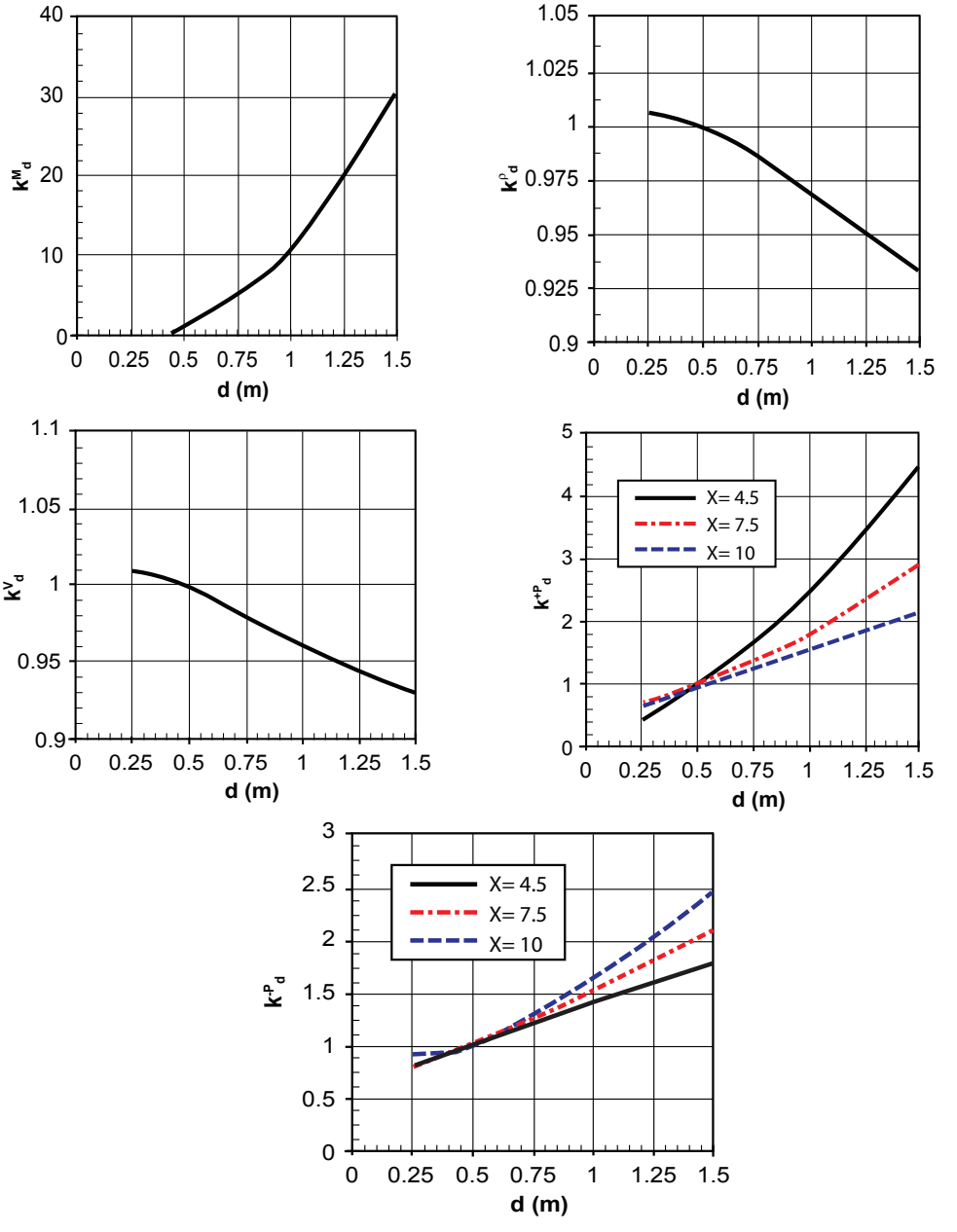

Figure 5.5 shows the correction factors for the pile length/tunnel depth ratios. It can be seen that induced bending moments, pile lateral movement and down drag forces increases with an increasing pile length/tunnel depth ratio. Pile head settlement can vary depending on the distance of the pile from the tunnel.

Figure 5.5 Design Charts: Correction Factors for Pile Length/Tunnel Depth Ratio - Short Pile

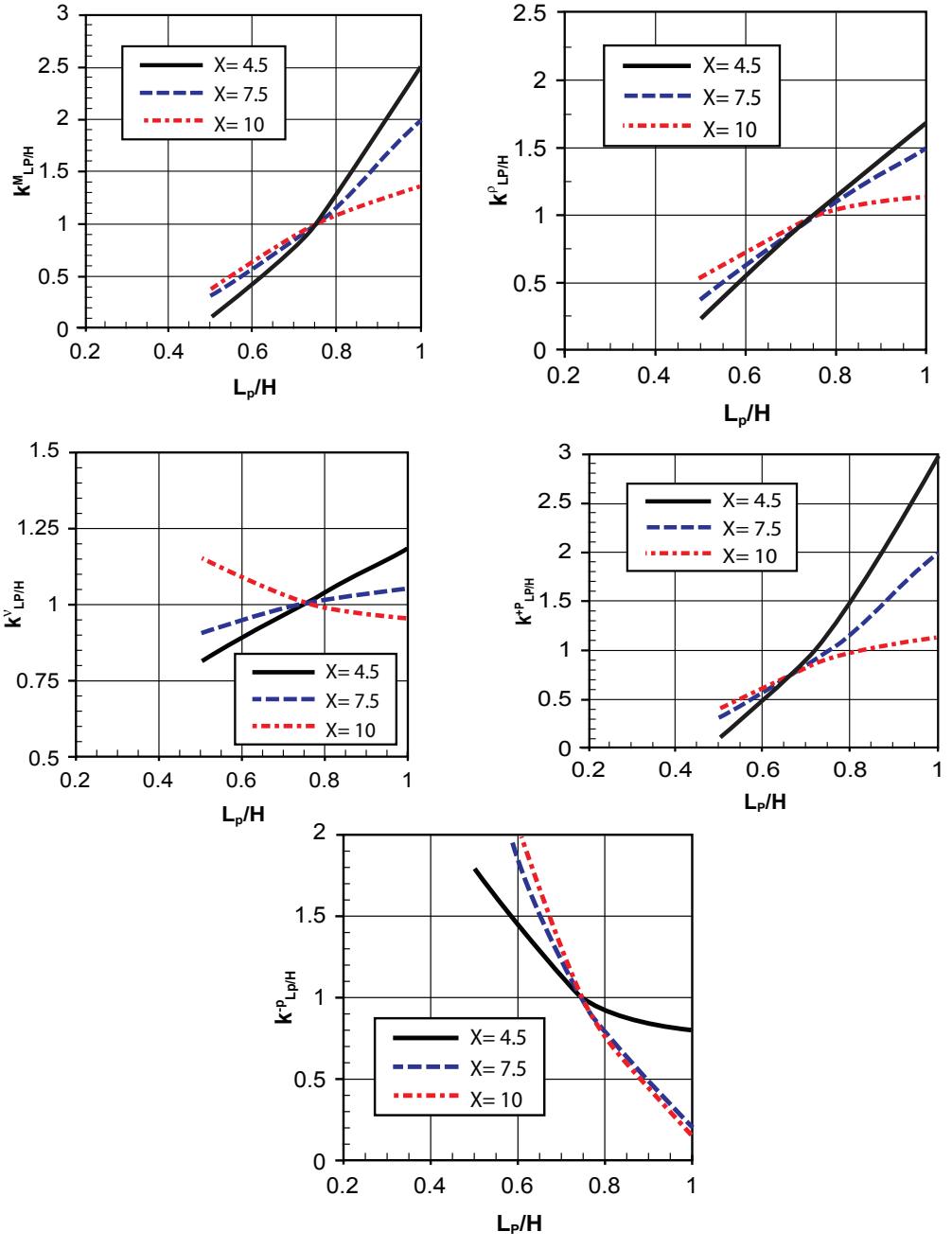

5.6 DESIGN CHARTS FOR LONG PILES

Design charts for long piles were developed as described for the short-pile case. Figure 5.6 shows the base values of the tunnelling-induced pile behaviour for a base value of ground loss factor $\varepsilon_{FB} = 0.09$.

Correction factors will be assessed based on the difference in parameters for a specific project from the base case.

- **Figure 5.6** shows the tunnelling-induced effects on long piles for the base case with the ground loss factor $\varepsilon_{FB} = R^2\varepsilon_0 = 3^2 \times 1\% = 0.09$.
- **Figure 5.7** shows the variation of correction factors for the undrained shear strength of the soil varying from 10 kPa to 300 kPa.
- **Figure 5.8** shows the variation of correction factors for the pile diameter varying from 0.25 m to 1.5 m (0.8 foot to 5 feet).
- **Figure 5.9** shows the variation of the correction factors for the pile length/tunnel depth ratio varying from 1.0 to 3.0. This ratio has the most influence on the response of the pile.

The steps involved in using the design charts are as follows:

STEP 1: Estimate the ground loss ratio, ε_F for a given problem using $\varepsilon_F = R^2\varepsilon_0$. Estimate the factor, $L_R = \varepsilon_F/\varepsilon_{FB}$, where $\varepsilon_{FB} = 0.09$.

STEP 2: Estimate the tunnelling-induced base behaviour from Figure 5.6 for the given horizontal distance, x, and multiply these values by the factor L_R.

STEP 3: Estimate undrained soil shear strength, pile diameter, and pile length/tunnel depth ratio correction factors from Figures 5.7, 5.8 and 5.9 and multiply the values estimated in Step 2 by these correction factors (via Equations 5.1 to 5.5).

Figure 5.6 Design Charts: Tunnelling-Induced Effects for Long Pile Base Case

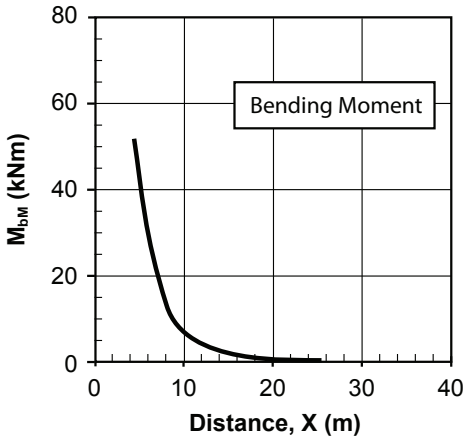

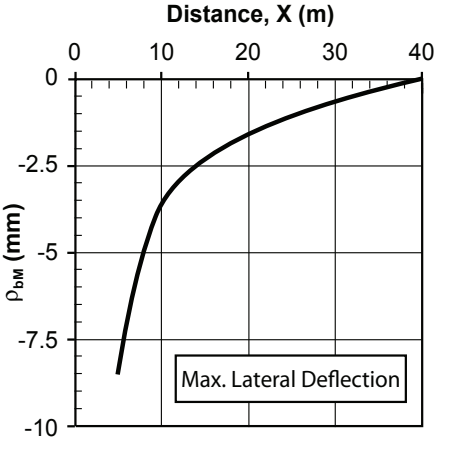

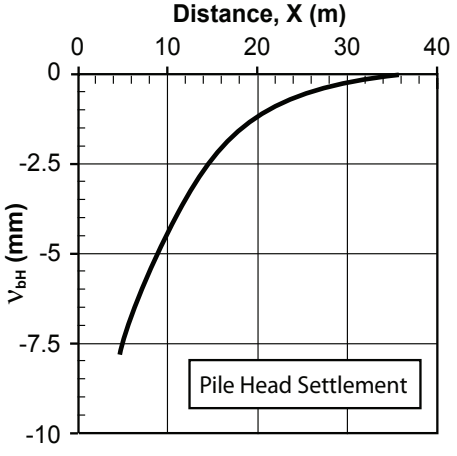

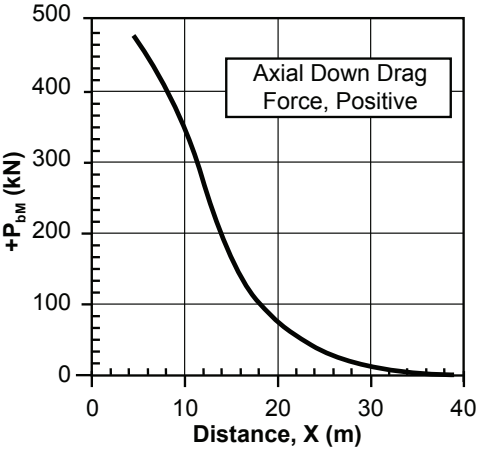

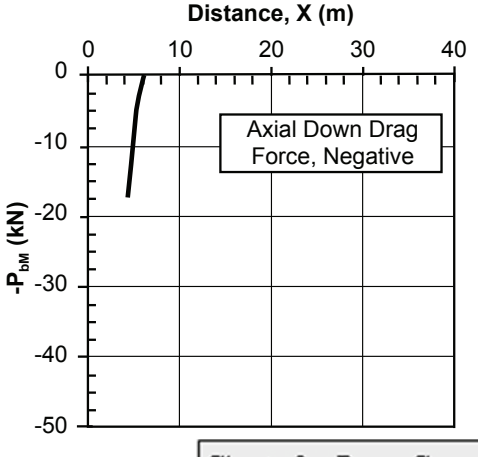

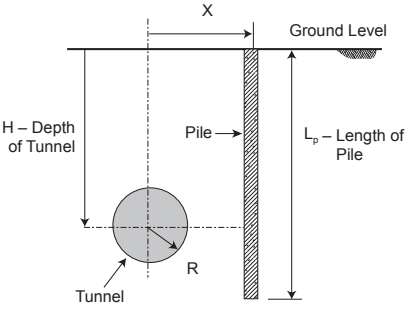

Charts for Base Ground Loss Ratio, $\varepsilon_{FB} = 0.09$

Figure 5.7 shows the correction factors for the undrained shear strength of the soil. It can be seen that all the tunnelling-induced behaviour parameters are increasing with increasing soil strength. Bending moment and axial down drag force vary considerably with the undrained shear strength of the soil.

Figure 5.7 Design Charts: Correction Factors for Strength - Long Pile

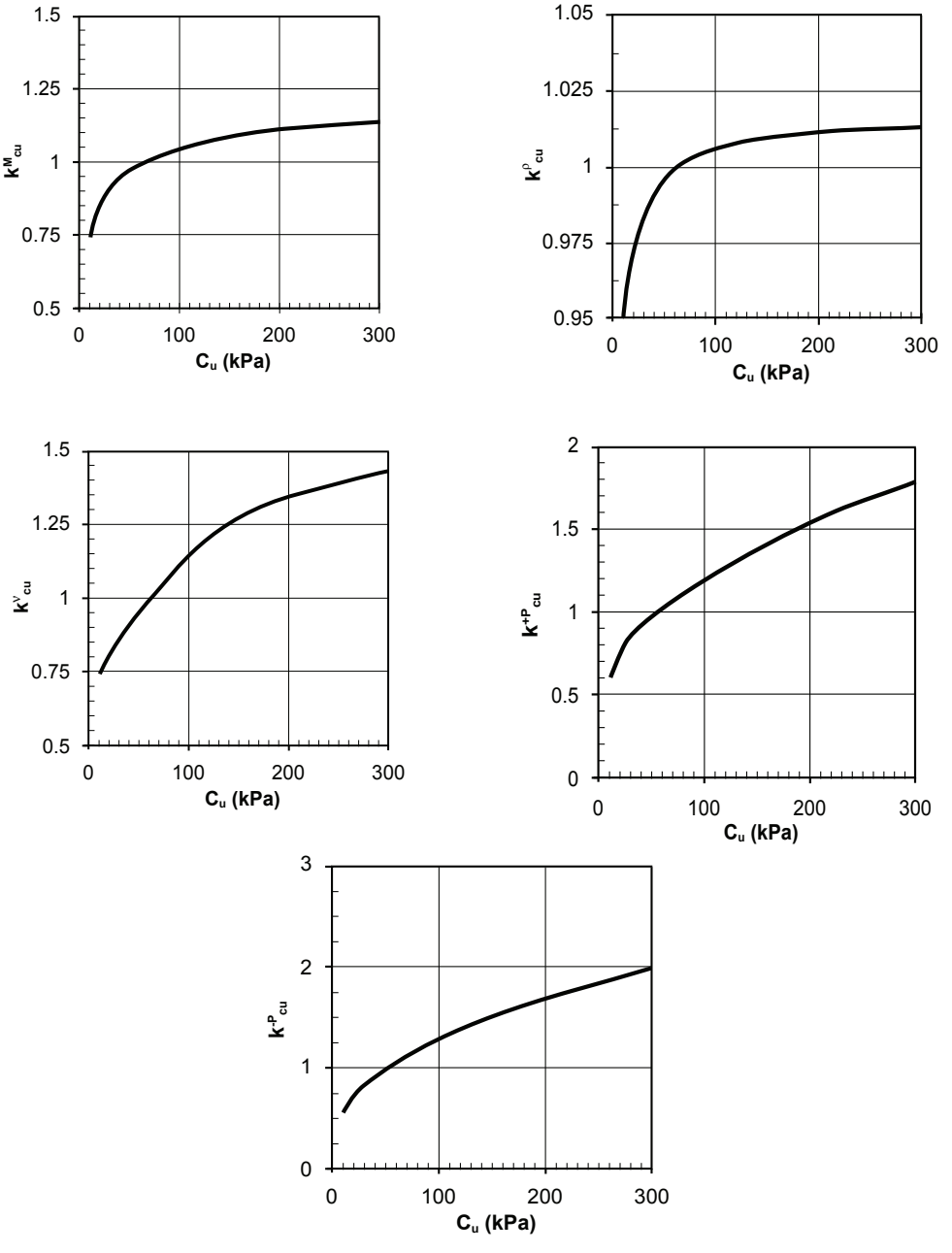

Figure 5.8 shows the correction factors for varying pile diameters. It can be observed that induced bending moments and axial down drag force are increasing with increasing pile diameter, but that the lateral deflection and settlement of the pile decrease with increasing pile diameter.

Figure 5.8 Design Charts: Correction Factors for Pile Diameter - Long Pile

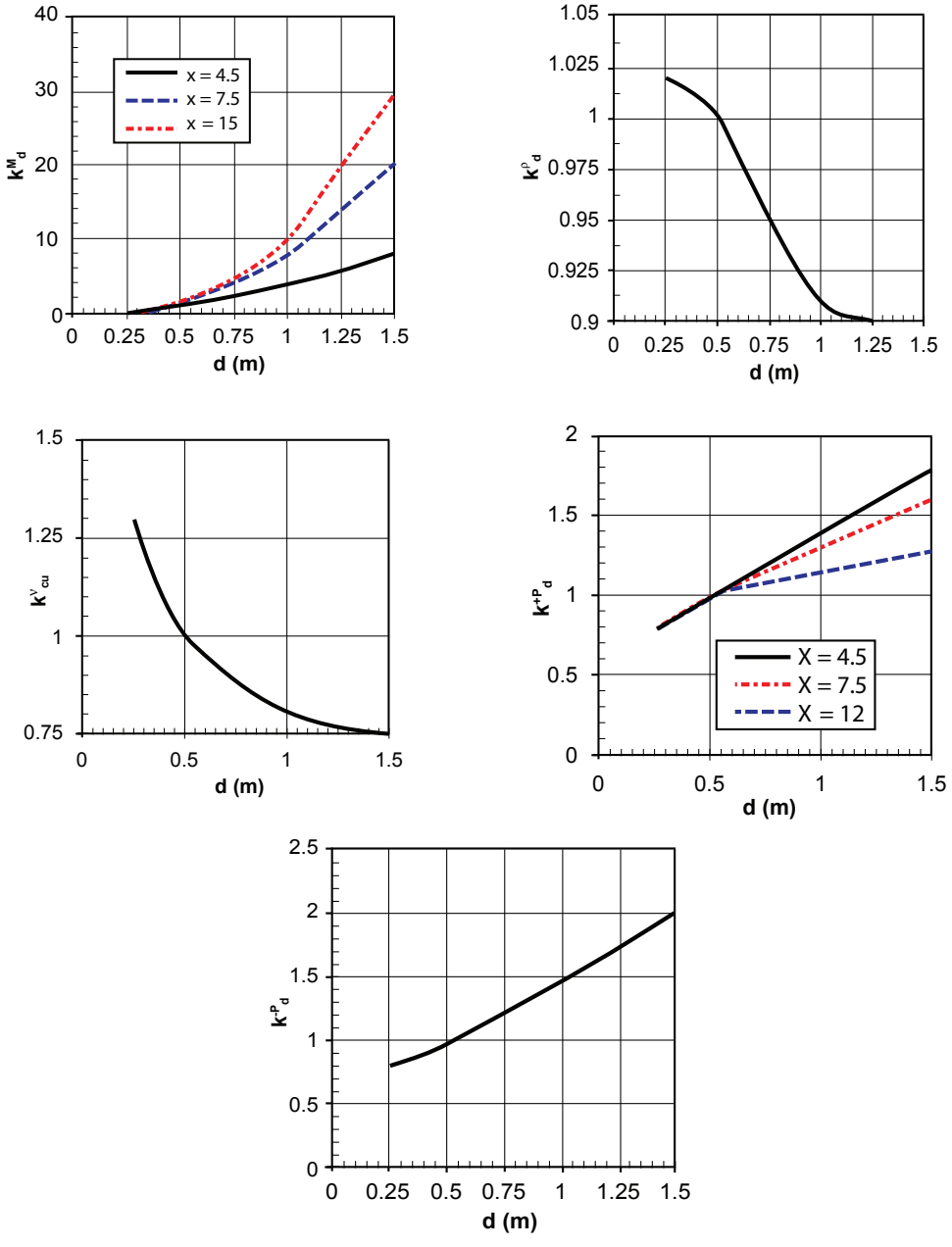

Figure 5.9 shows the correction factors for the pile length/tunnel depth ratios. It can be observed that induced bending moments and pile head settlements decrease with increasing pile length/tunnel depth ratio but the lateral deformation and the axial down drag forces increase.

Figure 5.9 Design Charts: Correction Factors for Pile Length/Tunnel Depth Ratio - Long Pile

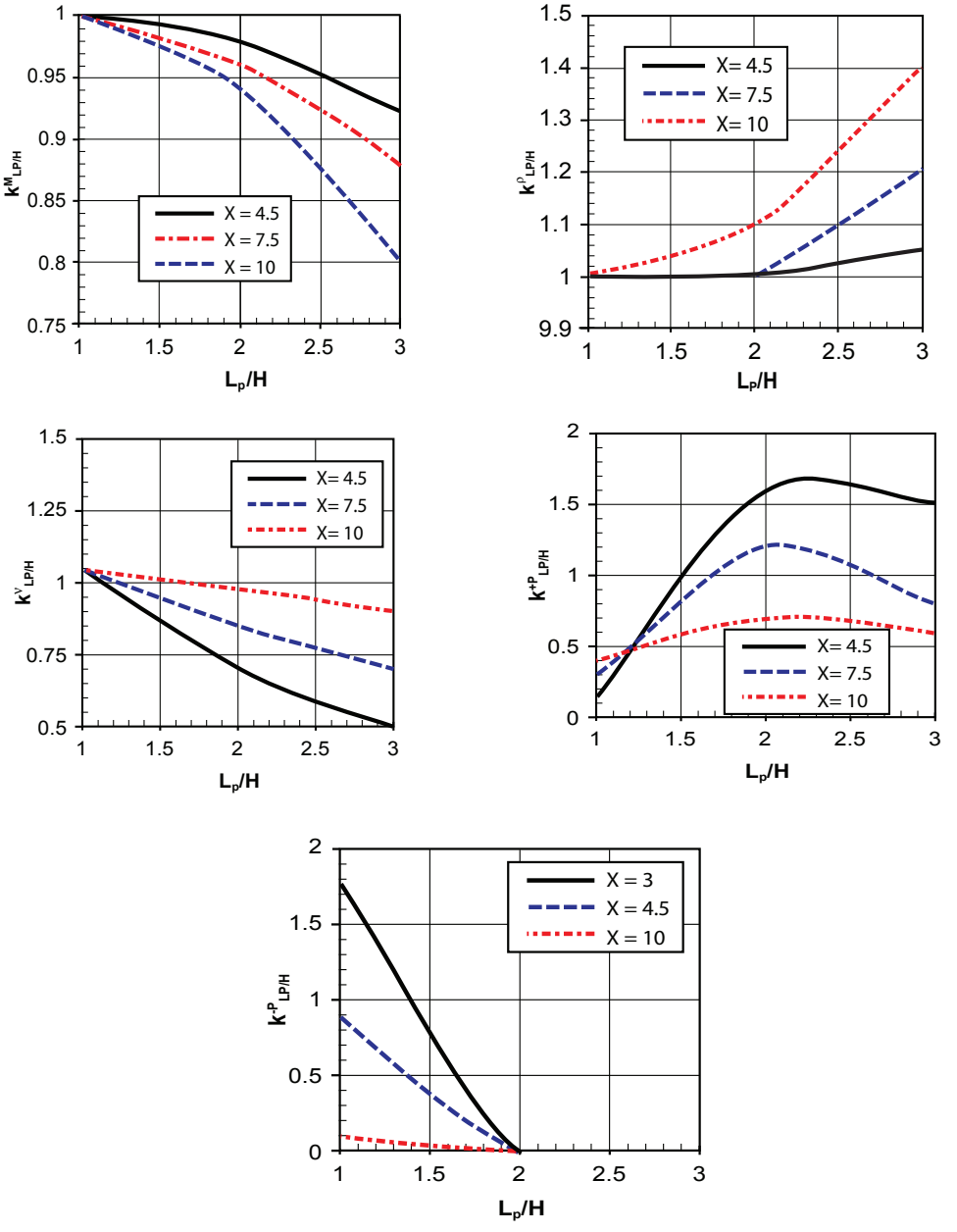

5.7 SUMMARY

Pile behaviour, especially the lateral movement, is rather different for long piles (tips below the tunnel axis level) and short piles (tips above the tunnel axis level) because the maximum soil movement occurs at or about the tunnel axis level. Simple design charts are presented to estimate the tunnelling-induced pile behaviour. It should be noted that the design charts are for computing tunnel excavation responses of the pile, assuming that the pile is initially stress free (both laterally and axially) before tunnelling. Also, these design charts have been derived for single isolated piles and are likely to provide an upper-bound estimate of response for piles in a group.

It should be noted that the design charts provided here may not predict the tunnelling-induced effects for extremely large ground loss (typically greater than 2.5 percent) values accurately because the ground interaction mechanism changes under such conditions.

6.0 RISK ASSESSMENT METHODOLOGY FOR PILES

6.0 RISK ASSESSMENT METHODOLOGY FOR PILES

6.1 INTRODUCTION

The design charts provided in Chapter 5 can be used to assess the ground movement-induced effects on the adjacent piles. The actual risk of damage depends, however, on the ground movement path at the pile location during the various stages of excavation. The critical condition can occur at an intermediate stage, for example, so it is important to understand the ground and induced pile movement path during each of the various stages of excavation.

The current practice of using total ground loss values to assess tunnelling-induced effects can result in quite conservative estimates. The method presented in this chapter results in more realistic values, thereby optimising the risk assessment and resulting in considerable potential savings for clients.

6.2 GROUND AND PILE MOVEMENT PATH

In current practice, tunnelling-induced effects on piles are estimated based on the pile displacements after the tunnel excavation has been completed; however, the piles may have experienced critical conditions at intermediate stages. To understand the actual net tunnelling-induced effects on adjacent piles, it is important to understand the pile movement path at the various stages of the tunnel excavation.

TBMs can be operated with a face pressure that is greater than the earth pressure, resulting in a negative face loss in such a way that the net movement of the adjacent pile due to tunnelling is negligible. This approach provides a minimum effect on the adjacent piles.

Piles experience displacements in various directions, depending on their location in relation to the TBM and the magnitude of the ground loss components; i.e., face loss, shield loss and tail loss. It is possible, therefore, to establish various displacement zones in the vicinity of the TBM.

Based on the maximum pile movement path, three displacement zones can be specified. These displacement zones are important when identifying the locations of piles that are subject to risk. The risk assessment method will vary for each zone.

Based on TBM operating face pressure, two different ground movements can occur, as described bellow.

CASE 1: Negative face loss. When a TBM face pressure is greater than the earth pressure at the face, the ground is pushed away from the TBM face, thereby inducing heave at the surface. When the TBM has passed, a positive shield and tail loss occurs (closing of the physical gap), meaning the ground will move toward the tunnel, resulting in ground settlement. Figure 6.1 shows the three different zones mentioned above (Z1, Z2 and Z3) and the maximum pile movement path for each zone.

It should be noted that, in some cases, shield pressure and back grouting pressure can be as high as face pressure and piles may not move towards the tunnel.

Case 1 can be adopted when tunneling adjacent to sensitive structures to minimise the net effect caused by ground movements.

Figure 6.1 Section and Plan View Showing Settlement Influence Zones and Pile Movements for Negative Face Loss

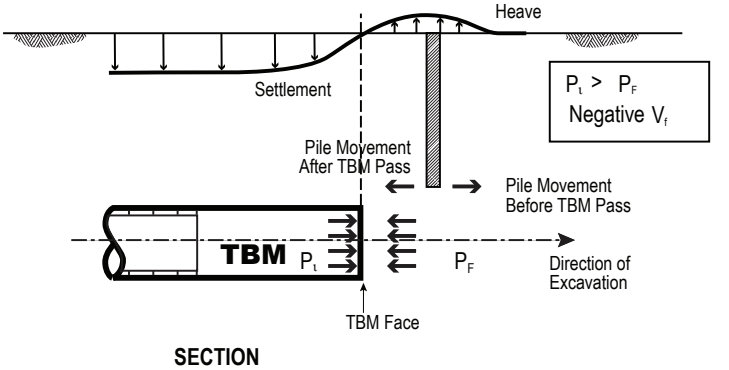

SECTION

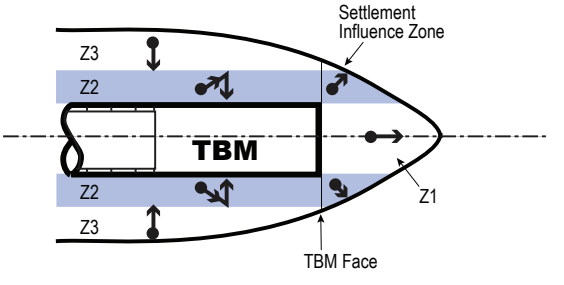

PLAN – Ground Movement Vector

Any pile located in front of the TBM face will be pushed away from the tunnel face, and after the TBM passes the pile, the pile will start to move in the opposite direction due to positive ground loss. The magnitude of these movements varies depending on various ground loss values and the pile's location relative to the tunnel alignment.

In Zone Z1, piles move only in the longitudinal direction, especially above the tunnel centreline. Lateral pile movements are negligible for Zone Z1.

Similarly, piles located in Zone Z2 will be pushed away from the TBM initially. After the TBM passes, the pile will move towards the tunnel. However, the direction of the movements will be different from the Zone Z1 movements. There are occasions where negative shield loss can occur, especially for slurry shield machines due to excessive slurry pressure. In this condition, piles will not move toward the tunnel.

Piles located in Zone Z3 will not be influenced by the face loss. After the TBM passes a pile, however, the pile will start moving toward the tunnel due to the shield and tail losses.

CASE 2: Positive face loss. When the applied TBM face pressure is less than the earth pressure, the ground moves toward the TBM face, thereby inducing positive face loss and settlement at the surface. When the TBM has passed, a positive shield and tail loss occurs that causes further ground settlement. There will be movement of the pile in the same direction when the TBM passes the pile. Figure 6.2 shows the three different zones (Z1, Z2 and Z3) and the maximum pile movement path for Case 2.

Figure 6.2 Section and Plan View Showing Settlement Influence Zones and Pile Movements for Positive Face Loss

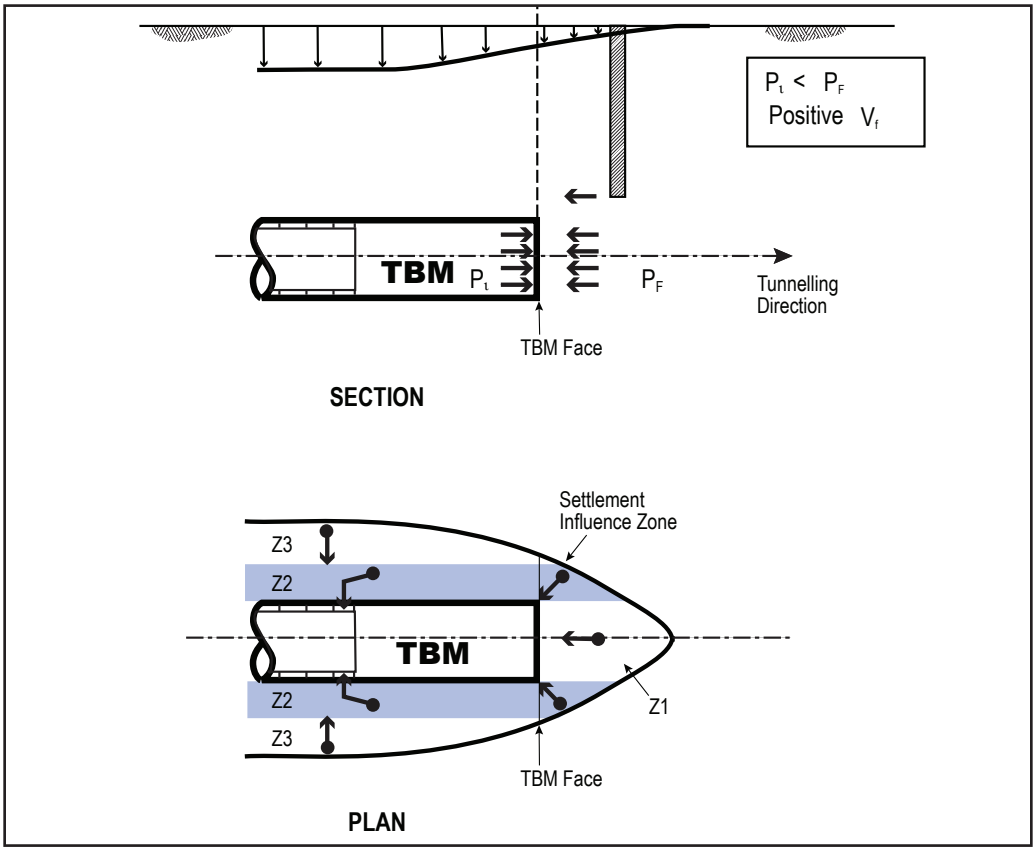

Piles located in Zone Z2 will move inward due to the positive face and shield losses. Piles located in Zone Z3 will not be influenced by the face loss; however, they will start moving toward the tunnel after the TBM passes the pile due to positive shield and tail losses.

It should be noted that any pile located in Zone Z3 will not be affected by the magnitude of face pressure and face loss because Zone Z3 is located outside the face pressure influence zone.

By adopting a stress influence zone or bearing pressure distribution concept for a circular footing to the TBM face, it can be assumed that 90 percent of the TBM face pressure effect will be felt within the two-diameter (2D) distance from the tunnel centreline (Bowles, 1996); i.e., Zone Z2 is located within twice the tunnel diameter distance from the tunnel centreline. It can be concluded that any piles located beyond about a 2D distance from the tunnel centreline will not be influenced by the TBM face pressure. The settlement induced in Zone Z3 will be due only to the shield and tail loss. The extent of Zone Z3 can be defined as three times the settlement trough width parameter (3i) as defined by Peck's (1969) settlement envelope (see Section 2.3.1).

A summary of the various displacement zones is shown in Figure 6.3.

The derivation of the extent of the displacement zones is an important aspect to determining the risk assessment requirement for piles located in various zones in the vicinity of a tunnel.

Figure 6.3 Extent of Various Displacement Zones

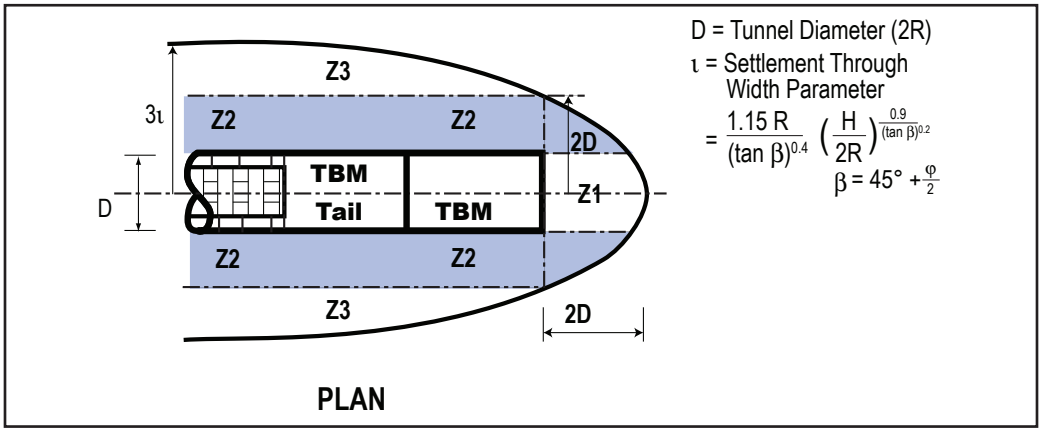

6.3 PILE LOCATION SPECIFIC INDUCED EFFECTS

The first step in assessing the risk of damage to buildings founded adjacent to a new tunnel is to estimate the tunnelling-induced bending moment, axial down drag, lateral deformation and settlements based on the design charts provided in Chapter 5 for the various ground loss components. The induced values derived from the design charts are the maximums that would be experienced. Based on the ground displacement and pile movement paths, the critical induced effects can be assessed as shown in Table 6.1.

Table 6.1: Critical Tunnelling-Induced Values on Piles

Induced Effects	Pile Location	Induced Design Value
Bending moment, ΔM (kNm)	Zone Z1	ΔM_f
	Zone Z2	$\Delta M_f + \Delta M_s + \Delta M_t$
	Zone Z3	$\Delta M_s + \Delta M_t$
Axial down drag force ΔP (kN)	Zone Z1	$\Delta P_f + \Delta P_s + \Delta P_t$
	Zone Z2	$\Delta P_f + \Delta P_s + \Delta P_t$
	Zone Z3	$\Delta P_s + \Delta P_t$
Lateral deflection, ρ (mm)	Zone Z1	ρ_f
	Zone Z2	$\rho_f + \rho_s + \rho_t$
	Zone Z3	$\rho_s + \rho_t$
Pile settlement v (mm)	Zone Z1	v_f
	Zone Z2	$v_f + v_s + v_t$
	Zone Z3	$v_s + v_t$

Where:

ΔM_f, ΔM_s and ΔM_t are induced bending moments due to face, shield and tail loss components.

ΔP_f, ΔP_s and ΔP_t are induced axial down drag forces due to face, shield and tail loss components.

ρ_f, ρ_s and ρ_t are induced lateral deflections due to face, shield and tail loss components.

v_f, v_s and v_t are induced pile settlements due to face, shield and tail loss components.

6.4 SUMMARY

As shown in Table 6.1, the actual tunnelling-induced effects on piles are different depending on their location. The actual induced bending moment may be smaller on piles in Zone Z1 and Zone Z3 than on piles located in Zone Z2. Similarly, the induced down drag force may be smaller for piles in Zone Z3 than for those in Zone Z1 or Zone Z2. In current practice, the total ground loss approach predicts higher values for all three zones. The method presented above optimises the risk assessment method and can result in considerable savings for clients.

7.0 BUILDING RISK ASSESSMENT TOOL

7.0 BUILDING RISK ASSESSMENT TOOL

7.1 INTRODUCTION

The successful completion of an urban tunnelling project with respect to risk depends on two critical factors, both of which are covered in this chapter:

1. A reliable and accurate building-risk assessment method or tool
2. An efficient risk-management procedure during construction.

In most cases, buildings are founded on mixed foundations consisting of both shallow foundations (pad and strip footings) and deep foundations (short and long piles), so it is also important to understand building risk assessments for shallow foundations. The global building risk assessment tool presented in this chapter covers both shallow foundations and pile foundations. It is intended to be used in the early stages of design, and it is applicable to tunnels excavated in either soft or hard ground.

It should be noted that the risk assessment methods presented for pile foundations are an outcome of this research, whereas methods used for shallow foundations are well established methods from the literature.

7.2 RISK ASSESSMENT FLOW CHART

Tunnelling-induced building risk assessments should be carried out systematically and in stages to identify the buildings that are truly exposed to increased risk. Figure 7.1 shows a flow chart that indicates the step-by-step procedure for conducting such risk assessments.

This flowchart includes the predictions of ground loss values based on the tunnel excavation methods. A method for assessing ground loss for TBM tunnels is described in Chapter 3. If the TBM configuration and geotechnical conditions are not provided for the estimation of ground loss components (as described in Chapter 3), then the ground loss values can be assumed based on previous projects under similar conditions. In such cases, however, back calculating the ground loss values once the TBM configurations are known is strongly recommended. At the later stages of the design, the risk assessment will need to be revised if the ground loss values assumed at the early stages vary considerably from the predicted ground loss values based on project specific geotechnical and TBM information that becomes available.

Similarly, for traditionally mined tunnels, numerical analysis is performed in longitudinal and lateral directions to assess the face loss and the total ground loss. In current practice, the ground loss values are assumed from previous similar projects. Again, comparing the assumed values with numerical predictions when the geotechnical conditions are available is strongly recommended.

In sequentially excavated conventional tunnels, an intermediate excavation stage may cause greater distortion to buildings than the full heading. It is important, therefore, to check the influence of the major intermediate headings; e.g., top heading drifts of substantial size.

Figure 7.1 Risk Assessment Tool: Flow Chart for Assessing Potential Damage to Existing Buildings

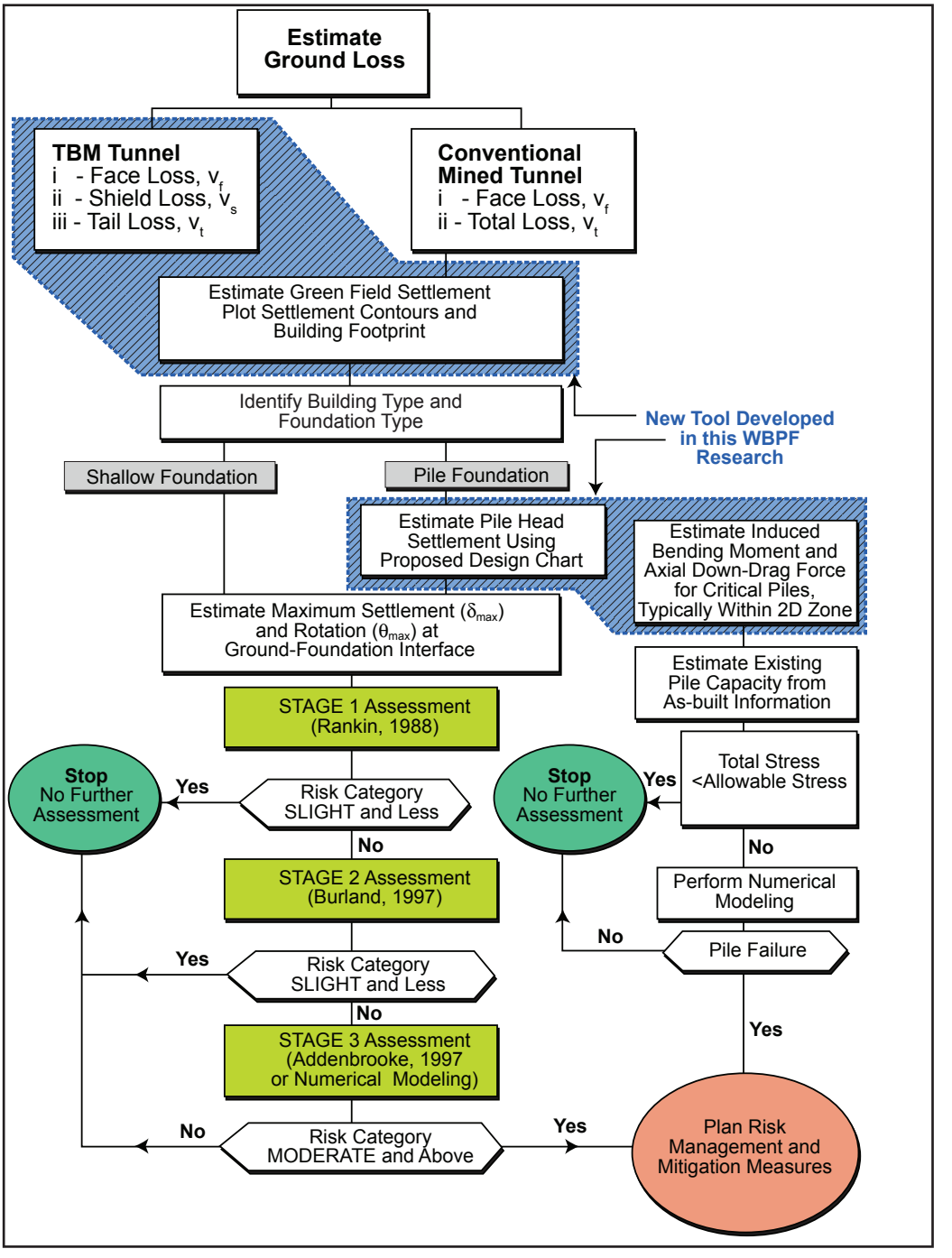

Based on the predicted or assumed ground loss, the tunnelling-induced ground movements can be predicted using the closed-form solutions provided in Chapter 4. These formulae predict surface and subsurface settlements, and lateral deformations. Example worksheets for estimating these settlement components are provided in Appendix A.2. These worksheets include alternate empirical prediction methods.

The design charts presented in Chapter 5, which provide quick assessment of tunnelling-induced settlements, lateral movements, bending moments and down-drag forces of the pile, allow the integration of the risk assessment of the piles with the existing risk assessment methods for shallow foundations.

7.3 TUNNELLING-INDUCED BUILDING RISK ASSESSMENT FOR SHALLOW FOUNDATIONS

Building risk assessment is based on the following three broad categories of damage:

- **Aesthetic:** Damage that affects only the appearance of the property
- **Serviceability:** Cracking and distortion that impair the weather tightness of the building or other functions (e.g., fracturing of service pipes, jamming of doors and windows)
- **Stability:** Damage that puts some part of the structure at risk of failure unless preventive action is taken.

Tunnelling-induced risk assessment for buildings on shallow foundations is well researched and widely used by the industry. The major steps involved are given below.

Step 1: Determine Total Settlement

Estimate tunnelling-induced ground movements using empirical, analytical or numerical methods as appropriate. Plot short-and long-term settlement contours along the tunnel alignment. Incorporate groundwater drawdown-induced settlements (if any) and the excavation-induced settlements to obtain the total settlements.

During construction and the long-term operation of a drained underground structure, groundwater drains into the excavation, resulting in the lowering of the original groundwater table (i.e., groundwater drawdown). Groundwater drawdown can be estimated by numerical predictions using two- or three-dimensional hydrogeological modelling software, depending on the complexity of the tunnel components and ground conditions.

Groundwater drawdown results in an increased effective weight of the ground, which will induce elastic compression of the ground in the short-term and consolidation settlement in the long term.

The settlement of a soil layer due to a uniform increase in the vertical effective stress can be calculated as shown in Equation. 7.1 (CIRIA 1996, C515, Sec 6.6.2).

$$\delta_v = \frac{D\Delta\sigma'_v}{E'_o} = \frac{D\gamma_w s}{E'_o} \quad (7.1)$$

Where:

D	= Thickness of soil layer
σ'_v	= Vertical effective stress increment
γ_w	= Unit weight of water
E'_o	= Soil stiffness in one dimensional compression
s	= Groundwater drawdown.

Step 2: Develop Contour Map

Plot the settlement and horizontal movements along the tunnel alignment. GIS software is useful for complex projects with interacting tunnels. Figure 7.2 shows a typical contour map along a tunnel alignment.

Figure 7.2 Typical Settlement Contour Map with Building Footprints

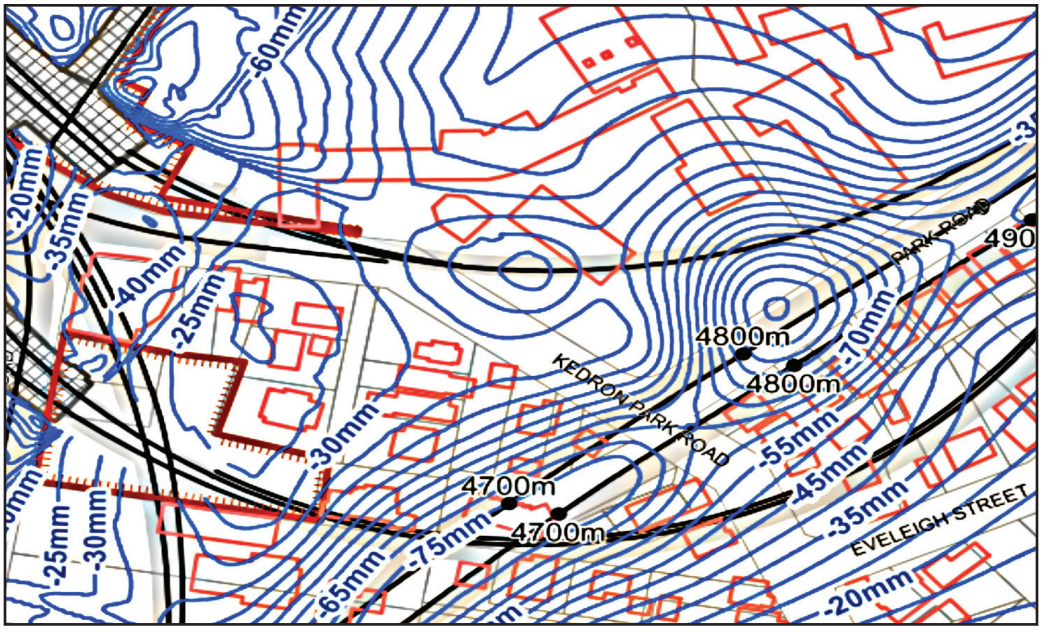

Step 3: Perform Initial Assessment (Stage 1)

Plot building footprints on the contour map and perform Stage 1 damage assessment (see also Section 2.4) by estimating the maximum settlement and differential movements under the building footprint. GIS software is often used to calculate such parameters for large complex projects that involve a large number of buildings. For small and less complex projects with only a few buildings, maximum and differential settlements can be estimated manually.

The Stage 1 assessment can be performed using Rankin's (1988) method, as recommended in CIRIA (1996) PR30.

Table 7.1: Damage Classifications – Typical Values for Maximum Building Slope and Settlement for Damage Risk Assessment (CIRIA PR30, 1996)

Risk category	Maximum slope of building	Maximum settlement of building (mm)	Description of risk
1	< 1/500	<10	***Negligible***: superficial damage unlikely
2	1/500 to 1/200	10 to 50	***Slight***: possible superficial damage which is unlikely to have structural significance
3	1/200 to 1/50	50 to 75	***Moderate***: expected superficial damage and possible structural damage to building, possible damage to relatively rigid pipelines
4	> 1/50	> 75	***High***: expected structural damage to buildings and rigid pipelines or possible damage to other pipelines

The criteria presented in Table 7.1 can be incorporated in a Microsoft Excel© worksheet by a simple macro function to determine the building risk category based on the predicted maximum settlement and the maximum rotation under the building footprint.

Figure 7.3 shows a typical worksheet used to assess the Stage 1 building risk assessment.

Figure 7.3 Typical Worksheet for Stage 1 Risk Assessment

Building ID	Address	Base Case Settlement					Revised Drain Case Settlement				Revised	Drained
		min (mm)	max (mm)	Differential	distance (m)	rotation	min (mm)	max (mm)	Differential	rotation	Tender	
K23		-28.50	-44.27	15.77	17.20	1091	-34.58	-53.42	18.84	913	Slight	Moderate
K24		-27.46	-42.86	15.40	43.66	2835	-32.63	-41.75	9.13	4784	Slight	Slight
K25		-21.96	-27.69	5.73	16.40	2861	-28.48	-34.26	5.78	2837	Slight	Slight
K26		-20.19	-35.13	14.94	38.64	2586	-27.44	-47.75	20.31	1902	Slight	Slight
K27		-45.45	-57.14	11.69	26.93	2304	-58.05	-72.66	14.61	1843	Moderate	Moderate
K28		-51.36	-78.99	27.63	30.89	1118	-64.57	-96.95	32.38	954	High	High
K29		-37.33	-42.04	4.71	9.06	1924	-41.95	-47.40	5.44	1664	Slight	Slight
K3		-47.89	-57.74	9.85	16.28	1653	-60.61	-73.01	12.41	1312	Slight	Moderate
K30		-63.07	-73.95	10.88	10.63	977	-79.82	-91.19	11.37	935	Moderate	Moderate
K31		-63.58	-69.43	5.85	7.81	1336	-79.38	-86.35	6.97	1120	Moderate	Moderate
K32		-35.05	-37.71	2.66	7.00	2629	-41.12	-43.27	2.15	3254	Slight	Moderate
K33		-92.84	-98.80	5.96	10.63	1785	-114.14	-119.66	5.52	1925	Moderate	High
K34		-79.82	-94.88	15.06	18.87	1253	-100.64	-115.44	14.80	1275	Moderate	High
K35		-32.21	-52.51	20.30	48.66	2397	-44.48	-69.32	24.83	1959	Slight	Moderate
K36		-46.20	-71.06	24.86	46.53	1871	-63.61	-93.68	30.07	1547	Moderate	Moderate
K37		-61.14	-75.07	13.93	21.84	1568	-83.89	-97.92	14.03	1557	Moderate	Moderate
K38		-49.09	-57.60	8.51	32.57	3829	-68.71	-79.91	11.20	2908	Slight	Slight
K39		-39.72	-50.64	10.92	28.65	2624	-55.81	-70.90	15.09	1899	Slight	Moderate
K4		-30.34	-38.89	8.55	17.49	2046	-39.13	-45.45	6.31	2770	Slight	Slight
K40		-44.56	-52.47	7.90	29.83	3774	-61.85	-73.13	11.28	2645	Slight	Slight
K41		-39.63	-44.38	4.76	17.16	3671	-55.73	-63.12	7.39	2362	Slight	Moderate

Step 4: Perform Stage 2 Assessment

This assessment is performed for buildings that earned a "Moderate" rating or worse in the Stage 1 assessment. First, estimate the "hogging" and "sagging" strains under the building footprint. Figure 7.4 shows the definition of the "hogging" and "sagging" strain calculation procedure.

Figure 7.4 Definition of "Hogging" and "Sagging"

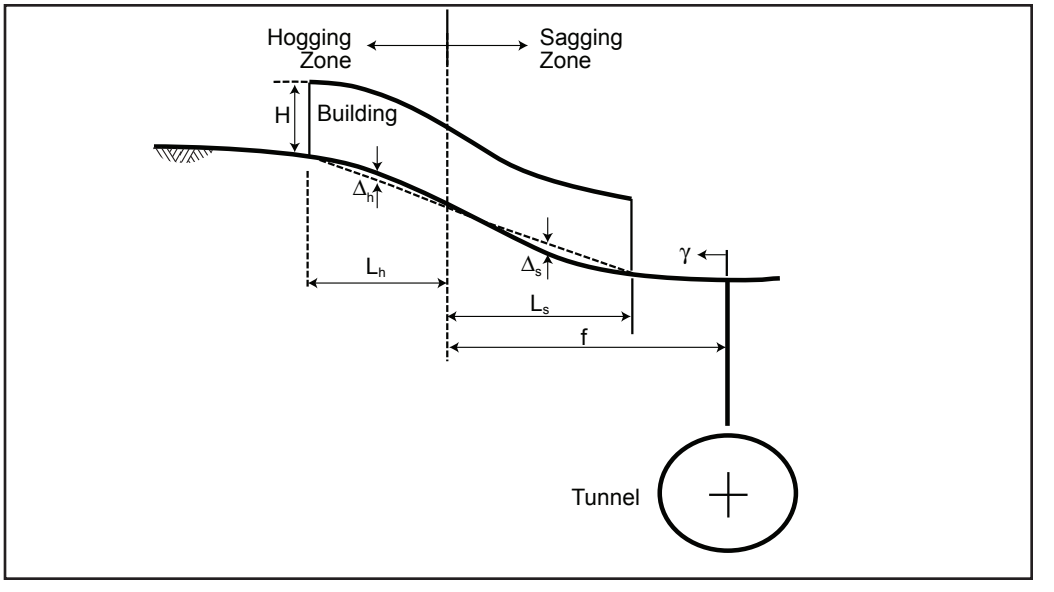

Next, estimate the bending strain (ε_b), diagonal strain (ε_d), and horizontal strain (ε_h) as shown below, as suggested by Burland and Wroth (1974).

$$\frac{\Delta}{B} = \left(\frac{L}{12t} + \frac{3IE}{2tLHG} \right) \varepsilon_b \tag{7.2}$$

$$\frac{\Delta}{B} = \left(\frac{HL^2G}{18IE} + 1 \right) \varepsilon_d \tag{7.3}$$

$$\varepsilon_h = \frac{\Delta_h}{B_d} \tag{7.4}$$

Where:

- H = Height of the building
- E/G = Relation between Young's modulus and shear modulus of the building
- L = Length of the considered building span
- I = Section moment of area of the equivalent beam height of the building at the respective zone (sagging zone: I=H3/12 and hogging zone: I=H3/3)
- t = Furthest distance from the neutral axis to the edge of the equivalent beam (sagging zone: t=H/2, hogging zone: t=H)
- Δ = Maximum relative settlement at the considered span
- Δ/L = Ratio between the maximum relative settlement at the considered span and the length of this span.

Estimate the total bending strain, diagonal strain and critical strain experienced by the building footprint as follows:

Total bending strain $\varepsilon_{bs} = \varepsilon_{b,max} + \varepsilon_h$ (7.5)

Diagonal strain $\varepsilon_{ds} = \varepsilon_h \left(\frac{1 - \nu}{2} \right) + \sqrt{\varepsilon_h^2 \left(\frac{1 - \nu}{2} \right)^2 + \varepsilon_d^2}$ (7.6)

Critical strain $\varepsilon_{critical} = \max(\varepsilon_{bs}, \varepsilon_{ds})$ (7.7)

The estimated critical strain can then be compared with Burland (1995) or Boscardin and Cording (1989) criteria as shown in Table 2.2 and Figure 2.6, respectively.

A detailed worksheet prepared for the Stage 2 building damage assessment is shown in Appendix C.1 with an example of a typical project.

Step 5. Illustrate Building Settlement Impacts

Plot the building damage designations to the building footprints shown in the contour map, as illustrated in Figure 7.5.

Figure 7.5 Building Risk Designation Plot

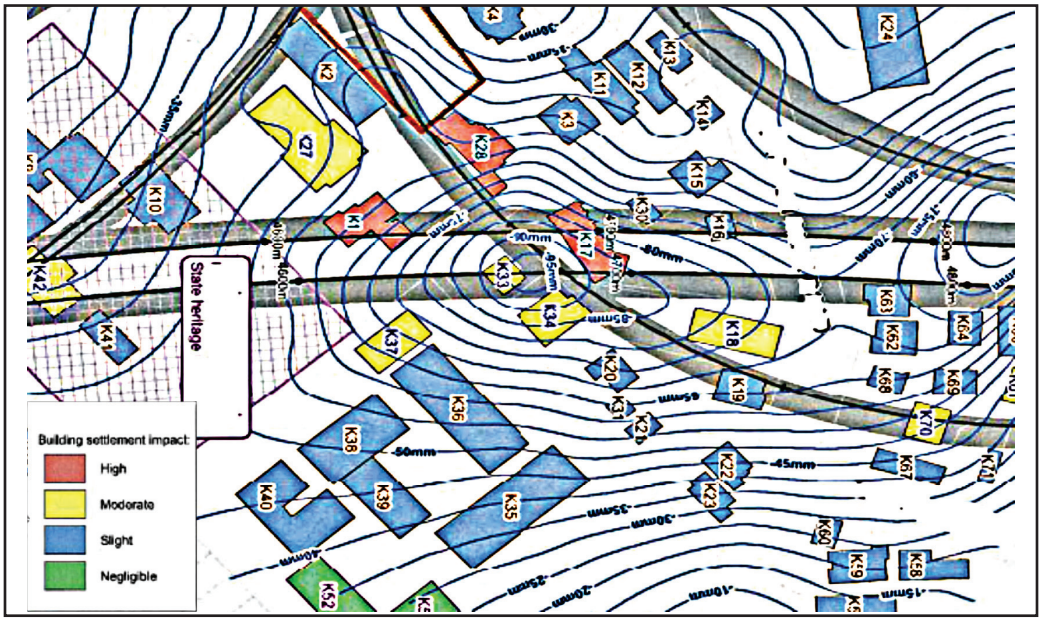

Step 6: Perform Stage 3 Assessment

The Stage 3 assessment is done by incorporating building stiffness for all buildings rated "Moderate" or "High" in Step 5. The Stage 3 assessment can be performed by using either the

methods proposed by Potts & Addenbrook 1996) or numerical modeling works. Appendix C.2 shows the Stage 3 assessment proposed by Potts & Addenbrook (1997).

The structural stiffness, a global structure parameter, is defined by the E/G ratio. Approximate values for E/G have been published by many authors. If the structure is assumed to be linear elastic, isotropic and homogenous, the E/G ratio depends upon the Poisson's Ratios used. This will range from 2.4 to 2.6 based upon Poisson's Ratios of 0.2 to 0.3 being used. Meils & Rodriguez Ortiz (2001) suggest: "for flexible buildings with big spans or steel structures, the E/G ratio can be as high as 12 to15." Further details about building stiffness are presented by Burland & Wroth (1974) and Mair et al. (1996).

7.4 TUNNELLING-INDUCED BUILDING RISK ASSESSMENT FOR PILE FOUNDATIONS

The stress-strain development mechanism induced by tunnel excavation is different for buildings founded on piles. It is not appropriate to consider green field settlements for building risk assessment for buildings founded on piles because the building will not settle along the ground settlement trough. Building settlement is the result of pile settlement.

Similar to buildings on shallow foundations, the following steps can be followed to assess the risk of buildings founded on piles.

Step 1: Assess Settlement and Lateral Movement

Assess the tunnelling-induced settlement and lateral movements of the piles using the proposed design charts. Plot the pile head settlement profile and estimate of the maximum settlement and maximum rotation below the building. The pile displacement paths described in Chapter 6 should be considered when assessing tunnelling-induced pile movements.

Figure 7.6 shows the schematic diagram of pile settlement profile and ground settlement trough for comparison.

Step 2: Obtain "As-Built" Information

Obtain as-built foundation details of the building and estimate the design capacity of each pile. Design capacity can be estimated based on the geotechnical capacity of the pile. In most as-built drawings, the pile capacity is provided.

- Design bending moment, $M=M_{design}$
- Design axial force, $P=P_{design}$.

If as-built drawings are not available, building foundation design drawings may be used to obtain foundation details.

Figure 7.6 Pile Head Settlement Profile

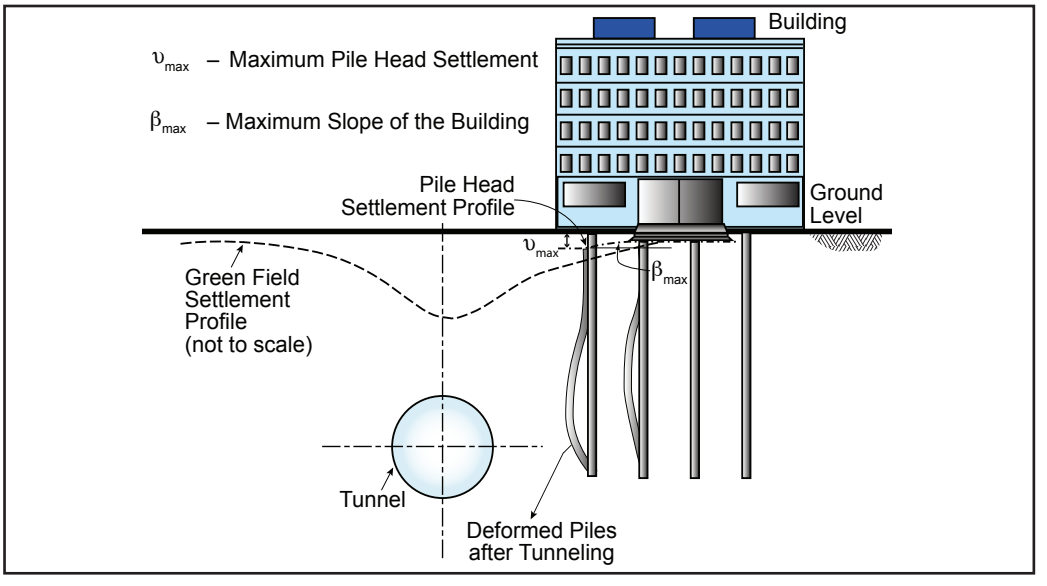

Step 3: Perform Stage 1 Assessment

Perform this risk assessment and categorise the building using the criteria provided in Table 7.1. The maximum settlement will be the maximum pile settlement and the maximum slope will be estimated based on the pile head settlement as shown in Figure 7.6.

Step 4: Perform Stage 2 Assessment

Estimate the tunnelling-induced bending moment and axial down-drag forces for all piles located within a 2D (D=tunnel diameter) distance using the design charts presented in Chapter 5. The induced effects should be estimated based on the guidelines provided in Chapter 6 for the three settlement influence zones.

- Induced bending moment, $\Delta M=\Delta M_{tunnelling}$
- Induced axial force, $\Delta P=\Delta P_{tunnelling}$

Determine the combined stress on the pile and check this against its capacity. If the combined (existing and induced) stress exceeds the pile capacity, the pile will fail. If any pile fails, the building can be placed in the “Moderate” or “High” risk categories.

$$\sigma_{max} = \frac{(M+\Delta M)}{Z} + \frac{(P+\Delta P)}{A} \qquad \text{(Z instead of I)}$$

$$\sigma_{min} = \frac{(M+\Delta M)}{Z} - \frac{(P+\Delta P)}{A} \qquad \text{(Z instead of I)}$$

Where Z is section modulus of area.

For concrete piles, however, designers should make a judgment to allow for the additional 25% compressive stress of the work cube strength at 28 days calculated on the total cross-sectional area of the pile, under working load. It is advised that the overstress assumption may not be applicable for old building foundations.

If $\sigma_{max} < \sigma_{allowable}$ then no pile failure.

Step 5: Verify Risk Level

Explore opportunities to downgrade the risk by adjusting tunnel construction methods, sequences and support details, and then reassess the risk of buildings rated “Moderate” or “High” in Step 4. Further risk assessment will not be required for buildings that are below the “Moderate” risk level.

Step 6: Perform Stage 3 Assessment

Perform detailed numerical modelling for buildings assessed “Moderate" or “High” in Step 5. If the numerical modelling does not show pile failure, then the damage risk for these buildings can be downgraded, depending on the risk category at the end on Step 3.

This step can be skipped if the contractor decides to implement mitigation methods for all buildings assessed “Moderate” and “High” in Step 5.

Step 7: Plan Mitigation

Implement remedial measures, such as ground improvement or foundation reinforcement to mitigate the tunnelling-induced risk to the building.

7.5 SUMMARY

The new tool presented in this chapter to assess the tunnelling-induced risk to the adjacent buildings considers both shallow and deep (pile) foundations. These risks are related to the tunnelling-induced effects on pile foundations that can be determined using the design charts presented in Chapter 5.

8.0 CONCLUSIONS

8.0 CONCLUSIONS

Ground movements around a tunnel excavation are always critical, particularly when the tunnel alignment is in an urban area and adjacent to high-rise buildings. Understanding tunnelling-induced ground loss mechanisms and the associated displacements is, therefore, key to successfully addressing the risks that tunnel excavation can impose on nearby buildings.

Gaining such an understanding early in the project design phase has not been possible until now, and the few methods that were available have proven to be inadequate or too complex. Now, using the innovative risk assessment tool presented in this monograph, designers can do the following easily and accurately:

1. **Predict various ground loss components for TBM tunnels in soft ground**

   The new methodology presented herein can be used prior to construction to assess various ground loss components, such as face loss, shield void loss and tail void loss. An automated worksheet developed as part of this effort is presented in Appendix A1. This methodology has been validated using published information on other projects. The ground loss components vary from project to project, however, so it is recommended that this method be validated for project specific conditions by carrying out a detailed monitoring programme at the early stages of the project.

2. **Predict tunnelling-induced ground settlement**

   The new closed-form solutions presented herein offer a marked improvement over methods used previously, and they provide accurate predictions of surface, subsurface and lateral ground movements. These solutions have been tested for accuracy in predictions by using case histories, centrifuge model test results and FLAC3D numerical predictions. These formulae are currently being used by practicing engineers to predict tunnelling-induced ground movements. They are as follows:

   Surface Settlement

$$U_{z=0} = \varepsilon_0 R^2 . \frac{4H(1 - \nu)}{H^2 + x^2} . \exp\left\{ \frac{1.38x^2}{(H \cot \beta + R)^2} \right\}$$

   Subsurface Settlement

$$U_z = \varepsilon_0 R^2 \left(\frac{z - H}{x^2 + (z - H)^2} + (3 - 4\nu) \frac{z + H}{x^2 + (z + H)^2} - \frac{2z[x^2 - (z + H)^2]}{[x^2 + (z + H)^2]^2} \right)$$

$$\cdot \exp\left\{ -\left[\frac{1.38x^2}{(H \cot \beta + R)^2} + \frac{0.69z^2}{H^2} \right] \right\}$$

Lateral Deformation

$$U_x = -\varepsilon_0 R^2 x \left[\frac{1}{x^2 + (H-z)^2} + \frac{3-4\nu}{x^2 + (H+z)^2} - \frac{4z(z+H)}{(x^2 + (H+z)^2)^2} \right]$$

$$\cdot \exp\left\{ -\left[\frac{1.38x^2}{(H \cot \beta + R)^2} + \frac{0.69z^2}{H^2} \right] \right\}$$

Where

$U_{z=0}$	= Ground surface settlement
U_z	= Subsurface settlement
U_x	= Lateral soil movement
R	= Tunnel radius
z	= Depth below ground surface
H	= Depth of tunnel axis level
ν	= Poisson's ratio of soil
ε_0	= Average ground loss ratio (not a displacement)
x	= Lateral distance from tunnel centreline
β	= Limit angle = 45 + ϕ/2.

Poisson's ratio value (ν) can be estimated from lateral earth pressure at-rest coefficient (k_0) values using the following relationship:

$$k_0 = \frac{\nu}{(1-\nu)}$$

3. Predict tunnelling-induced effects on foundation piles

The new design charts presented herein enable designers to quickly, easily and accurately estimate the tunnelling-induced bending moments, down-drag forces and movements of pile foundations early in the design process. This method is a vast improvement over the current practice of basing the tunnelling-induced effects on pile foundations on complex numerical modelling—a time consuming exercise that requires detailed geotechnical modelling. The new design charts were based on a series of detailed numerical studies and then test verified using published centrifuge model test results. Figures 5.2 to 5.9 provide a series of design charts for short piles (tip above the tunnel centreline) and long piles (tip below the tunnel centreline). It should be noted that these design charts may not accurately predict the tunnelling-induced effects for extremely large ground loss values (typically greater than 2.5 percent) because the ground interaction mechanism changes for extremely high ground loss values.

4. Evaluate a building's risk assessment

Tunnelling-induced building risk assessment and risk management are important aspects in urban tunnelling. The risk assessment and management should be carried out systematically, in stages, to identify the buildings that are truly subject to potential damage risk due to the tunnel excavation. In current practice, various procedures are used by practicing engineers for shallow foundations. The risk associated with pile foundations are typically handled separately by performing detailed numerical analysis.

The new risk assessment and management procedure presented in this monograph incorporates all structures founded on both shallow and deep foundations. Figure 7.1 shows the new building damage risk assessment and management flow chart.

9.0 REFERENCES

9.0 REFERENCES

Addenbrooke, T, Potts, D M and Puzrin A M (1997). The influence of pre-failure soil stiffness on the numerical analysis of tunnel construction, Geotechnique 47, No. 3, pp. 693-712.

Atkinson J H and Potts D M (1979). Subsidence above shallow tunnels in soft ground, Journal of Geotechnical Engineering, American Society of Civil Engineers, GT4, pp. 307-325.

Attewell P B (1977). Ground movements caused by tunnelling in soil, Proc. of the Large Ground Movements and Structures Conference, Cardiff, Edited by Geddes, Pentech Press, London, pp. 812-948.

Banerjee P K and Driscoll R M C (1976). Three-dimensional analysis of raked group, Proceedings, Institute of Civil Engineering, 61, pp. 653-671.

Bezuijen A and Bakker K J (2007). Bentonite and grout flow around a TBM, Proc. WTC 2007, Prague.

Boscardin M. D. and Cording E. J. (1989). "Building Response to Excavation-Induced Settlement," Journal of Geotechnical Engineering, American Society of Civil Engineers, Vol. 115, No. 1, pp. 1-21.

Bowles J E(1996). Foundation analysis and design, 5th Ed, McGraw-Hill International.

Burland J B (1997). Assessment of risk of damage to buildings due to tunnelling and excavation, Earthquake Geotechnical Engineering, Ishihara (ed), Balkema, Rotterdam, pp. 1189-1201.

Burland J B and Wroth C P (1974). Settlement of buildings and associated damage. State of the Art Review, Proceedings, Conference on Settlement of Structures, Cambridge, Pentech Press, London, pp. 611-654.

CIRIA (1996). “Prediction and effects of ground movements caused by tunnelling in soft ground beneath urban areas,” Construction Industry Research and Information Association, Project Report 30.

Clough G W and Schmidt B (1977). Design and performance of excavations and tunnels in soft clays, State-of-the-art report, International Symposium on Soft Clays, Bangkok.

Clough G W and Schmidt B (1981). Excavations and Tunnelling, Soft Clay Engineering, Chapter 8, Edited by E W Brand and R P Brenner, Elsevier.

Cording and Hansmire (1975). Tunnels in Soils-general report. Proceedings, Session IV, 5th Pan American Congress of Mechanical and Foundation Engineering, Buenos Aires, p. 63.

Gatti M.C and Cassani G (2007). Ground loss control in EPB TBM Tunnel excavation, Underground Space - The 4th Dimension of Metropolices - Taylor&Frances Group, London, Eds: Bartak, Hrdina, Romancov & Ziamal.

Gunn M J (1993). The prediction of surface settlement profiles due to tunnelling, predictive soil mechanics, Proc. of the Wroth Memorial Symposium, edited by G T Houlsby and A N Schofield, Oxford, pp. 304-316.

Ingles O G (1972). Soil Stabilisation, Text Book, Butterworths, Sydney.

Lagerblad B, Fjallberg L and Vogt C (2010). Shrinkage and Durability of Shotcrete, Proceeding of Shotcrete Elements of a System, ed: Bernard, ES, 2010 Taylor & Francis Group, London, pp. 173-180.

Lee K M, Rowe R K and Lo K Y (1992). Subsidence owing to tunnelling. I. Estimating the gap parameter, Canadian Geotechnical Journal 29, pp. 929-940.

Lo K Y, Ng R M C and Rowe R K (1984). Predicting settlement due to tunnelling in clays, Tunnelling in Soil and Rock, American Society of Civil Engineers, Geotech III Conference, Atlanta, Ga., pp.48-76.

Loganathan N and Poulos H G (1998). "Analytical Predictions of Tunnelling Induced Ground Movements", Geotechnical Engineering Journal, American Society of Civil Engineers, Sept., 1998, Vol. 124, No. 9.

Loganathan, N, O'Carroll, J, Flanagan, R and Tan BT (2005). 'EPB TBM tunneling in Singapore old alluvium', Proceedings of the Rapid Excavation and Tunneling Conference, Seattle, Washington, United States, June.

Loganathan, N and Flanagan, RF (2001). 'Prediction of tunnelling-induced ground movements: assessment and evaluation,' Proceedings of the Underground Singapore 2001, Singapore.

Loganathan, N, Poulos, HG and Bustos-Ramirez, A (2000). 'Estimation of ground loss during tunnel excavation,' paper presented at GeoEng2000, Melbourne, Australia, November.

Mair R J, Gunn M J and O'Reilly M P (1981). Ground movements around shallow tunnels in soft clay, 10th International Conference on Soil Mechanics and Foundation Engineering, Stolkhom, pp.323-328.

Mair, R.J. (1993). Developments in geotechnical engineering research: application to tunnels and deep excavations, Unwin Memorial Lecture 1992, Proceedings Institution of Civil Engineers. Civil Engineering, Vol. 93, pp.27-41.

Mair, R.J. (1996). Settlement effects of bored tunnels. Session report, Geotechnical Aspects of Underground Construction in Soft Ground - Proceedings International Symposium, City University, London, 15-17 April 1996 (eds: R J Mair and R N Taylor), Balkema, Rotterdam.

Mair, R.J., Taylor, R and Burland, J (1996). Prediction of ground movements and assessment of risk of building damage due to bored tunnelling, Conference on Geotechnical Aspects of Underground Construction in Soft Ground, London.

Meils, M and Rodriguez Ortiz, J (2001). Consideration of the stiffness of buildings in the estimation of subsidence damage by EPB tunnelling in the Madrid Subway, CIRIA Response of Buildings to Excavation-induced Ground Movements.

Norgrove W B, Cooper I and Attewell P B (1979). Site investigation procedures adopted for the Northumbrian water authority's Tyneside sewerage scheme, with special reference to settlement prediction when tunnelling through urban area, Tunnelling '79, pp. 79-104.

O'Reilly M P and New B M (1982). Settlements above tunnels in the U.K – Their magnitude and prediction, Tunnelling '82. pp. 173-181.

Peck R B (1969). Deep excavations and tunnelling in soft ground, Proceedings. of 7th International Conference on Soil Mechanics and Foundation Engineering, Mexico City, State-of-the-art volume, pp. 225-290.

Phienwej et al. (2006). International Symposium on Underground Excavation and Tunnelling, 2-4 February 2006, Bangkok, Thailand.

Potts D M and Addenbrooke T I (1996). The influence of an existing surface structure on the ground movements due to tunnelling, International Symposium on Geotechnical Aspects of Underground Construction in Soft Ground, City University, London, (eds: R Mair and R Taylor), Rotterdam, pp. 573-578.

Poulos H G (1979). An approach for the analysis of offshore pile group, Proc. Conf. on Numerical Methods in Offshore Piling, Institution of Civil Engineers, London, pp.119-126.

Poulos H G (1990). DEFPIG Users Guide, Center for Geotechnical Research, University of Sydney, Australia.

Randolph M F (1980). PIGLET: A computer program for the analysis and design of pile groups under general loading conditions, Soil Report TR91, CUED/D, Cambridge University, Cambridge, England.

Rankin, W J (1988). Ground movements resulting from urban tunnelling: Predictions and effects. Engineering Geology of Underground Movements, Engineering Geology Special Publication No 5, Geological Society, London, pp. 79-92.

Rowe R K and Lee K M (1989). Parameters for predicting deformations due to tunnelling. Proceedings, 12th International Conference on Soil Mechanics and Foundation Engineering, Rio de Janeiro, pp. 793-796.

Rowe R K and Kack G J (1983). A theoretical examination of the settlements induced by tunnelling: Four Case Histories, Canadian Geotechnical Journal, Vol. 20, pp. 299-314.

Rowe R K and Lee K M (1992). An evaluation of simplified techniques for estimating three-dimensional undrained ground movements due to tunnelling in soft soils, Canadian Geotech–nical Journal, 29, pp. 39-52.

Sagaseta C (1987). Analysis of undrained soil deformation due to ground loss, Geotech–nique 37, pp. 301-320.

Simpson B, Atkinson J H and Jovicis V (1996). The influence of anisotropy on calculations of ground settlements above tunnels, Proceedings of International Symposium on Geotechnical Aspects of the Underground Construction in Soft Ground, London preprint vol., pp. 511-514.

Sternath, R and Baumann, K (1997). Face support for tunnels in loose ground, Tunnels for People, Balkema, Rotterdam, 1997.

Vermeer P A and Bonnier P G (1991). Pile settlements due to tunnelling, Proceedings of European Conference On Soil Mechanics and Foundation Engineering, 10, Florence, May 1991, pp. 869-872.

Verruijt, A. and Booker, J.R. (1996). Surface settlements due to deformation of a tunnel in an elastic half plane, Geotechnique, Vol. 46, No. 4, pp. 753-756.

Xu K J and Poulos H G (1999). Principles of Program GEPAN for General Pile Elastic Analysis, University of Sydney, Dept. of Civil Engineering, Research Report No: R782.

APPENDICES

APPENDIX A
DESIGN WORKSHEETS

APPENDIX A1: GROUND LOSS ESTIMATION

Parsons Brinckerhoff
CALCULATION SHEET

Design Date:
Check Date:
Description:

Project:
Subject:

ESTIMATION OF TUNNELLING-INDUCED GROUND LOSS

Project Title:

General Project Information

Location:

Depth: 30 m (CL)
Diameter : 6 m (OD)

Soil Type:

Poisson's ratio:	0.5	
Stability number:	5.9	
Undrained modulus, E:	75000	kPa
SPT, N value:	50.0	
Unconfined shear strength, q_u:	150	kPa
Earth press. coef , k_0:	0.80	
Unit weight:	18	kN/m^3
Depth of WT:	25	m (from surface)
Tunnel support Pressure, P_i=	100	kPa
P_0 =	292.8	kPa
k=	*0.9*	
Ω=	*3.7*	

Tunneling Method Information

Method:
Earth pressure balance, shield tunnelling

TBM Configuration

Length of the shield:	9.14	m
Thickness of tail skin, t:	15	mm
Clearance for erection of lining, δ:	25	mm
Cutter bead overcut thickness, t_b:	0	mm
TBM shield taper, t_t: (change in radius)	30	mm

Used reduced TBM face pressure to induce larger ground movement to demonstrate ground loss predictions.

Face loss, Vf
Equivalent radial gap, gf = 19.6 mm
Face loss V_f = 0.65 %

Shield Loss, Vs
Radial gap, gs= 12.18 mm
Shield loss V_s= 0.4 %

Tail Loss, Vt
Radial gap, gt = 4.0 mm
Tail Loss V_t= 0.1 %

Total ground loss

$$V_L = 1.15\ \%$$

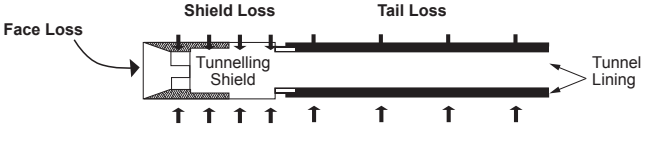

Parsons Brinckerhoff Pte Ltd
CALCULATION SHEET

Prepared by: Logan Date:
Check Date:
Description:

Project:
Subject:

TUNNEL FACE PRESSURE ESTIMATION

Tunnel depth, H =	30	m
Tunnel diameter, D =	6	m
Friction angle =	1	deg
UCS =	150	kPa
Cohesion =	75	kPa
Average unit weight =	18	kN/m^3
Earth Pressure coef. =	0.80	
Surcharge pressure =	0	kPa
Depth of WT, hw = (from ground surface)	25	m
Water height from crown Hw =	5	m

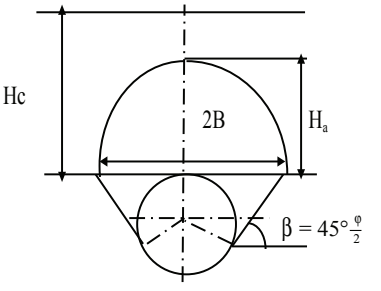

According to Terzaghi's Silo theory, loading width "B" can be expressed as;

$$B = R\ \tan(45^\circ - \frac{\varphi}{2}) + \frac{R}{\cos(45^\circ - \frac{\varphi}{2})} \quad = 7.15 \text{ m}$$

The vertical earth pressure at depth Hc can be expressed as;

$$\sigma_v = \frac{\gamma B - C}{k_0 \tan\varphi}\left(1 - e^{-k_0 \tan\varphi H / B}\right) + P_0 e^{-k_0 \tan\varphi H / B} \quad = 197.54 \text{ kPa}$$

Arching height, Ha = 10.97 m

Effective earth pressure loaded on cutter head face is given as;

If Hw> Ha $P_F = K_1\ (H_a + \frac{D}{2})\gamma$ = 89.44 / 111.80 $K_1 = \frac{1-\sin\varphi}{1+\sin\varphi}$

Else $K1$ = 0.80

$$P_F = K_1\left[\gamma(H_a - H_w) + \gamma'(H_w + \frac{D}{2})\right] \quad = 138.45 \text{ kPa}$$

(Effective) P_F = 138.45kPa

Total pressure on TBM face = FP

(Total)	FP =	188.45 kPa	Crown
		218.45 kPa	Spring Line
		250.63 kPa	Invert

APPENDIX A2: GROUND MOVEMENT PREDICTIONS

Parsons Brinckerhoff
CALCULATION SHEET

Design Date:
Check Date:
Description:

Project:
Subject: Surface Settlement Prediction

INPUT DATA

Tunnel depth (tunnel centreline)	H =	30	m
Tunnel diameter (outer diameter)	D =	6	m
Poisson's ratio of soil	ν =	0.5	
Friction angle (soil at tunnel crown)	ϕ =	1	deg.
Tunnel face pressure (applied)	P_i=	100	kPa
Estimated ground loss (total)	V_L=	1.15	%
Ground loss at face	V_f=	0.65	%
Ground loss at shield	V_s=	0.4	%
Ground loss at tail	V_t=	0.1	%

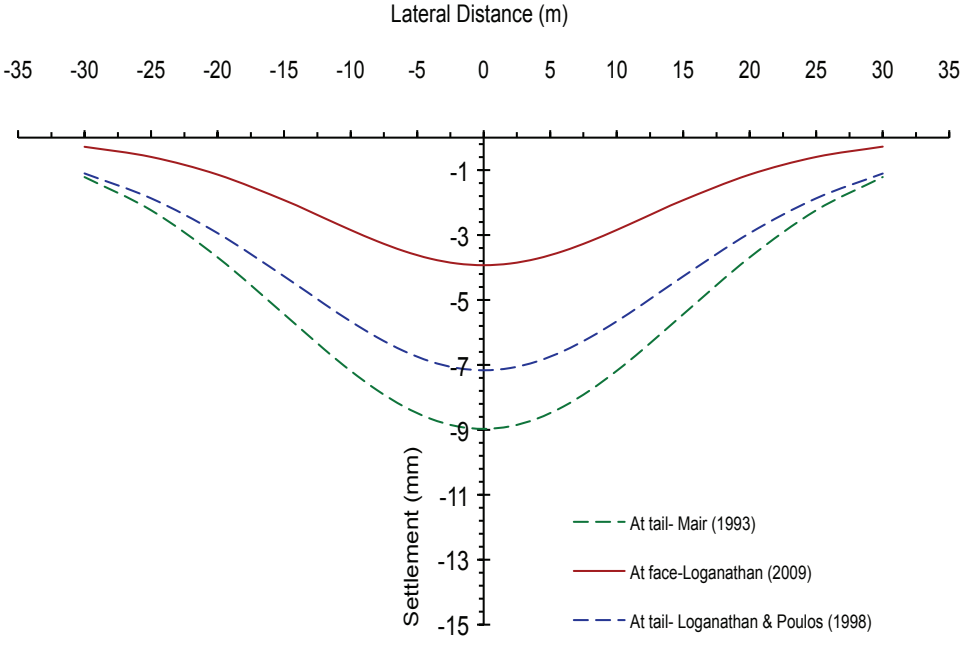

Parsons Brinckerhoff
CALCULATION SHEET

Prepared by: Logan Date:
Check Date:
Description:

Project:
Subject: Sub-Surface Settlement Predictions

INPUT DATA

Tunnel depth (tunnel centreline)	H =	30	m
Tunnel diameter (outer diameter)	D =	6	m
Poisson's ratio of soil	ν =	0.5	
Friction angle (soil at tunnel crown)	ϕ =	1	deg.
Tunnel face pressure (applied)	P_i=	100	kPa
Lateral distance from tunnel centreline	x=	0	m
Estimated ground loss (total)	V_L=	1.15	%
Ground loss at face	V_f=	0.65	%
Ground loss at shield	V_s=	0.4	%
Ground loss at tail	V_s=	0.1	%

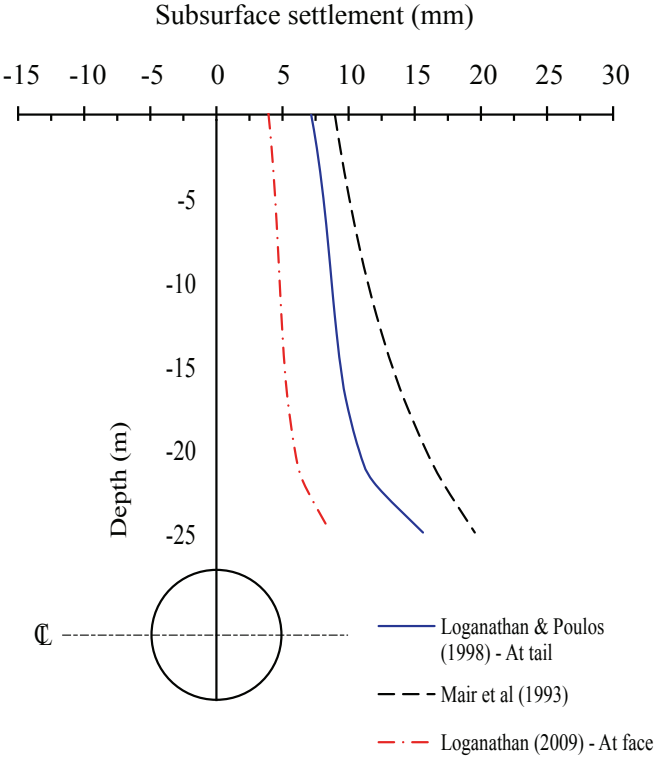

Parsons Brinckerhoff
CALCULATION SHEET

Prepared by: Logan Date:
Check Date:
Description:

Project:
Subject: Lateral Deflection Prediction

INPUT DATA

Tunnel depth (tunnel centreline)	H =	30	m
Tunnel diameter (outer diameter)	D =	6	m
Poisson's ratio of soil	ν =	0.5	
Friction angle (soil at tunnel crown)	ϕ =	1	deg.
Tunnel face pressure (applied)	P_i=	100	kPa
Lateral distance from tunnel centreline	x=	5	m
Estimated ground loss (total)	V_L=	1.15	%
Ground loss at face	V_f=	0.65	%
Ground loss at shield	V_s=	0.4	%
Ground loss at tail	V_t=	0.1	%

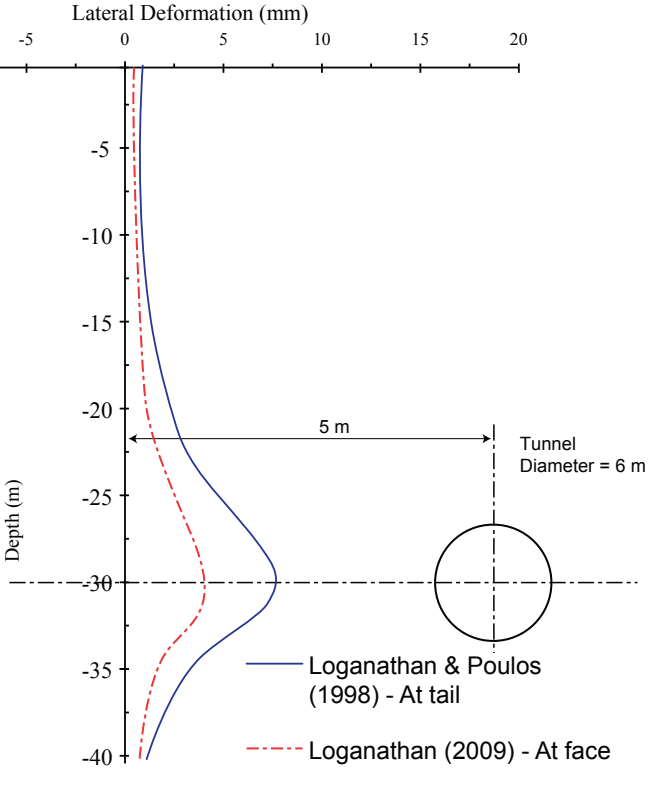

APPENDIX B
GENERAL PILE ANALYSIS (GEPAN) COMPUTER PROGRAM

DETAILS OF GEPAN COMPUTER PROGRAM

At present, various numerical approaches have been used to estimate pile group responses to combinations of external loadings. Computer programs for the analysis of pile groups vary in the types of approaches used and in the sophistication of their treatment of different aspects of group behaviour. Among the most widely used general programs for pile group analysis are PGROUP (Benerjee, 1976), DEFPIG (Poulos, 1979, 1990), and PIGLET (Randolph, 1980). These programs are based on elastic continuum analysis, although DEFPIG can also be extended into the non-linear range by specifying limiting values of skin friction and lateral pressure along the pile.

Although these programs have been used widely, they all involve simplifications and idealizations, including the following:

1. Pile-to-pile interactions are used instead of individual pile-element-to-pile-element interactions.
2. The actual non-uniform stress distributions around the pile (especially in the lateral loading case) are modified to an equivalent uniform stress distribution over each pile element.
3. Load-deformation behaviour is modeled individually without considering the deformation coupling effects due to three dimensional loading.
4. Off-pile loading conditions arising from adjacent constructions such as embankments, excavations, tunnelling etc. are not considered.

GEPAN was developed at Sydney University (Xu and Poulos, 1999) to overcome some of the limitations and idealizations in existing computer programs. A three-dimensional boundary element analysis together with the virtual image technique for an elastic half-space has been used to carry out analyses of multiple single piles and pile groups that incorporate the effect of external soil movements due to embankments, tunnels and excavations. Figure B.1 shows a typical pile element discretization used in GEPAN. Each pile is subjected to a total of six components of load.

Figure B.1: Schematic Diagramme Showing 3D Boundary Element Discretization and Loads and Stresses Acting on the Pile and Adjacent Piles

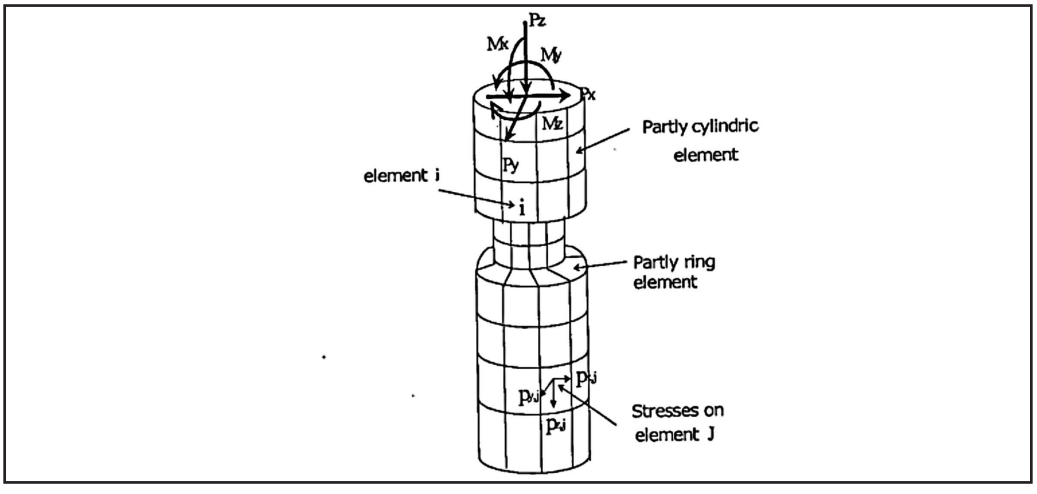

More accurate load-deformation pile responses are obtained by assuming that load-deformation interactions occur between each element of each pile of each group. Twelve kinds of influence factors are classified and presented by corresponding influence factor matrixes (IFM), which are of a hierarchical nature. The resulting global equation for pile response is shown in Equation (B.1).

$$\begin{pmatrix} A & B & \varnothing & D \\ \varnothing & \varnothing & G & H \\ O & P & Q & R \\ S & \varnothing & \varnothing & V \end{pmatrix} \begin{pmatrix} X_e \\ X_b \\ X_c \\ X_t \end{pmatrix} = \begin{pmatrix} Y_q \\ Y_c \\ \varnothing \\ Y_p \end{pmatrix} \tag{B.1}$$

Where:

A=IFM of element displacement and stress (=SIF+PIF), SIF=IFM of element soil displacement and stress, PIF=IFM of element pile displacement and stress,

B=IFM of element displacement and pile tip displacement,

D=IFM of element displacement and pile head load,

G=IFM of cap displacement and cap-tie-cap beam force (to allow for pile caps jointed by tie beam,

H=IFM of cap load and pile head load,

O=IFM of pile head displacement and element stress,

P=IFM of pile head displacement and pile tip displacement,

Q=IFM of pile head displacement and cap displacement,

R=IFM of pile head displacement and pile head load,

S=IFM of pile head load and element stress,

V=IFM of pile head load and pile head load,

Yq=vector of element stress offset (=Yq,t + Yq,e),
Yq,t=vector of element displacement due to pile head load,
Yq,e=vector of element displacement due to extra soil displacement/stress/force,
Yc=vector of cap load,
Yp=vector of pile head load,

Xe=vector of pile-soil stress,
Xb=vector of pile tip displacement,
Xc=vector of cap displacement,
Xt=vector of capped pile head force.

Details of the various matrices and vectors are given by Xu and Poulos (1999).
The global Equation (B.1) contains the following four kinds of independent equations:

1. Compatibility equations at the pile-soil interfaces
2. Equilibrium equations for pile heads and caps
3. Compatibility equations for pile heads and caps
4. Equilibrium equations for piles.

The results obtained from GEPAN for the direct loading of a group generally agree well with the other standard programs such as PIGLET and DEFPIG (Xu and Poulos, 1999). One of

the most attractive advantages of the proposed 3D-boundary element modeling method is that externally imposed ground movements are very easily incorporated into the governing equations if the distributions of these ground movements are known. These ground movements are absorbed into the vector $\{Y_{q,e}\}$ in governing Equation (B.1) and the soil displacement vector $\{Y_q\}$ at element 'i' is given as;

$$\{Y_q\} = \{Y_{q,t}\} + \{Y_{q,e}\} \tag{B.2}$$

Where:

$\{Yq,t\}$ = soil displacement vector on element 'i' due to pile head load on individual piles

$\{Yq,e\}$ = soil displacement vector due to external sources.

The effects of external ground movements can be considered in two ways:

1. Displacements imposed directly, based on the known ground movements
2. Induced stresses based on the known ground movements.

In the first case, the free-field soil movements at the pile-soil interface are indicated by a vector $\{u_{soil}\}$ as shown in Equation (B.3):

$$\{Y_{q,e}\}=\{u_{soil}\} \tag{B.3}$$

In the second case, the induced stresses are represented by a vector $\{\sigma_{soil}\}$. The corresponding soil movements due to the soil stresses are the product of the soil influence factor matrix [*SIF*] and the soil stress vector $\{\sigma_{soil}\}$ as shown in Equation (B.4):

$$\{Y_{qe}\}=[SIF]\{\sigma_{soil}\} \tag{B.4}$$

The head displacements of individual piles can be determined from Equation (B.5).

$$\{X_i\} = [O]\{X_e\} + [P]\{X_b\} + [R]\{Y_p\} \tag{B.5}$$

The analytical closed-form solutions presented in this study to predict the tunnelling-induced ground movements have been incorporated in Equation (B.3) within GEPAN.

APPENDIX C
TYPICAL WORKSHEET FOR BUILDING DAMAGE ASSESSMENT

APPENDIX C.1
TYPICAL STAGE 2 ASSESSMENT WORKSHEET

Parsons Brinckerhoff

BUILDING DAMAGE ASSESSMENT- STAGE 2

Project:

Calc by: Date:

Checked by: Date:

Building adress Building ID K1

Building detail

Length, L	21	m (approx.)
Height, H	2.5	m (approx.)
Width, W	19	m (approx.)
Poisson's ratio, ν	0.3	
Description	Single level brick structure	
E/G =	2.6	

E/G = 2.6 for Masonry structure
E/G = 12.5 for Framed structure

E = Young's Modulus of Building
G = Shear Modulus of Building

Aerial Photogaph

Remarks

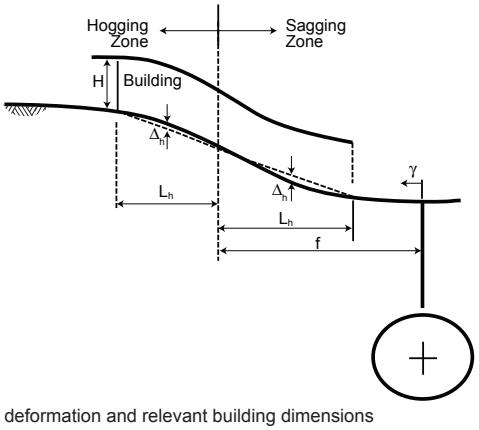

Building deformation and relevant building dimensions

Settlement and lateral deformation profile under the building

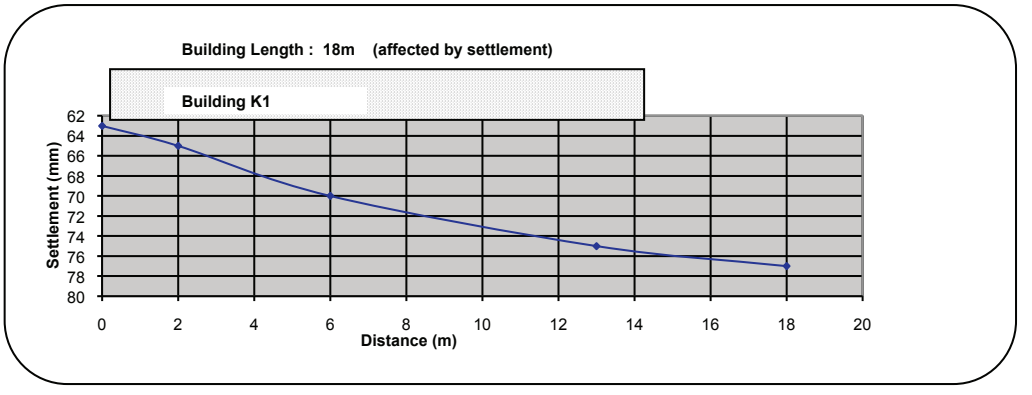

Sagging			**Hogging**		
Length, L_s	**14**	m	Length, L_h	**4**	m
Deflection, Δ_s	**2**	mm	Deflection, Δ_h	**0.8**	mm
t = H/2	1.25	m	t = H	2.5	m
$I = H^3/12$	1.3	m^3	$I = H^3/3$	5.2	m^3
Length B_s	**14**	m	Length B_h	**4**	m
H_movement Δ_{hs}	**10**	mm	H_movement Δ_{hh}	**10**	mm

Building has been considered as a beam, Burland & Wroth (1974)
t = furthest distance from the neutral axis to the edge of the beam
I = average horizontal strain along the building footprint that interacts with horizontal displacement
B = length of the building interacting with the horizontal movement

Building has been considered as a beam with the neutral axis in the middle of the beam.
This assumption is appropriate for buildings on shallow foundations.

Using the method proposed by Burland & Wroth (1974):

		Sagging	**Hogging**
Bending strain, εb			
$\frac{\Delta}{B} = \left(\frac{L}{12t} + \frac{3IE}{2tLHG}\right)\varepsilon_b$	$\varepsilon_{b,\,max}$ =	0.000136	0.0002115
		0.0136%	0.0211%
Diaganol strain, εd			
$\frac{\Delta}{B} = \left(\frac{HL^2G}{18IE} + 1\right)\varepsilon_d$	$\varepsilon_{d,\,max}$ =	0.000016	0.000172
		0.0016%	0.0172%

Horizontal strain, εh

$\varepsilon_h = \Delta_h / B$

$\varepsilon_{h,\,max}$ = 0.000714 0.002500

0.0714% 0.2500%

Total bending strain,

$\varepsilon_{bs} = \varepsilon_{b,max} + \varepsilon_h$

$\varepsilon_{bs,\,max}$ = 0.000850 0.002711

0.0850% 0.2711%

Total diagonal strain, εds

$$\varepsilon_{ds} = \varepsilon_h \frac{1-\nu}{2} + \sqrt{\varepsilon_h^{\,2}\left(\frac{1-\nu}{2}\right)^2 + \varepsilon_d^{\,2}}$$

$\varepsilon_{ds,\,max}$ = 0.000500 0.001767

0.0500% 0.1767%

ν **- Poisson's ratio**

Critical tensile strain, $\varepsilon_{critical}$

$\varepsilon_{critical} = \max(\varepsilon_{bs}, \varepsilon_{ds})$

$\varepsilon_{critical}$ = 0.000850 0.002711

0.0850% 0.2711%

Governing Condition $\varepsilon_{critical,\,max}$ = **0.2711%**

Risk Category **Moderate Damage**

Stage 3 assessment is required.

Reference

Category of Damage	Normal Degree of Severity	Limiting Tensile Strain
0	Negligible	0 - 0.05
1	Very-Slight	0.05 - 0.075
2	Slight	0.075 - 0.15
3	Moderate*	0.15 - 0.3
4 to 5	Severe to Very Severe	>0.3

* Note: Boscardin & Cording (1989) describe the damage corresponding to the tensile strain in the range 0.015-0.3%, as "moderate to severe." However, none of the cases quoted by them exhibit severe damage for this range of strains. There is no evidence, therefore, to suggest that tensile strains up to 0.3% will result in severe damage.

Burland (1995) and Boscardin & Cording (1989)

Description of Risk Category ---- ***Moderate Damage***

Moderate - The cracks require some opening up and can be patched by a mason. Repointing of external brickwork and possibly a small amount of brickwork to be replaced. Doors and windows sticking. Service pipes may fracture. Weathertightness often impaired. Typical crack widths are 5 to 15mm or several > 3mm.

Negligible - Hairline cracks less than about 0.1mm.
Very Slight - Fine cracks which are easily treated during normal decoration. Damage generally restricted to interior.
Slight - Cracks easily filled. Redecoration probabley required. Recurrent cracks can be masked by suitable linings.
Moderate - The cracks require some opening up and can be patched by a mason. Repointing of external brickwork may be required.
Severe - Extensive repair work involving breaking-out and replacing sections of walls, especially over doors and windows.
Very Severe - This requires a major repair job involving partial or complete rebuilding. Beams lose bearing, walls lean badly and require shoring.

APPENDIX C.2
TYPICAL STAGE 3 ASSESSMENT WORKSHEET

Parsons Brinckerhoff

BUILDING DAMAGE ASSESSMENT- STAGE 3

Project:

Calc by: Date:

Checked by: Date:

Building adress Building ID 10

Building detail

Length, L	25	m (approx.)
Height, H	2.5	m (approx.)
Width, W	20	m (approx.)
Poisson's ratio, ν	0.3	
Building Description	Single level brick structure	
E =	3.0E+07	kPa
Area, A_{slab} =	0.150	m^2/m
Second Moment, I =	2.81E-04	m^4/m

E/G = 2.6 for Masonry Structure
E/G = 12.5 for Framed structure

E: Young's Modulus of Building
G: Shear Modulus of Building

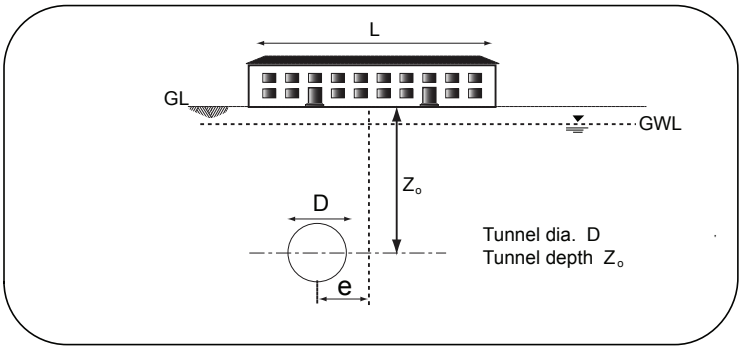

Remarks

Settlement and lateral deformation profile under the building

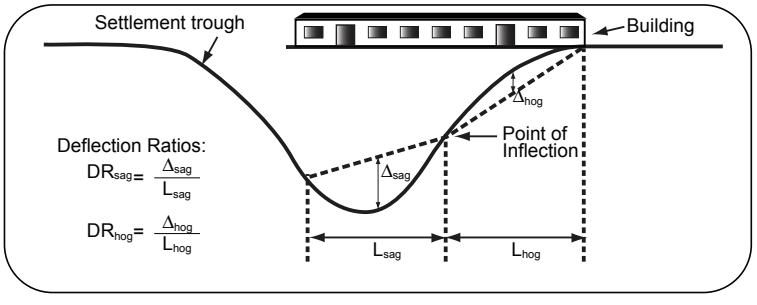

Sagging			Hogging		
Length, L_s	12	m	Length, L_h	12	m
Deflection, Δs	50	mm	Deflection, Δh	3	mm
Length B_s	12	m	Length B_h	12	m
H_movement Δhs	11	mm	H_movement Δhh	11	mm
Tunnel Dia, D	6	m	Eccentricity, e	3.5	m
Tunnel Embedded Depth	30	m			
Representative Soil Stiffness, E_s	4000	kPa			

Building has been considered as a beam, Burland & Wroth (1974)
Average horizontal strain along the building footprint that interacts with horizontal displacement
Building has been considered as a beam with the neutral axis in the middle of the beam.
This assumption is appropriate for buildings on shallow foundations.

Using the method proposed by Addenbrooke et al (1997):

Eccentricity ratio, e/L

e/L = 0.14

Relative bending stiffness, ρ*

$$\rho^* = \frac{16EI}{E_s L^4}$$

ρ* = 8.64E-05

Relative axial stiffness, α*

$$\alpha^* = \frac{2EA}{E_s L}$$

α* = 9.00E+01

Deflection ratios - greenfield		Sagging	Hogging
DR^g_{sag} =	Δ_s/L_s	DR^g_{sag} = 0.004167	
DR^g_{hog} =	Δ_h/L_h	DR^g_{hog} =	0.000250

Horizontal strains - greenfield

Compression (sagging), ε_{hc} =	Δ_{hs}/L_s	ε_{hc} = 0.000917	
Tension (hogging), ε_{ht} =	Δ_{hh}/L_h	ε_{ht} =	0.000917

Modification factors - read from curves at Fig. 16

Sagging	M^{DR}_{sag} = 0.35	Compression	$M^{\varepsilon hc}$ = 0.000000
Hogging	M^{DR}_{hog} = 0.2	Tension	$M^{\varepsilon ht}$ = 0.000000

Modified deflection ratios	Sagging	Hogging
$M^{DR_{sag}} = \frac{DR_{sag}}{DR^g_{sag}}$	DR_{sag} = 0.001458	
	1.46E-03	
$M^{DR_{hog}} = \frac{DR_{hog}}{DR^g_{hog}}$	DR_{hog} =	0.000050
		5.00E-05

Modified horizontal strains

	Compression	Tension
$M^{\varepsilon hc} = \frac{\varepsilon_{hc}}{\varepsilon^g_{hc}}$	ε_{hc} = 0	
	0.00E+00	
$M^{\varepsilon ht} = \frac{\varepsilon_{ht}}{\varepsilon^g_{ht}}$	ε_{ht} =	0
		0.00E+00

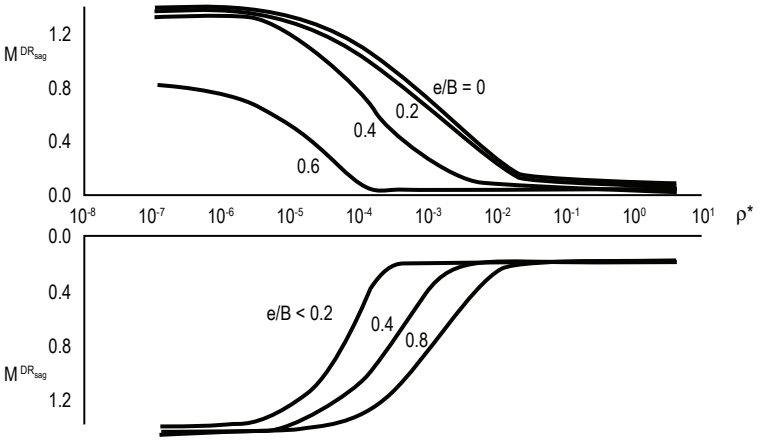

Fig. 16. Design curves for modification factors for deflection ratio

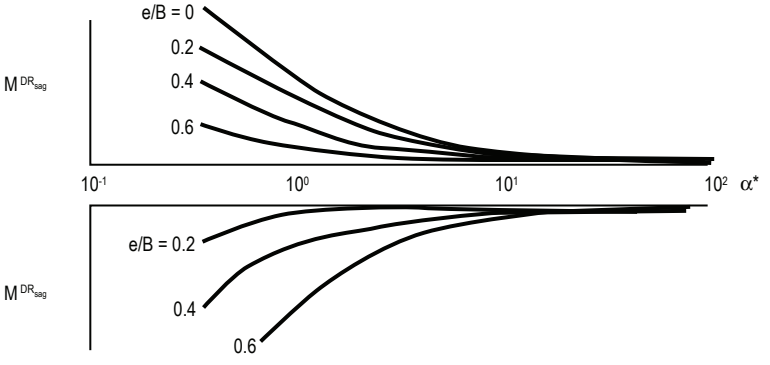

Fig. 17. Design curves for modification factors for horizontal strain